COMPARISON OF EPISODIC AND NON-EPISODIC NON-VOLCANIC TREMORS IN THE NORTHERN CASCADIA SUBDUCTION ZONE

by

Gillian Thérèse Royle

B.Sc.Joint-Honors, Memorial University of Newfoundland, 2002

A THESIS SUBMITTED IN PARTIAL FULFILLMENT
OF THE REQUIREMENTS FOR THE DEGREE OF
MASTER OF SCIENCE
in the Department
of
Earth Sciences

SIMON FRASER UNIVERSITY
Spring 2006

APPROVAL

Name: **Gillian Royle**

Degree: Master of Science

Title of Thesis: Comparison of Episodic and Non-Episodic Non-Volcanic Tremors in the Northern Cascadia Subduction Zone

Examining Committee:

Chair: **Dr. Brian Coffey**
Assistant Professor

Dr. Andrew Calvert
Senior Supervisor
Associate Professor

Dr. Doug Stead
Supervisory Committee Member
Professor

Dr. Honn Kao
Supervisory Committee Member
Geological Survey of Canada

Dr. John Cassidy
External Examiner
Geological Survey of Canada

Date Approved: August 18, 2005

Abstract

Sequences of non-volcanic tremor have been identified along the Nankai and Cascadia subduction zones [41, 15]. The source mechanisms of tremor have been attributed to flow-induced resonance in fluid-filled conduits [23]. In northern Cascadia, transient surface deformation indicates that slow slip occurs every 13-16 months on the inter-plate boundary and landward of the locked zone. Elevated levels of tremor activity have been found to coincide spatially and temporally with slow slip episodes [46]. I image two tremor sequences: one which occurs during a slow slip episode (episodic) and another which occurs in between slip episodes (non-episodic). Episodic tremors migrate 150 km along strike from south to north and correlate with the subduction megathrust. Non-episodic tremors do not migrate, and are found mostly at 5-10 km depth within the continental crust. Non-episodic tremors could arise from readjustment of the crust following the preceding slow slip episode.

For Ross and my family.

Acknowledgements

I would like to express my sincere gratitude towards my thesis supervisor Dr. Andy Calvert, who has provided expert guidance and supervision throughout my thesis research. He has been consistently enthusiastic to discuss and implement new ideas, and has been crucial in the development of my research career. I have been very lucky to have had a supervisor who has provided so much support, and with whom I can communicate so easily. I will miss working with him.

I had a wealth of resources made available to me while conducting this research. Tremor location programs, publications and documentation on relevant research, and advice from experienced researchers were easily and continuously accessible. Dr. Honn Kao was the first to generate an automated method to image tremor sources, and provided the tremor source-scanning algorithm and corresponding documentation that was implemented in this thesis. His helpful discussion clarified many of the technical points of imaging tremor sources, and saved me a significant amount of time in the lab. I am very grateful for his cheerful guidance and support, and eagerness to help when I needed. I am very grateful to Dr. John Cassidy and Dr. Doug Stead for their guidance and commitment to my research as my committee members. Their valuable discussion and suggestions substantially improved the quality of this work. I would like to express thanks to Dr. Kumar Ramachandran, who provided the 3-D velocity model he developed during his PhD research. I also received support from Dr. Kelin Wang, Dr. Gary Rogers, and Dr. Herb Dragert, who provided permissions to implement figures from their respective publications within this thesis.

Thanks to the departmental grad students for their friendship and support. In particular, my lab-mate Nathan, Kenna, Majid, Pat, Smudge, Megan, Sarah, Ryan, and Mike. Things become overwhelming and sometimes you just need to laugh about it - that was so easy to do with all of you. I will miss you all very much.

I owe so many thanks to my wonderful family, who have provided so much loving support

throughout my studies and who have been a constant source of inspiration. They have always maintained full confidence in my abilities, and have given tremendous encouragement, moral support, and laughter when it was needed.

Finally, I would like to express so many thanks to my love, Ross Hickey. He knows, perhaps better than anyone, the amount of work that went into this thesis. Unfortunately, he was also the one to suffer the consequences of my stress. Ross has provided unwavering patience, understanding, respect and support throughout my entire experience in Graduate School. I will always cherish our days at Simon Fraser University, which were filled with love and happiness.

Contents

List of Tables

List of Figures

Chapter 1

PROJECT SCOPE AND SIGNIFICANCE

1.1 INTRODUCTION

Recent discovery by surface-based deformation monitoring of episodic slip on the subduction megathrust faults in Japan and the Pacific Northwest [15, 41] has opened new avenues for research into the dynamics and seismic hazard assessment of subduction zones. In northern Cascadia, these slow slip events occur periodically every 13-16 months and last 2-3 weeks [46]. Though the time sequence of slip events has been identified, their depths are poorly constrained. In May 2003, it was found that low amplitude non-impulsive vibrations referred to as non-volcanic tremors are temporally and spatially associated with these slow slip episodes [46]. Identification of the spatial location and sequence of episodic tremor activity coinciding with slow slip may make it possible to better estimate the depth at which slow slip occurs. The implications of such possibilities are significant in that stress loading on the shallow part of the fault caused by one of these slip events will likely be a trigger for a great subduction earthquake. Lower levels of non-volcanic tremor activity have also been detected in between episodes of slow slip. These non-episodic tremor sequences have never before been imaged, and their origins are unknown. In this thesis, I image both an episodic and a non-episodic tremor sequence, with the objectives of further understanding tremor source mechanisms by comparing their source locations and characteristics. The source locations of both classes of tremor will also provide important information on the rheology of the megathrust interface. Identifying the locations of tremors, and understanding their association with megathrust, and perhaps other earthquake-related processes significantly advances the understanding of the tectonics of the Cascadia subduction zone and may lead to a more accurate assessment of the seismic hazard in the Pacific Northwest.

1.2 THE CASCADIA SUBDUCTION ZONE

1.2.1 EARTHQUAKE SEISMICITY IN CASCADIA

The Cascadia subduction zone extends 1,100 km from northern California to southwestern British Columbia. The region is characterized by complicated tectonics due the interactions of three main lithospheric plates: the large Pacific and North American plates and the intervening Juan de Fuca plate system, which includes the Explorer, Juan de Fuca and Gorda plates [11].

At the Northern Cascadia margin, the oceanic Juan de Fuca plate underthrusts North America at a rate of approximately 46 mm/yr [13] along the megathrust interface, generating damaging levels of seismicity in the forearc crust and downgoing plate (Figure 1.1). Three different classes of earthquakes occur along the Cascadia margin:

1. Megathrust events on the shallow (< 25 km depth) portion of the megathrust interface where the Juan de Fuca and North American plate are currently locked [3, 47]. Megathrust earthquakes have moment magnitudes $M_w > 8$ and re-occur every 200-600 years [19]. The most recent megathrust event occurred January 26, 1700 with a magnitude estimated to be approximately 9 [47, 10]. The rupture associated with this event appears to have extended along most of the margin [19].

2. Crustal earthquakes occur within the overriding North America plate in response to subduction. High rates of crustal earthquakes occur in Puget Sound and southwestern Washington [6] with moment magnitudes that may exceed $M_w = 7$.

3. Inslab earthquakes, also called Wadati-Benioff earthquakes, whose magnitude is usually less than 7, occur at depths as great as 80 km. Despite great depths, inslab earthquakes dominate current seismicity in the northern Cascadia subduction zone. Canada's fourth generation seismic hazard model [2] has found inslab earthquakes to occur at a rate up to five-fold higher per unit area than crustal events, and their predicted shaking is stronger than crustal events of the same size [1].

The conditional probability of a megathrust event occurring within the next 100 years is constrained by the time since the last event, the main recurrence interval of characteristic earthquakes, and the distribution of these intervals [33]. Earthquake recurrence intervals and distributions are largely dependant on the deformation associated with post-seismic relaxation. Shortly following fault rupture, a part of the fault downdip may slip aseismically. Later in the interseismic period,

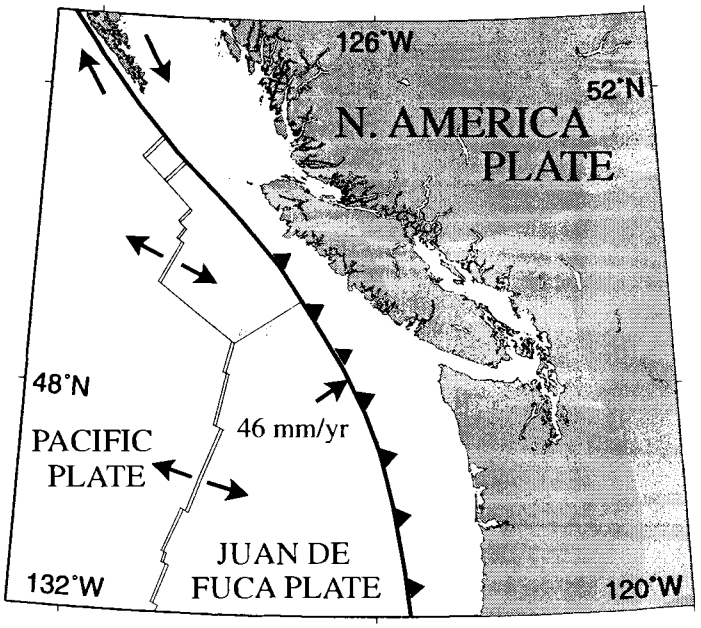

Figure 1.1: Lithospheric plates at the northern Cascadia margin. The Juan de Fuca plate underthrusts North America at a rate of approximately 46 mm/yr.

deformation is dominated by fault locking. Seismic hazard assessment therefore translates to the appraisal of slab and crustal stresses due to the (interseismic) locking and (coseismic) unlocking of the subduction fault.

Contemporary geodetic deformation along the Cascadia margin is used to measure elastic strain accumulation due to the locked subduction fault. A 3-D viscoelastic finite element model developed at the Pacific Geoscience Center takes into account along-strike variations of fault geometry, geodetic plate convergence parameters and asthenospheric viscoelasticity [52]. The model represents interseismic deformation as a combined effect of the previous megathrust event and subsequent loading on the locked fault. Surface displacements along the Cascadia margin have been measured with respect to a stationary site at Penticton (on the North America plate) by Global Positioning System (GPS) sensors. Seaward GPS sites were found to have larger velocities in the plate convergence direction than landward sites. This observation is interpreted as evidence for the locking of the subduction fault [15]. The 3-D viscoelastic model predicts post-rupture elastic deformation due to the relaxation of a low-viscosity asthenosphere. Model-predicted strain rates for the present day define a locked fault zone extending 60 km landward of the deformation front. The transition zone to stable sliding on the megathrust extends from the locked zone to more than 120 km from the

deformation front, and becomes progressively wider as the fault remains locked.

1.2.2 Regional Geology

The Intermontane superterrane, made up primarily of sedimentary and volcanic rocks, collided with the North America plate approximately 200 My ago [43]. The last major collisional episode occurred during the mid-Cretaceous, which accreted the Insular superterrane against the Intermontane superterrane. The mid-Cretaceous to early Tertiary intrusive rocks of the Coast Belt were generated in the suture region [43]. Onshore, Vancouver Island is largely composed of the Wrangellia terrane (part of the Insular superterrane), which is composed of Devonian through Lower Jurassic igneous sequences and sedimentary rocks which are interpreted to represent a Jurassic island arc [21, 35]. The Pacific Rim and Crescent terranes were the last to be accreted to the continent and reached their present locations during the late Cretaceous and Tertiary periods [20]. The Pacific Rim terrane, composed of a mainly Mesozoic metasediments, is found along the west coast and southern part of Vancouver Island [11]. The Eocene volcanic Crescent terrane is found at the southern tip of Vancouver Island and northwest Washington, which is largely composed of basalt, diabase and gabbro [36]. The mafic rocks of the Crescent terrane are considered correlative to the Metchosin volcanics of southern Vancouver Island [36].

1.2.3 The Structure of the Megathrust from Reflection and Refraction Imaging

The imaging of reflection data has identified a thin reflection zone, which broadens from 2 km off the west coast of Vancouver Island into a thick (5-7 km) reflection package at the island's eastern margin [40]. This reflection zone is commonly referred to as the E-reflectors, and is interpreted to represent interlayered mafic and/or sedimentary rocks [54, 12], or intensely sheared sediments in which fluids released from the subducting plate are trapped [8]. Complementary to these interpretations is the identification of a low velocity zone (6.4-6.6 km/s) at depths of 25-35 km beneath southern Vancouver Island in 3-D P-wave velocity model images of southwest British Columbia and northwest Washington [55, 44]. Additionally, magnetotelluric surveying and modelling [30] has located a landward dipping highly conductive zone in the 20-50 km depth range beneath Vancouver Island, landward of the transition zone determined by viscoelastic modelling, and coinciding with the E-reflector package. A highly conductive E-layer may indicate the presence of hydrated rocks [17, 9]. Water-rich fluids are thought to be released at the 40-50 km depth range, resulting in

hydration of the overlying mantle and crust material. Temperature estimates on the megathrust [19] and fluid-filled porosity estimates within the E-reflectors [17] indicate that the fully developed E-reflector package most likely defines the zone of aseismic stable sliding downdip of the seismogenic zone. This is supported by the observation that earthquake seismicity terminates abruptly at the top of the E-reflectors, which indicates that ductile processes are the dominant form of deformation within this zone [7].

Seismic refraction and normal incidence reflection profiles acquired west of Vancouver Island locate the top of the subducting oceanic plate immediately beneath a reflector dipping landward between 12 and 25 km depth [50, 12, 7]. This reflector is observed intermittently at depths 2-6 km deeper than the E-reflectors. This reflection is referred to as the F-reflector, and has been interpreted to be the oceanic Moho [40] or the top of the subducting plate [7]. Common among both interpretations is the idea that the F-reflector originates from a very thin region or single interface.

Across southern Vancouver Island, the E-reflectors dip shallowly east northeast (ENE) at 4^o. The package bends downward at the eastern margin, dipping sharply at 15^o and reaching depths of 45 km [7]. The F-reflector is found to dip at 15^o at the western margin of Vancouver Island, and flatten out to the east. The E- and F-reflectors are therefore thought to define a duplex thrust structure extending 110 km in width [7] in which crustal rocks are imbricated (Figure 1.2). The top of the E-reflectors (roof thrust) and the F-reflector (floor thrust) are interpreted to accommodate slow slip.

1.3 Transient Deformation in Cascadia

1.3.1 Episodic Aseismic Slip

Data from continuously recording GPS sites have recently provided evidence for sudden periods of aseismic slip [15]. Over a two-week period in August of 1999, displacements of 14 GPS stations (relative to the GPS site at Penticton) have indicated a total horizontal displacement of 2 to 4 mm over a 6 to 15 day period in the direction opposite to that of longterm plate convergence [15] (Figure 1.3).

With increased GPS station coverage, aseismic slip has been found to reoccur every 13 to 16 months (Figure 1.4). The largest horizontal motions are found 100 km landward of the locked zone, roughly bounded by the 30- and 40-km depth contours of the plate interface. Slip appears to migrate from stations in the southeast along strike to the northwest at a rate of approximately 6 km/day. The

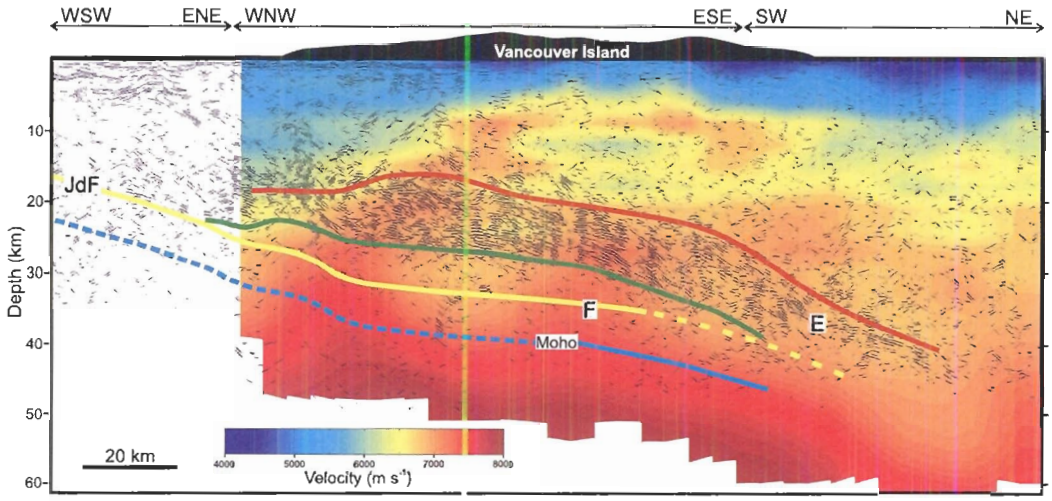

Figure 1.2: Composite seismic cross-section across the northern Cascadia forearc, showing migrated reflection data superimposed on *P*-wave velocities derived by 3-D tomographic inversion of first arrivals. Seismic profiles were projected onto an azimuth of 063°, which is a representative dip direction for the subducting plate near the seismic profiles. Source: [7], by permissions.

surface deformation has been modelled by a slip of 2.1 cm on a landward-dipping interface at 30-40 km depth, which is equivalent to approximately half a year of plate convergence and generates a maximum surface strain signal on the order of 20×10^{-9} to 30×10^{-9} [15]. Discontinuous slip rates along the plate interface imply that the convergent plate motion across the deeper plate interface varies with time. Silent deep-slip events could indicate cumulative stress loading of the shallower seismogenic zone, each event bringing the locked zone closer to failure.

1.3.2 Episodic Tremor and Slip

Non-volcanic tremor-like signals, identified by visual inspection of seismograph station records from the Canadian National Seismic Network (CNSN), have recently been found to accompany transient slip. Moreover, these findings parallel the discovery of non-volcanic tremors close to the Moho of the overriding plate in the Nankai subduction zone of southwest Japan [41, 27]. The tremors of northern Cascadia have been observed only in the subduction zone region and specifically in the same general region as the deep slip events [46]. No correlation between local (deep or shallow) earthquake patterns and tremor activity has been found. The temporal correlation between non-volcanic tremors and slow slip suggests that the tremor source region is in some way associated with the location of slow slip. However, the depth of slow slip is poorly constrained because it is

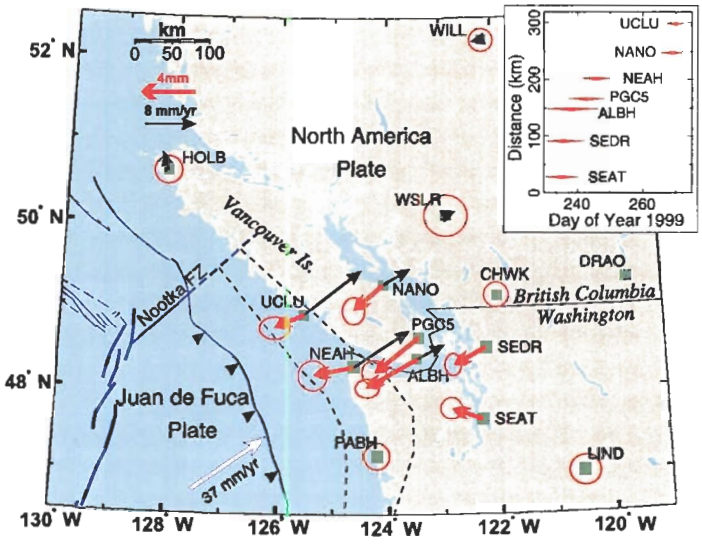

Figure 1.3: Location of continuous GPS sites that are included in routine analysis of GPS data by the GSC. Red arrays show displacements with respect to North America due to the 1999 slip event. Black arrays show the 3- to 6-year average GPS motion. Source: [15], by permissions.

determined by surface deformation monitoring. The association between tremor activity and slow slip - referred to as episodic tremor and slip (ETS) - has led to the hypothesis that the depth of slow slip thrusting can be constrained by the location of tremor activity.

Each tremor comprises multiple pulses of energy that last tens of seconds to several minutes, with a frequency content between 1 and 5 Hz [46]. Seismic waves emitted from the source region propagate at close to the *S*-wave velocity, and tremor amplitudes are often barely visible above background environmental noise. Tremor signals can therefore be detected only by correlating records from multiple stations. Identification of the first *P* arrivals and discrimination of phases is virtually impossible by visual inspections alone. An added complication is that tremor waveforms have been found to be inconsistent from one seismograph station to another, the cause of which may be due to either a poor signal to noise ratio, the source radiation pattern, or site effects beneath the seismograph station.

Resonance of fluid-filled cracks and flow-induced oscillations in conduits are seen as the current descriptions of tremor sources [23]. The modelling of flow stability through narrow conduits [4] has indicated that fluid-induced oscillations in conduit walls may provide a source for sustained seismicity. Balmforth *et al.* (2005) have found that rapid flow of low-viscosity fluids is required to generate resonance [4]. The propagation of water and CO_2-rich fluids at sufficiently high speeds is

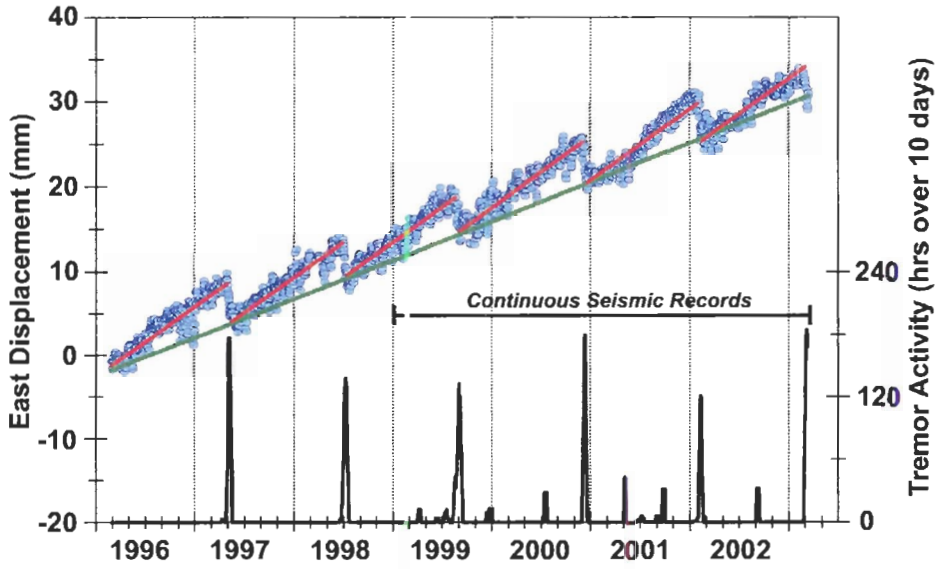

Figure 1.4: Comparison of slip and tremor activity for the Victoria area. Blue circles indicate day-by-day changes in the east component of GPS site ALBH relative to the GPS site near Penticton. The bottom graph shows the total number of hours of tremor activity observed for southern Vancouver Island within a sliding 10-day period. Source: [46], by permissions.

a viable tremor source mechanism, though the nature and origin of the fluid motion has not yet been determined.

Because the onset of tremor activity could indicate the occurrence of slip, and possibly an increased probability for the occurrence of a megathrust earthquake, the investigation into Cascadia tremors has focused on the development of a systematic and automated method to identify and locate tremor sources. Kao and Shan [25] have developed an algorithm - referred to as the source-scanning algorithm - to image the distribution of tremor sources in space and time using the coherence of tremor waveforms across a recording array. They compute the likelihood that a seismic source exists at a particular origin time and position. Tremors have been located by the source-scanning algorithm within an error of ± 3 km. It may prove possible to infer the region of slow slip from the spatial distribution of tremor sources.

It has been found, however, that tremor activity associated with the March 2003 slow slip event is not confined to a single localized interface but distributes along a wide depth range [26]. If it is found that tremor activity and slow slip events occur in the same geographic area, but that tremors are distributed in a broad vertical zone, then this may indicate a broad zone of shearing or multiple shear zones. This structural mechanism might support the two megathrusts proposed on the basis

of seismic reflection surveys in northern Cascadia [7]. If it is found that tremor activity and slow slip events are spatially decoupled, tremor source mechanisms independent of slow slip must be considered. It has been suggested that tremors are created by fluid flow in subsurface conduits at high pressure, which can create a resonance-like phenomena [24]. If this is in fact the process that is generating non-volcanic tremor in Cascadia, then tremor and slow slip need not be coincident. In this case, the tremor locations may not indicate the depth of slow slip events, but could be related to stress perturbations arising from slow slip. Finally, though peak occurrence of tremor activity in Cascadia correlates with slow slip, there are several other peaks in tremor activity that occur at times when slow slip has not been inferred. These periods of tremor activity may indicate that slow slip occurred below the limit of detection by the existing GPS monitoring array.

1.4 Project Objectives and Impact

The primary objective of this thesis is to determine the spatial and temporal location of tremors from previous slow slip and non-slip tremor sequences along the Cascadia margin near southern Vancouver Island. I will focus on locating tremors associated with two sequences of activity: September 2002, which is not presently linked to slow slip, and February 2002, which corresponds to a known slow slip event of the 13-16 month cycle.

Slow slip causes stress loading along the megathrust interface and can potentially trigger megathrust earthquakes. It is therefore of interest to refine the estimated duration and periodicity of slow slip thrusting. If the spatial distribution of tremors in the September 2002 sequence is similar to that of both the March, 2003 and February 2002 sequences, then we might reasonably associate the September 2002 sequence with slow slip. This in turn would indicate that slow slip can occur outside the defined 13-16 month cycle.

If tremors and slow slip are found to be spatially correlated, the distribution of deep tremors will help to constrain the landward limit of the locked megathrust fault. A more accurately-defined landward limit of this locked zone will allow better estimates of ground shaking and damage from a megathrust earthquake.

Alternatively, if it is found that the September 2002 sequence is not linked to slow slip but that a temporal association to local earthquakes exists, then it is possible that tremor activity may be associated with seismic sources unrelated to the megathrust. This possibility would be supported by the location of tremor sources away from the inter-plate boundary.

By using data from all available seismograph stations, including CNSN and POLARIS, I will

attempt a thorough search of the recorded data in southwest British Columbia to produce results of direct relevance to the populated areas of northern Washington State and southern British Columbia.

Chapter 2

THEORY AND METHODS

2.1 SEISMIC SOURCE HYPOCENTER DETERMINATION

Conventional methods for hypocenter determination are based on minimizing differences between the observed and predicted arrival times of various seismic phases recorded on a seismograph array. Minimum error estimates of seismic source location parameters (coordinates, depth, and origin time) typically require impulsive *P*- and *S*-wave arrivals for accurate picking of arrival times, accurate velocity models, and sufficient seismograph coverage about epicentres. Consequently, phase-picking methods are most useful for individual events that are well separated in time and generate clear arrivals at seismic stations with a relatively low level of background noise. Tremor waveforms are characteristically non-impulsive, emergent, and low amplitude. Typically, only *S*-wave arrivals of tremor sources are observed from waveform data, and are commonly difficult to identify on a single station above the background noise. Tremor events are therefore identified by correlating waveform data from various seismograph stations (Figure 2.1).

In 2004, Kao and Shan [25] developed the source-scanning algorithm: an automated method to image the source distributions and origin times of non-volcanic tremors. The algorithm estimates the likelihood that a seismic source exists at a particular location and origin time based on the coherence of the strongest phase arrival across a seismograph network. Essentially a grid-search method, the source-scanning algorithm calculates a measure of coherence for each combination of trial location and origin time in the search volume. The spatial and temporal distribution of tremor sources is determined by isolating the combination of spatial location and origin time that yield the highest measures of coherence.

2.2 THEORY OF THE SOURCE-SCANNING ALGORITHM

The coherence measure calculated by the source-scanning algorithm, referred to as "brightness", is recovered from the constructive additions of seismic waveform amplitudes from each station of the seismograph array. The brightness of a hypothetical tremor source at trial location (η) and origin time (τ) estimates the likelihood that the tremor source exists at this location and origin time. Assuming that a tremor event is recorded by a seismic network of N stations, the N recorded seismograms are first normalized to partly correct for geometrical spreading during wave propagation. The brightness of a potential source at location (η) and origin time (τ) is defined by

$$br(\eta,\tau) = \frac{1}{N}\sum_{n=1}^{N}|u_n(\tau+t_{\eta n})| \tag{2.1}$$

where u_n is the normalized seismogram recorded at station n and $t_{\eta n}$ is the predicted travel time of the largest phase from point η to station n. Large brightness values will be found if the maximum amplitude of each seismogram originates from the same source-point η and origin time τ. In this way, the source locations and origin times of tremor sources within the search volume are identified by local brightness maxima.

Assuming an elastic and isotropic medium, predicted arrival times $t_{\eta n}$ from each trial location η to each seismic station n are calculated by a 3-D finite difference solution to the Eikonal equation [16, 51] at a grid-spacing of 1km. The calculation uses a 3-D S-wave velocity model, which is scaled from the SHIPS 3-D P-wave model [42] using the approximate $\frac{V_p}{V_s}$ ratio of 1.76. To accommodate possible errors in the velocity model and travel-time calculations, equation (1.1) is modified to calculate brightness from amplitudes within a time window centered on the predicted arrival time rather than the single amplitude $u_n(\tau+t_{\eta n})$ at predicted arrival time $t_{\eta n}$, such that

$$br(\eta,\tau) = \frac{1}{N}\sum_{n=1}^{N}\left\{\frac{\sum_{m=-M}^{M} W_m|u_n(\tau+t_{\eta n}+m\delta t)|}{\sum_{m=-M}^{M} W_m}\right\} \tag{2.2}$$

where the duration of the time window equals the number of samples $2M$ multiplied by the sample interval δt. W_m specifies the weighting factor applied to amplitudes within the time window about the predicted arrival time (either constant or a Gaussian centered on the arrival time). As a first order approximation, the length of the time window should be comparable to the possible travel time error

caused by velocity model inaccuracies.

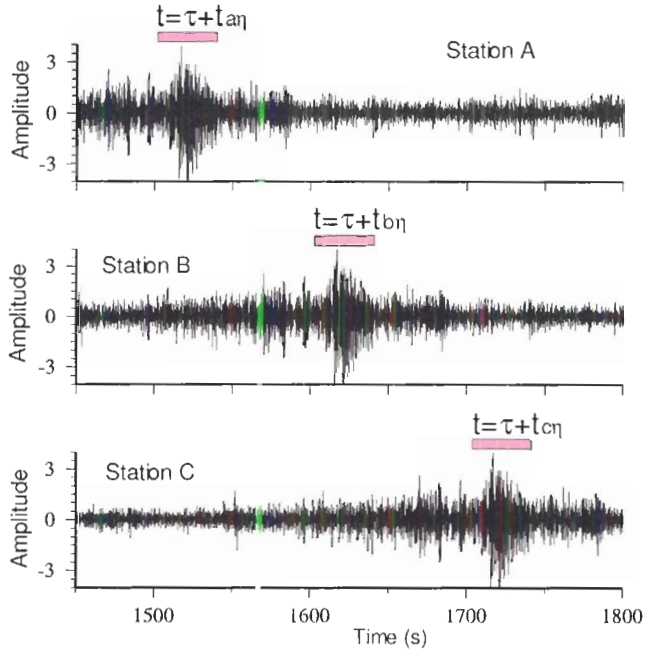

Figure 2.1: A schematic of tremor trace amplitudes plotted (downward) in order of increasing epicentral distance. The brightness of a tremor source at point η at origin time τ is computed by summing the normalized absolute trace amplitudes from stations A, B, and C at the predicted arrival times (τ plus respective travel times $t_{a\eta}$, $t_{b\eta}$, and $t_{c\eta}$). A large brightness value is found in cases where the location η and origin time τ are consistent with the arrival of the largest amplitude at each station. Pink bars indicate the time window, centered at the arrival time of the largest phase, within which trace amplitudes are summed to yield the brightness value.

2.3 METHODOLOGY

The dimensions of the 3-D *S*-wave velocity model were used to define the dimensions of the scanned volume. The velocity model extends from 1-87 km in depth, 46.9^{o}N to 50.95^{o}N in latitude and -126^{o}E to -121^{o}E in longitude, which translates to 1-361 km in the x-direction and 1-451 km in the y-direction. For the purposes of comparing the onset, distribution, and migration of episodic and non-episodic tremor sequences, vertical component waveform data were acquired for the entire months of February and September of 2002 from a combination of 3-component broadband and vertical component short period seismograph stations. A combination of eight regional Canadian National Seismograph Network (CNSN) short-period and broadband stations were online during

February 2002 (Figure 2.2). An additional three POLARIS broadband stations were available during September 2002. All waveform data were downloaded from the Geological Survey of Canada's National Waveform Archive. Travel times from each station to all grid points in the search volume

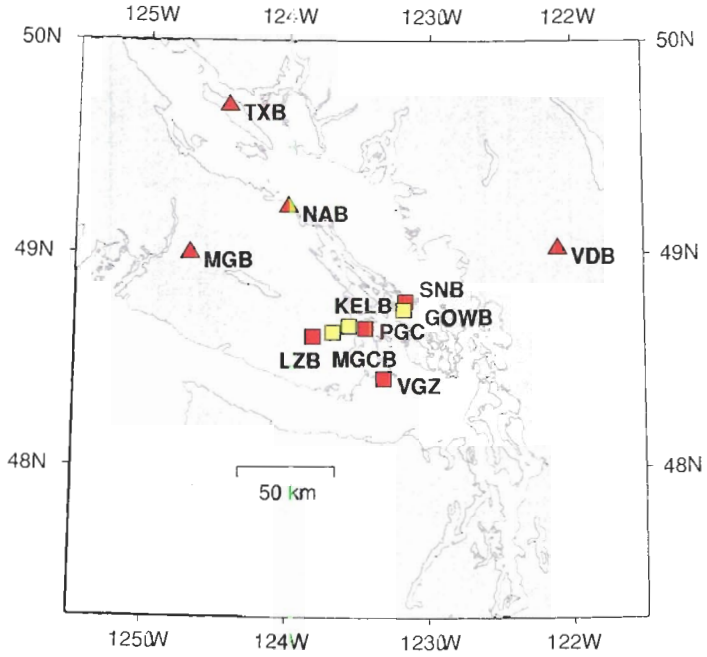

Figure 2.2: Seismograph stations from which waveform data were acquired. Red triangles indicate CNSN short-period vertical component stations, red squares indicate CNSN 3-component broadband stations, yellow squares indicate POLARIS 3-component broadband stations which became available for September 2002 waveform processing.

were calculated using a 3-D finite-difference travel time code [16], and at a spatial mesh interval of 1 km. These travel times were used to generate a set of reference travel time files for each station. The source-scanning algorithm uses the travel times from each station's reference file and the absolute trace amplitude of corresponding waveforms to compute brightness values for each combination of source location and origin time.

2.3.1 Waveform Processing

All waveform pre-processing was carried out on one-hour segments of waveform data using the Seismic Analysis Code (SAC) for seed format data. Waveforms were anti-aliased and down-sampled to a sampling interval of 0.1 s. Waveform means, glitches, and linear trends were removed, and the

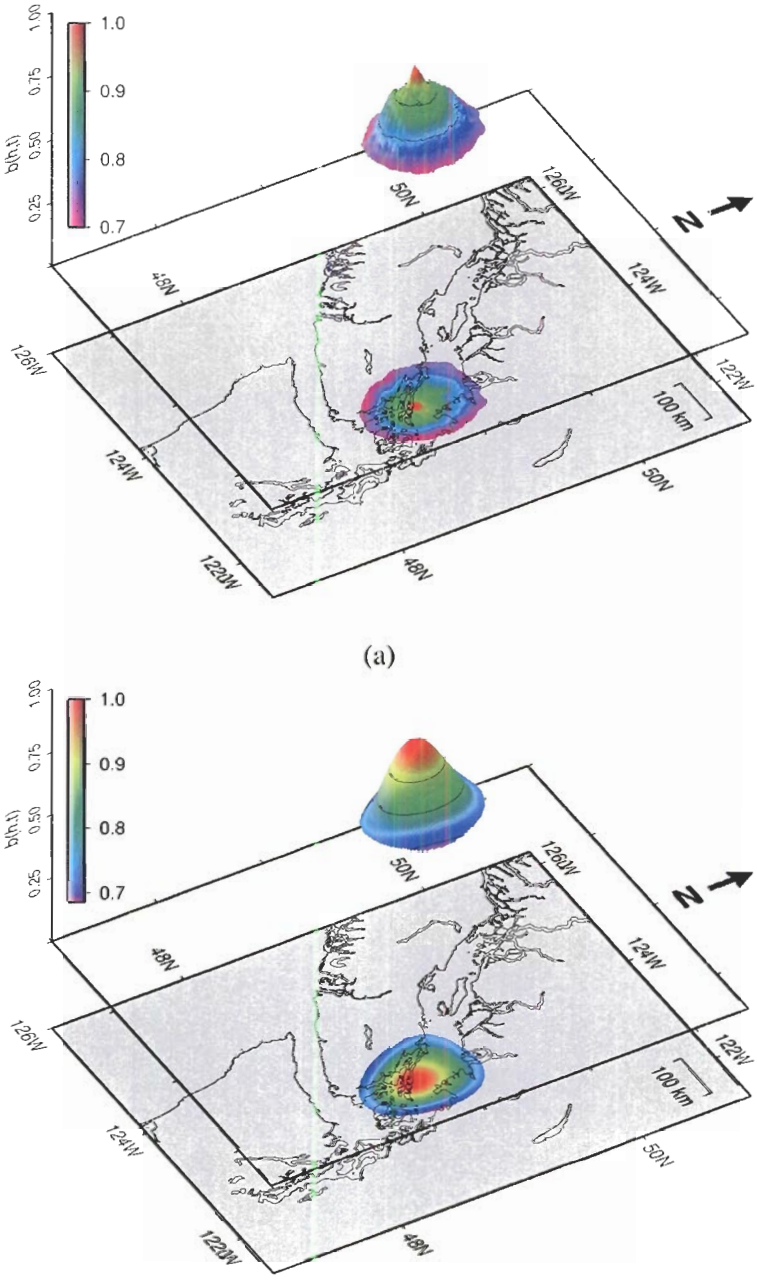

Figure 2.3: Tremor source location solutions from (a) absolute trace amplitude waveform data and (b) trace envelope waveform data. Brightness values are normalized and define a probability distribution that a tremor source exists at the defined origin time and source location.

data were deconvolved to remove instrument responses. A high-pass filter was applied using a corner frequency of 1.5 Hz to remove low-frequency background noise. These pre-processing methods have been found to produce clearer, more distinct tremor arrivals [25]. Each waveform trace was normalized to compensate for amplitude variations due to transmission losses and geometric spreading. Tremor waveforms were normalized such that 2 standard deviations of the absolute amplitude is set to 1.0. This normalization has been found to improve the visibility of tremor arrivals and facilitate the search method. Smoothed envelopes of trace amplitude data were also calculated, using a 25-point (2.5 s) running average of trace amplitudes. Brightness values were calculated for each one-hour segment of waveform data using both absolute trace amplitudes and trace envelopes. Due to a smoother amplitude variation, brightness values calculated using waveform envelopes generate a broader, more Gaussian-like distribution about local brightness maxima. Brightness values calculated using absolute trace amplitude data define a more irregular, though higher resolution brightness distribution (Figure 2.3). Tremor source locations and origin times determined from brightness distributions calculated using absolute trace amplitude and trace envelope waveforms were compared for consistency and location accuracy.

2.3.2 Search Method

All brightness values were calculated by summing Gaussian-weighted waveform amplitudes (either absolute trace amplitudes or envelopes) along a time window ($2M\delta t$) of 1.5s centered at the predicted arrival time (equation 2.2). These parameters were employed in previous tremor location studies in Cascadia [25]. The source-scanning algorithm is applied to the waveform data in 3 steps:

1. Brightness values are initially calculated at time steps of 5 s along each waveform trace, and for trial source locations spaced every 10 km within the entire search volume. Each 5 s time step defines a reference time for the calculation, which is considered to be the arrival time at a reference station. For each trace of waveform data, the arrival time of a hypothetical source at trial location η was calculated by adding to the reference time the difference in travel time between the current seismograph station and the reference station. Gaussian weighting is applied to the waveform amplitudes within the time window centered at this arrival time, and the weighted amplitudes are summed. The summed amplitude values from all stations are averaged to yield a brightness value for each time step.

2. Reference time and trial location combinations which yield brightness values greater than 0.7 using absolute trace amplitude data and 1.0 using trace envelope data are used to define

reference time intervals and subvolumes for further scanning at higher resolution. Subvolumes with dimensions of 100 km in the x- and y-directions and 50 km in the z-direction were re-scanned at time steps of 0.1 s over a reference time interval of 30 s. For this second, more refined search, a spatial mesh interval of 1 km was used to define trial source locations. The origin time of the tremor source is determined by subtracting the travel time to the reference station from the reference time corresponding to the maximum brightness value. The trial location corresponding to the maximum brightness value is used to define a search subvolume.

3. The final step involves calculating the distribution of brightness values within a subvolume for a single tremor origin time. In this step, the arrival times are obtained by adding the travel time to the origin time. A search volume with dimensions of 80 km in the x- and y-directions and 40 km in depth is scanned. Brightness values are calculated for trial source positions defined by grid locations every 1 km. The spatial distribution of brightness values indicates the probability that a tremor source exists at the define combination of origin time and source location.

Located tremor sources that occur within a 20 km radial distance and 20 s origin time of local earthquakes were rejected. Tremor sources that are considered well-located are those that have been obtained using both absolute trace amplitudes and trace envelopes of the waveform data, and agree to within ± 15 km in x-, y-, and z-directions, and have origin times within 10 s. Brightness values computed using trace amplitude data must exceed 0.7, and those computed using trace envelopes must exceed 1.0. Brightness values which define a tremor source must be the largest within a time window of ± 30 s about the origin time. Tremor events which are located at depths less than 5 km are excluded, since these events could be surface-related environmental noise.

2.4 Error Assessment

A set of controlled tests was conducted to determine the accuracy of tremor source locations determined by the source-scanning algorithm, and the error to be expected due to the seismograph station geometry. The spatial accuracy in tremor locations was determined by the gradient of the brightness function - a large brightness gradient indicates a higher spatial accuracy. The spatial range in the x-, y-, and z-directions defined by brightness values above a specified threshold was used to estimate tremor location accuracy. To determine an appropriate brightness threshold for error estimation, the source-scanning algorithm was used to locate earthquake epicenters (Figure 2.4). The deterioration

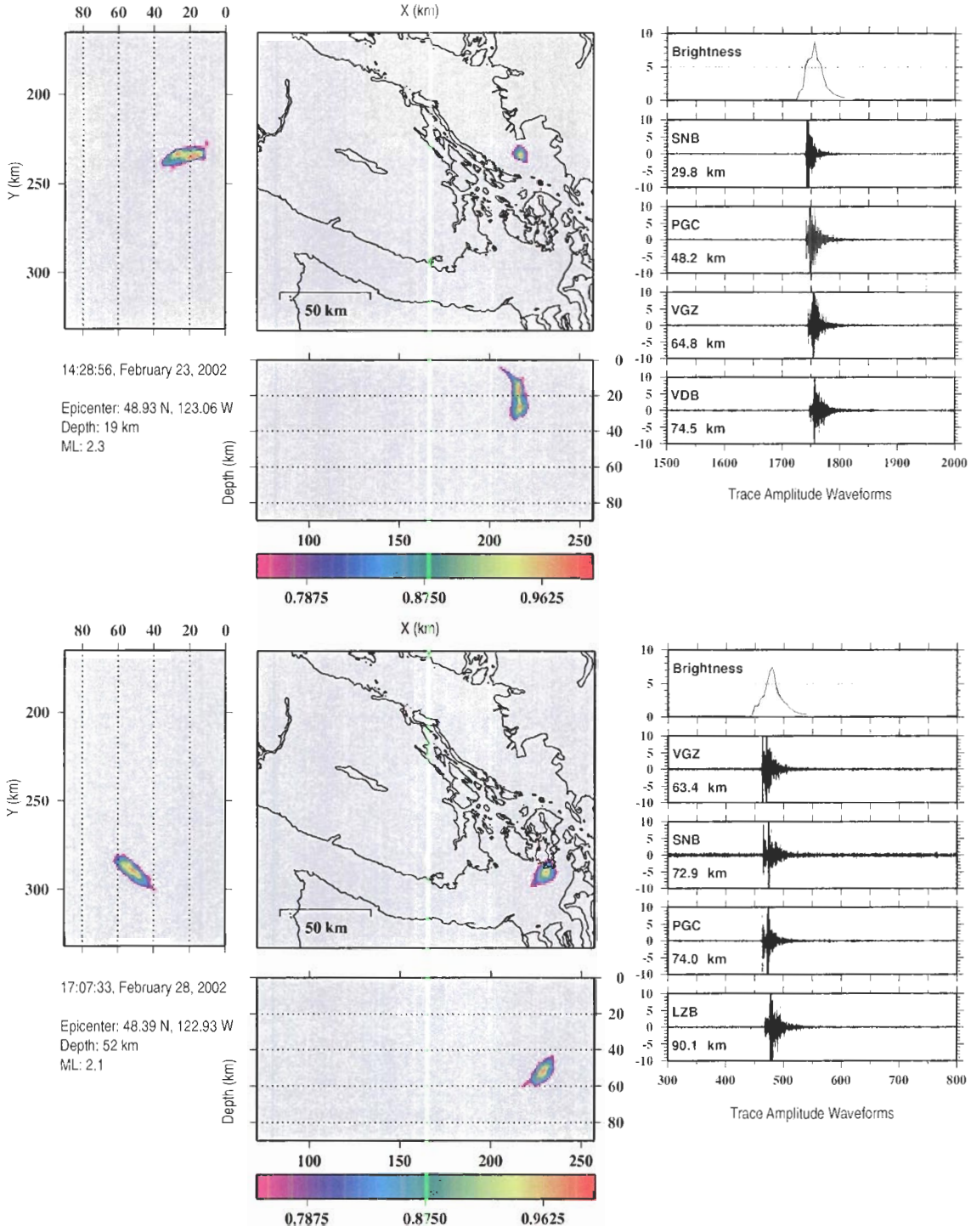

Figure 2.4: Top: Brightness distribution for an earthquake (M_L=2.3) that occurred February 23, 2002 and at a depth of 19 km. Bottom: Brightness distribution for an earthquake (M_L=2.1) that occurred February 28, 2002 and at a depth of 52.2 km. The deterioration of the brightness function by 15% corresponds horizontal spatial error of 3 km and a vertical spatial error of 5 km.

of the brightness function corresponding to an acceptable spatial error of 3 km in the x- and y-directions and 5 km in the z-direction was used. Waveform data from the eight seismograph stations available during the month of February 2002 were acquired for two earthquakes, one at a depth of 19.0 km and another at a depth of 52.2 km [39]. The source-scanning algorithm was implemented to locate the earthquake epicenters using the absolute trace amplitude waveforms. The deterioration in the brightness function corresponding to a horizontal (x, y) spatial error of 3 km and a vertical (z) error of 5 km was found to be approximately 15% for both earthquakes. The deterioration of the brightness function by 15% of its maximum value was therefore used to define the spatial errors of tremor source locations.

Regions of high and low tremor location accuracy within the search volume were determined by distributing synthetic tremor sources at different grid points, recovering their source locations using the source-scanning algorithm, and calculating their spatial accuracy as outlined above. Trial locations were positioned every 40 km in the x- and y-direction and every 20 km in depth (Figure 2.5(a)). Travel times from each trial location to each seismograph station were calculated using the 3-D finite-difference travel time code [16] and the S-wave velocity model. To generate a synthetic tremor source, a representative tremor waveform was selected from the data set, filtered, and normalized (Figure 2.5(b)). This tremor source was effectively positioned at each trial location by time-shifting the waveform by the travel time between the corresponding trial location and each recording station. Absolute trace amplitude and trace envelope waveforms files were generated and used to calculate brightness values corresponding to each synthetic tremor source trial location. All eleven seismograph stations available for the month of September 2002 were used in recovering the tremor source distribution. The average of the distance along the $+x/-x/+y/-y$ directions from the recovered tremor source location corresponding to a decay in brightness by 15% was used to define the horizontal error of recovered tremor locations. The average of the distance along the $+z/-z$ directions was used to estimate the vertical error. The horizontal and vertical errors of the recovered tremor source locations at depths of 6, 26, 46, and 66 km were plotted as a function of radial distance between the tremor source and the center of the recording station array. Horizontal error was found to increase in an exponential manner with increasing radial distance from the array center (Figure 2.6(a), (c)). Tremor locations recovered using absolute trace amplitude and trace envelope waveform data produce comparable results. At radial distances beyond 200 km from the center of the station array, the horizontal error becomes large, reaching values up to 30 km. One may therefore presume acceptable horizontal spatial error for tremor sources within 200 km of the center of the station array. The lowest horizontal errors were found for tremor sources positioned at a depth of 26 km,

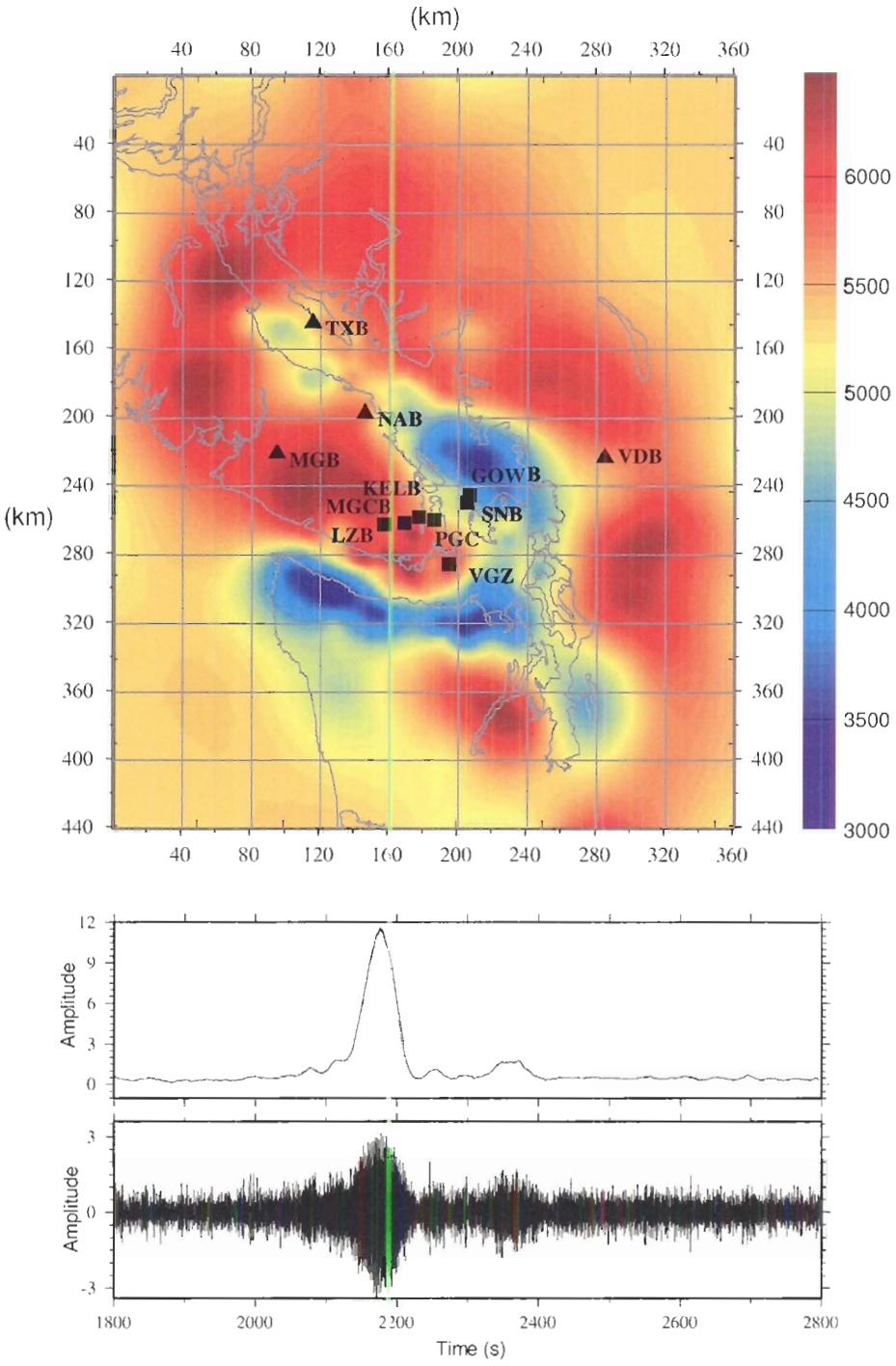

Figure 2.5: Top: Grid points used to position synthetic tremor sources for error assessment tests. Velocities correspond to the *S*-wave velocity model used in the location method at a depth slice of 3km. Four short-period vertical stations (triangles) and seven broad-band stations (squares) were used to recover the synthetic tremor source distribution. Bottom: Tremor trace amplitude waveform (bottom) and trace envelope waveform (top) used to generate synthetic tremor sources within the search volume. Waveform amplitudes and envelopes are time-shifted by the travel time between the trial location and seismograph station position.

and highest horizontal errors were found for sources at a depth of 6 km. The vertical spatial errors of tremor locations do not appear to be as dependant on the distance of the tremor source from the station center, but remain fairly consistent at approximately 7 km (Figure 2.6(b), (d)). Large vertical errors have been found for shallow tremor sources at a depth of 6 km, which average approximately 8 km. Beyond 150 km from the center of the station array, vertical errors in tremor locations become highly variable. This indicates that acceptable vertical spatial errors in tremor source locations may be obtained within 150 km of the center of the station array.

The absolute spatial error ξ of the recovered tremor source location was determined by calculating the radial distance between the trial location and the location of the source determined by the source-scanning algorithm, such that

$$\xi(\eta, \tau) = \sqrt{|x_t - x_r|^2 + |y_t - y_r|^2 + |z_t - z_r|^2} \tag{2.3}$$

where x_r, y_r, and z_r denote the x-, y-, and z-position of the recovered tremor source, and x_t, y_t, and z_t define the trial source location. Acceptable absolute error (< 10 km) is achieved up to radial distances of 250 km from the center of the seismograph station array for tremor sources at 6, 26, 46, and 66 km. Both trace amplitudes and envelopes yield comparable results up to this range (Figure 2.7, 2.8). At larger radial distances from the array center, the absolute error of source locations becomes increasingly variable and may reach values up to 20 km towards the edges of the search volume. Source locations obtained using trace envelope data contain less variability than those acquired with absolute trace amplitudes, which is to be expected, as waveform envelopes contain less amplitude variability.

The above spatial error tests indicate that the source-scanning algorithm is indeed robust to within approximately 200 km of the center of the seismograph array. These error estimates may be used for comparison with spatial accuracies of tremor source locations found using all available waveform data for the months of September 2002 and February 2002. Located tremor sources with spatial accuracies that are comparable to the estimates determined through the above series of tests may been seen as reasonable tremor solutions.

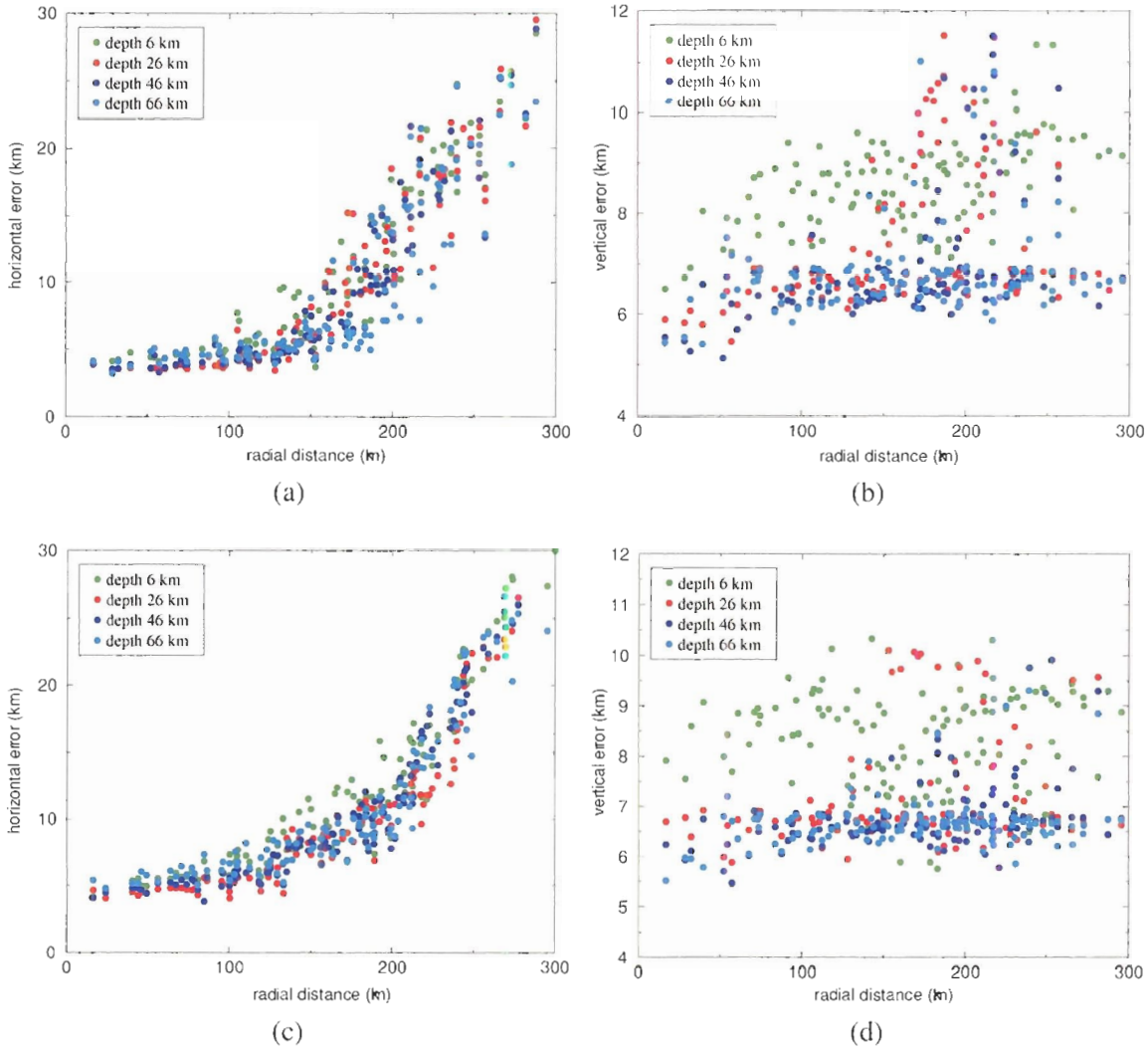

Figure 2.6: Horizontal and vertical errors of located tremor sources plotted as a function of radial distance of the source location from the array center. (a) Horizontal error of tremor sources determined using absolute trace amplitude data. (b) Vertical error of tremor sources determined using absolute trace amplitude data. (c) Horizontal error of tremors located using trace envelope data. (d) Vertical error of tremors located using trace envelope data.

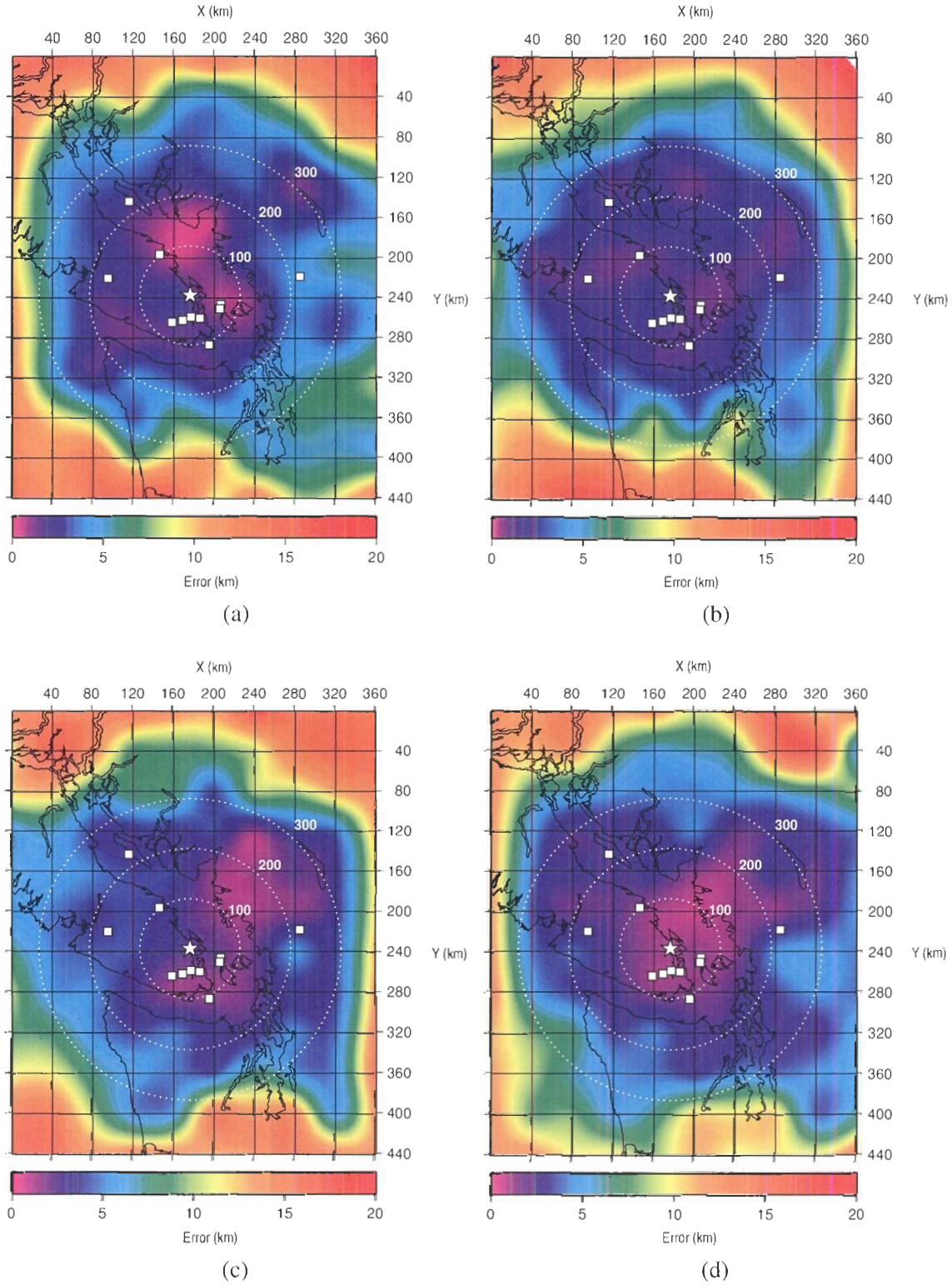

Figure 2.7: Absolute spatial error of tremor source locations recovered from (a) tremor sources at 6 km depth using absolute trace amplitude waveform data, (b) sources at 6 km depth using trace envelopes, (c) sources at 26 km depth using absolute trace amplitudes, and (d) sources at 26 km depth using trace envelopes.

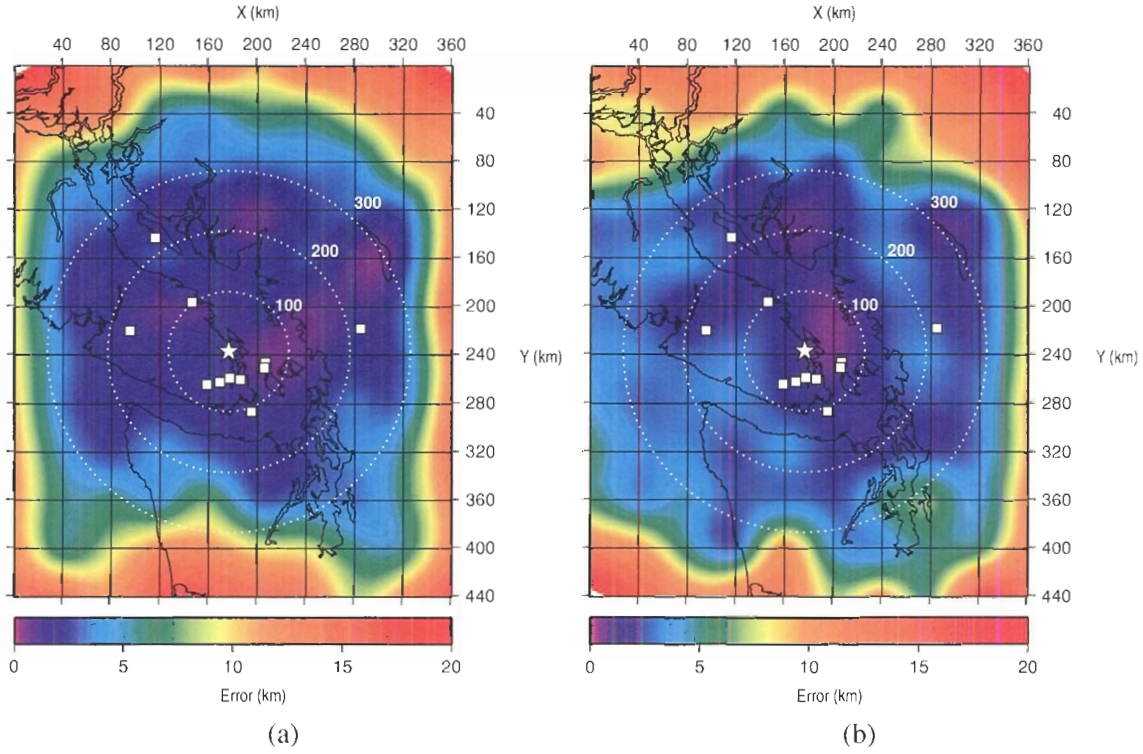

Figure 2.8: (a) Absolute spatial error of tremor source locations recovered from (a) tremor sources at 46 km depth, using absolute trace amplitude waveform data, and (b) sources at 46 km depth using trace envelopes.

Chapter 3

COMPARISON OF TREMOR SEQUENCES

The spatial distributions, magnitudes and spectral content of episodic and non-episodic tremor sequences will be examined and compared in this chapter in order to identify the distinct characteristics of each tremor class. The spatial distributions of tremor sequences indicate regions of stress release along the Cascadia margin, which will be related to the structure of the megathrust interface and the zone of slow slip in the following chapter. The magnitudes and spectral content of episodic and non-episodic tremor classes will be used to indicate whether or not tremor sequences occur in relation to earthquake seismicity. The properties of episodic and non-episodic tremors will provide additional information to clarify their source mechanisms and rheological environment, and further indicate regions of stress accumulation and release along the subduction zone. It has been proposed that the location of tremor sequences may be used to constrain the depths at which slow slip occurs [46] because episodic tremor and slow slip have been found to correlate spatially and temporally. Since it is believed that tremor activity originates from flow-induced resonance in subsurface conduits [24], tremor distributions and slow slip need not spatially coincide. Rather, tremor source locations might indicate the location of flow conduits, which may provide important information on the rheology of the subduction zone and the potential for stress accumulation. The comparison of episodic and non-episodic tremor classes will provide the basis for discussions on tremor source mechanisms and rheological environments in Chapter 4.

3.1 EPICENTRAL DISTRIBUTION OF EPISODIC TREMORS

3.1.1 TEMPORAL DISTRIBUTION OF FEBRUARY 2002 TREMORS

A significant amount of tremor activity was detected by implementation of the source-scanning algorithm during the month of February 2002, which has been anticipated since a slow slip episode has occurred during this time. 482 tremor events were identified by brightness values in excess of 0.7 using absolute trace amplitude waveforms, and by brightness values of 1.0 using trace envelope waveforms. 187 of the tremor source locations identified by trace amplitude waveforms and trace envelopes waveforms were consistent to within $\pm$ 15 km in the x-, y-, and z-directions, and 10 s in origin time. Based on these criteria, the 187 tremor sources are considered well-located. The low proportion of well-located tremor sources (38% of those identified) is likely a consequence of the availability of only 8 seismograph stations within the scanning region during February 2002. All identified and well-located tremor locations were compared with local earthquake epicentres, and rejected if tremor sources occurred within 20 km of earthquake epicentres and within 20 s. of earthquake origin times. A histogram of daily tremor frequency during February 2002 was generated to monitor the build-up and decline of the episodic tremor sequence (Figure 3.1). Two 8-day periods of elevated tremor activity are identified, separated by two days of reduced tremor detection: the first between February 2^{nd} - 9^{th} and the second between February 11^{th} - 18^{th}. During February 2^{nd} - 9^{th}, 2002, 132 tremor sources were identified (27% of those identified for the month) and 55 tremor sources were found to be well-located (29% of those well-located for the month). During February 11^{th} - 18^{th}, 2002, 248 tremor sources were identified (51% of those identified for the month) and 107 tremor sources were well-located (57% of those well-located for the month). The background level of episodic tremors is approximately 5 events per day.

3.1.2 SPATIAL DISTRIBUTION OF WELL-LOCATED EPISODIC TREMORS

At the onset of the episodic tremor sequence, tremors were located near the southeast tip of Vancouver Island. A gradual migration of tremor sources from south to north and along the strike of the subduction zone was detected the first pulse in tremor activity. This migration coincides with the movement of the surface displacement transient that has been found to occur during each slow slip episode [15]. During the second pulse in elevated tremor activity, tremors undergo enhanced migration to the northwest, reaching a rate of over 5 km/day (Figure 3.2). No migration is detected during the last 10 days of the month. Over the entire month, episodic tremors were found to migrate

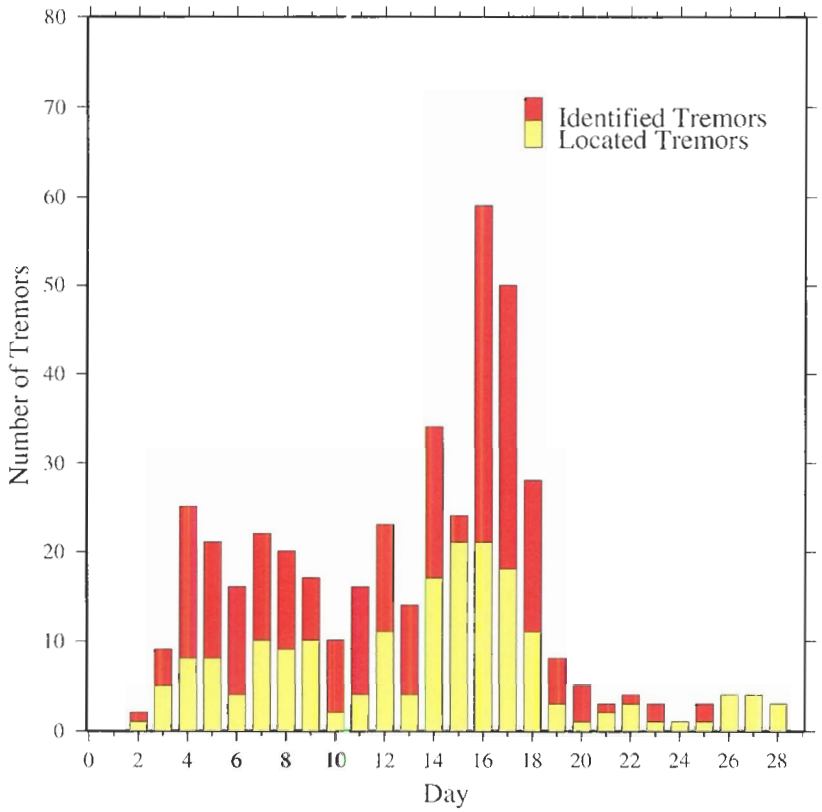

Figure 3.1: Number of identified and located episodic tremors during February 2002. Two 8-day pulses of elevated tremor activity are identified, separated by a two-day period of reduced detection. The first pulse of elevated activity (February 2^{nd} - 9^{th}, 2002) contains 29% of well-located tremor sources for the month. The second pulse (February 11^{th} - 18^{th}, 2002) contains 57% of well-located tremor sources.

over 200 km from south to north and along the strike of the subduction zone.

3.2 Epicentral Distribution of Non-Episodic Tremors

3.2.1 Temporal Distribution of September 2002 Tremors

The grid-search location of non-episodic tremors during September 2002 identified 194 tremors based on large brightness values above the thresholds of 0.7 using absolute trace amplitude waveforms and 1.0 using waveform envelopes. 99 tremor source locations acquired from trace amplitude and trace envelope waveforms were consistent to within ± 15 km in the x-, y-, and z-directions and with 10 s. in origin time. A larger proportion of tremor sources have been well-located (51% of those identified) relative to February 2002 (38% of those identified) due to an additional 3 seismograph

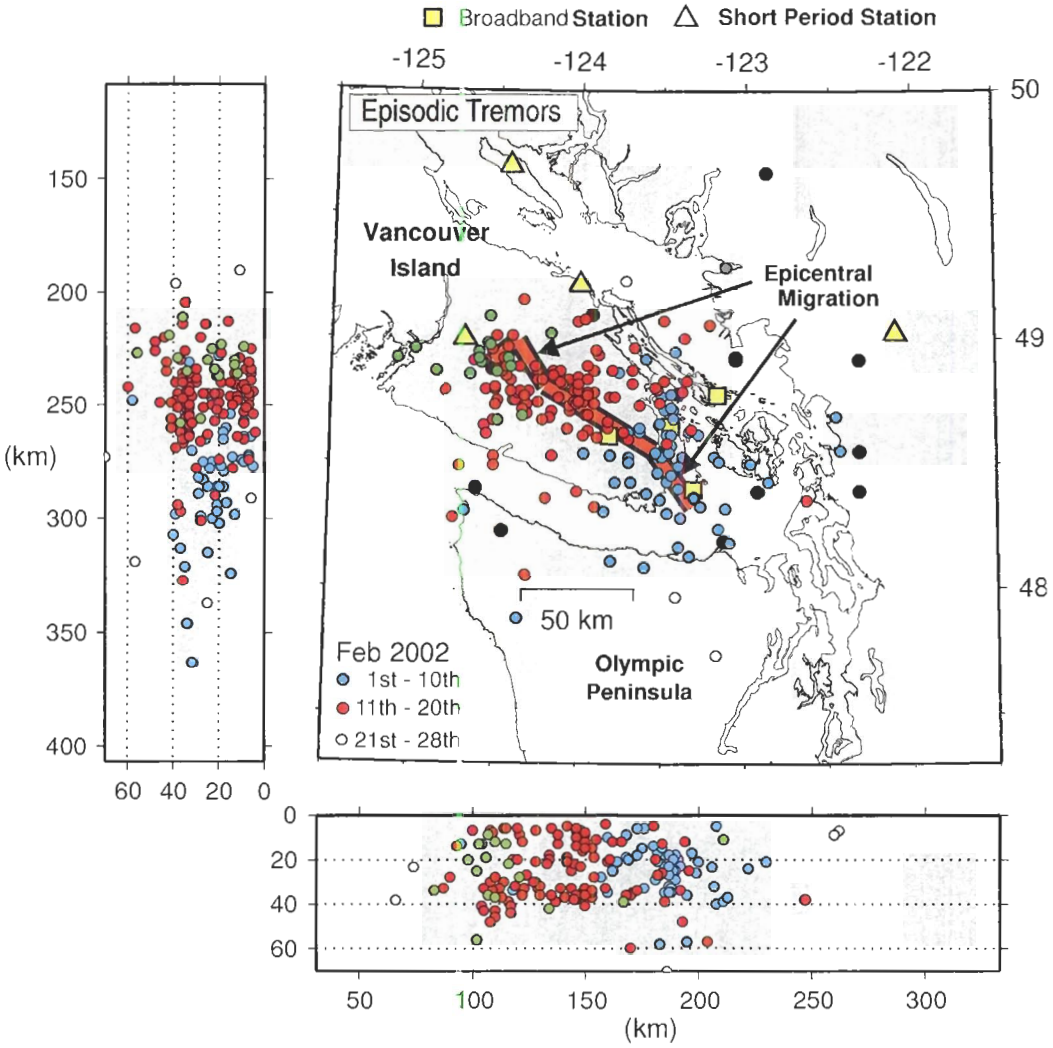

Figure 3.2: Map showing the distribution of well-located episodic tremor hypocenters. Tremors located during February 1^{st} - 10^{th} are shown in blue, during February 11^{th} - 20^{th} in red, and during February 21^{st} - 28^{th} in green. Local earthquake hypocenters during February 2002 are shown by black circles. Tremor migration over the course of the month is indicated by the orange line, which represents the mean epicentral location during each 5-day period. CNSN Broadband and short period seismograph stations are shown by yellow squares and triangles, respectively.

stations that became available during September 2002. A histogram of daily tremor occurrence indicates a short 3-day pulse of elevated activity during September 4^{th} - September 6^{th} above a background level averaging 4 events daily (Figure 3.3). 41% of identified tremors and 29% of well-located tremors have been detected during this period. Several isolated 1-2 day periods of elevated activity are also identified (September 16^{th}, 21^{st}, 25^{th}, 2002). Aside from the short pulse in elevated tremor activity at the beginning of the month, tremor occurrence appears sporadic - no gradual rise and decline in tremor detection is apparent, as has been found in February 2002.

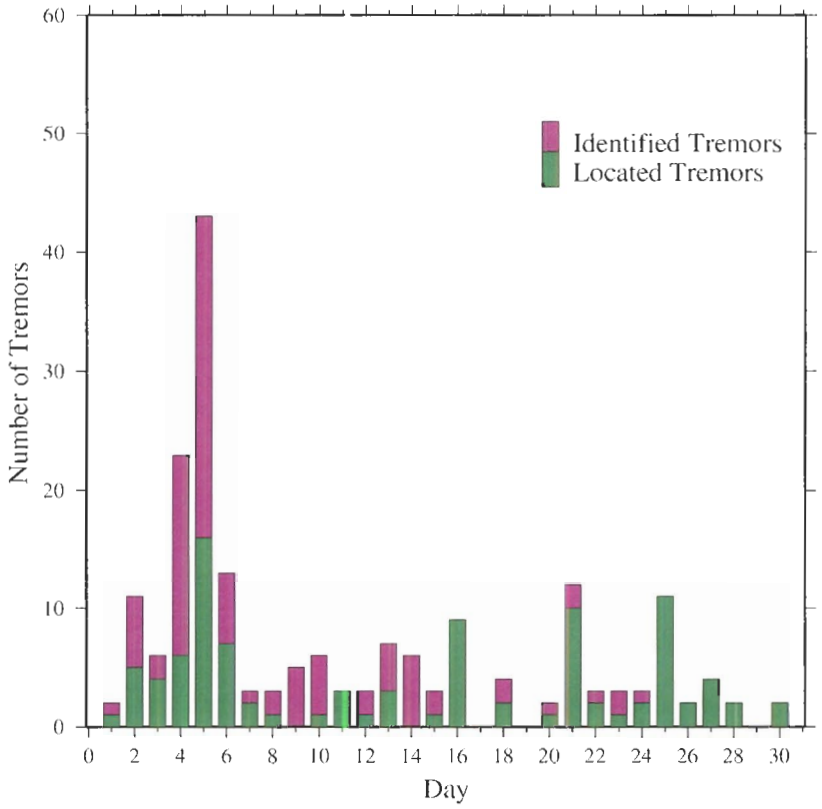

Figure 3.3: Number of identified and located tremors during September 2002. A single pulse of elevated tremor activity occurs at the beginning of the month, followed by several isolated days of increased activity above a background level of approximately 4 events/day. 41% of identified tremors and 29% of well-located tremors were detected during September 4^{th} - September 6^{th}.

3.2.2 Spatial Distribution of Well-Located Non-Episodic Tremors

The 99 well-located tremors detected during September 2002 were located in a circular region of approximately 100 km in diameter near the southeast tip of Vancouver Island (Figure 3.4). In contrast to episodic tremors, no apparent migration of non-episodic tremor sources has been observed. A large number of non-episodic tremors were located at shallow depths, predominant in the range of 5-10 km, also in contrast to episodic tremor distributions.

3.3 Tremor Depth Distribution

3.3.1 Episodic Tremor Depth Distribution

To compare the depths at which episodic tremors distribute during each pulse in elevated activity, histograms of tremor occurrence *vs.* depth were generated for the February 2002 sequence. Well-located tremor sources detected during each pulse were sorted into 2-km bins (Figure 3.5). During the first pulse in elevated activity (February 2^{nd} - 9^{th}, 2002), tremor sources are fairly evenly distributed along a wide depth-range of 5 - 40 km. During this period, tremor sources slowly begin to migrate northwest. During the second and stronger pulse in activity (February 11^{th} - 18^{th}, 2002), a larger amount of tremor sources are detected at greater depths, up to 48 km. What is most evident from the depth histogram for this period is a highly variable depth distribution relative to the first pulse in activity. Large amounts of tremors are found on three depth ranges: 5-9 km (8% of well-located tremors), 19-23 km (7% of well-located tremors), and 34-39 km (18% of well-located tremors). Tremor sources detected during this second pulse in elevated activity undergo rapid migration to the northwest.

3.3.2 Episodic *vs.* Non-Episodic Tremor Depth Distributions

A depth histogram of located episodic *vs.* non-episodic tremors was generated to emphasize the distinct depth distributions of both tremor classes. Well-located tremors detected during September 2002 and February 2002 were grouped into bins of 2 km and plotted together on one histogram for comparison (Figure 3.6). Non-episodic tremors occupy a shallower depth range relative to episodic tremors, and locate predominantly in the overriding North American plate. The number of September 2002 tremors shows a peak at a depth range of 5-10 km, and decreases smoothly and rapidly with increasing depth. Episodic tremors distribute over a 5-60 km depth range, and therefore are detected in both the subducting Juan de Fuca plate and the overriding North American plate.

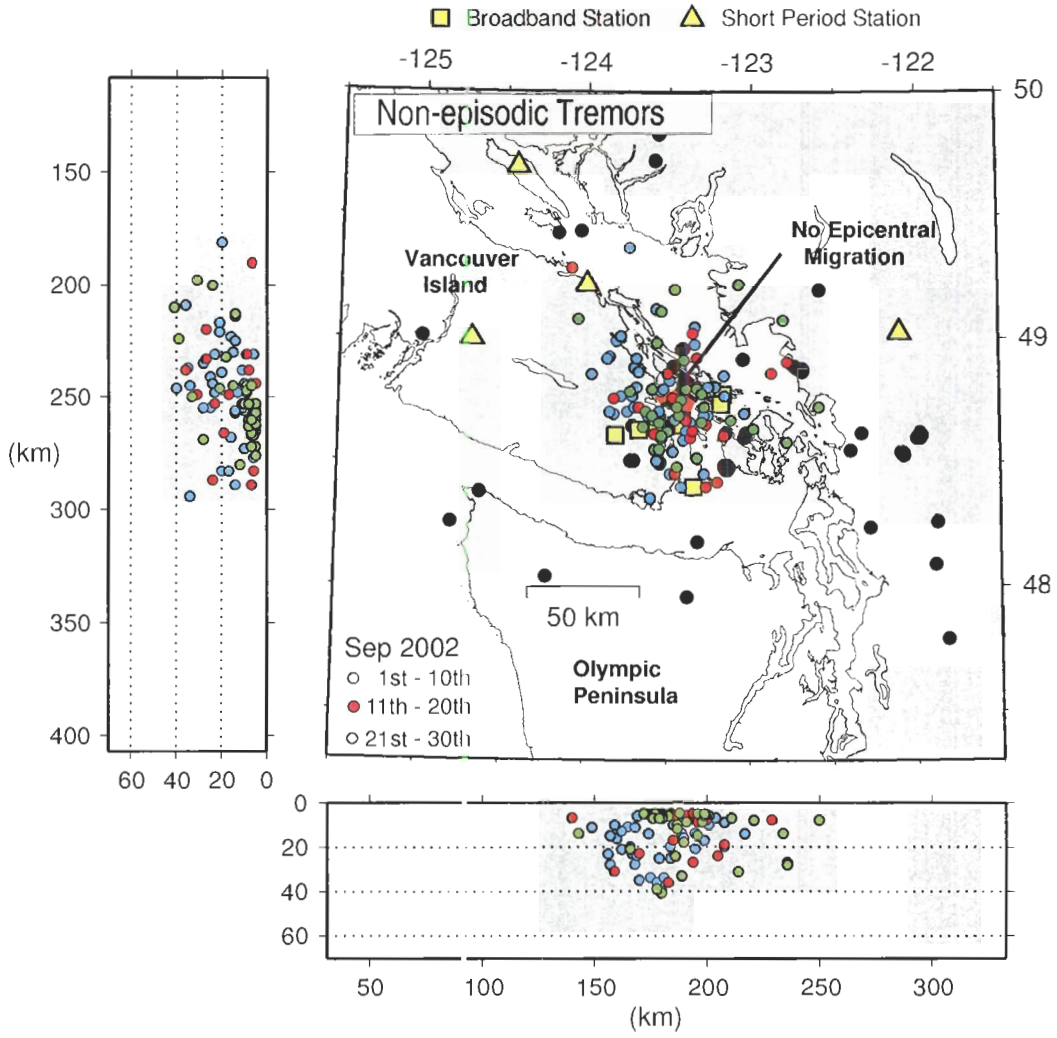

Figure 3.4: Map showing the distribution of well-located non-episodic tremor hypocenters. Tremors located during September 1^{st} - 10^{th} are shown in blue, during September 11^{th} - 20^{th} in red, and during September 21^{st} - 28^{th} in green. Local earthquakes during September 2002 are indicated by black circles. No migration of non-episodic tremors is observed. CNSN Broadband and short period seismograph stations are shown by yellow squares and triangles, respectively.

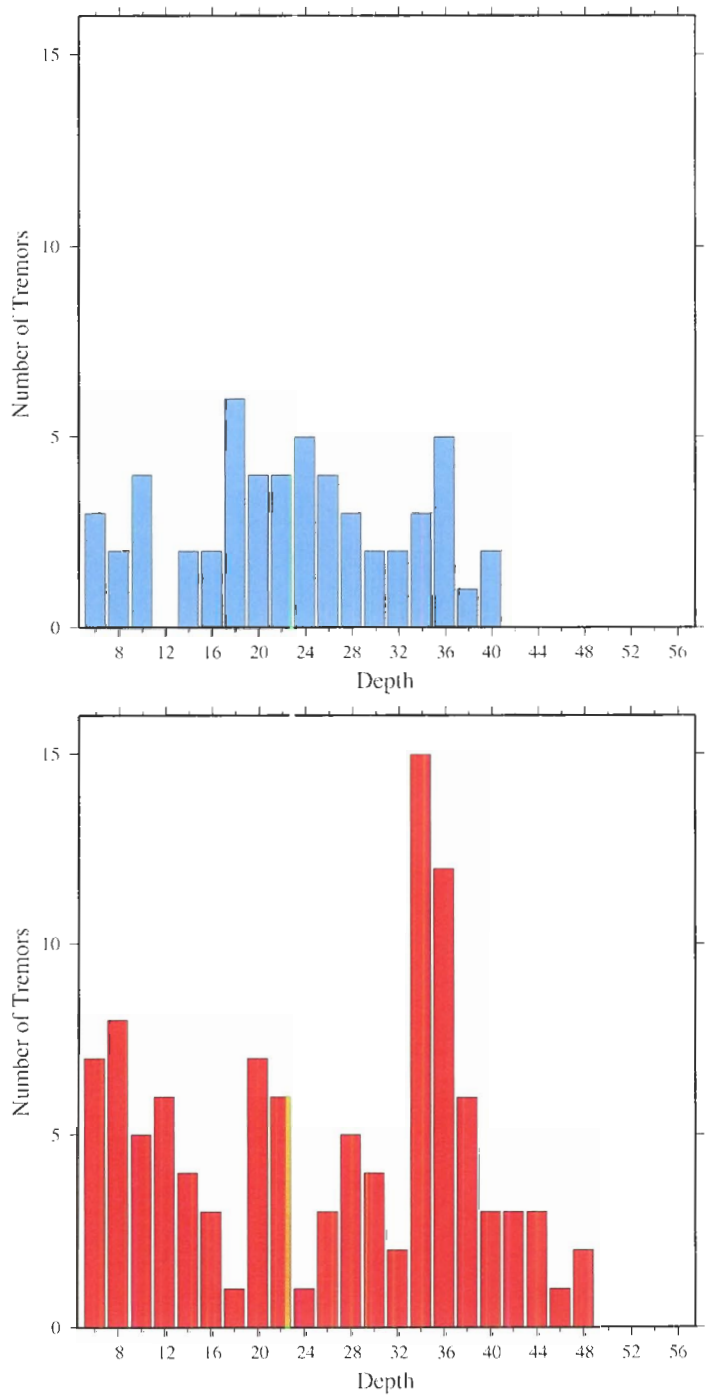

Figure 3.5: Top: depth distribution of well-located episodic tremors during the first pulse of tremor activity (February 2^{nd} - 9^{th}, 2002). Generally, tremors are evenly distributed across a wide depth range extending 40 km. Bottom: depth distribution of well-located episodic tremors during the second pulse in tremor activity (February 11^{th} - 18^{th}, 2002). A large number of tremors distribute along narrow depth ranges of 5-9 km, 19-23 km, and 34-39 km.

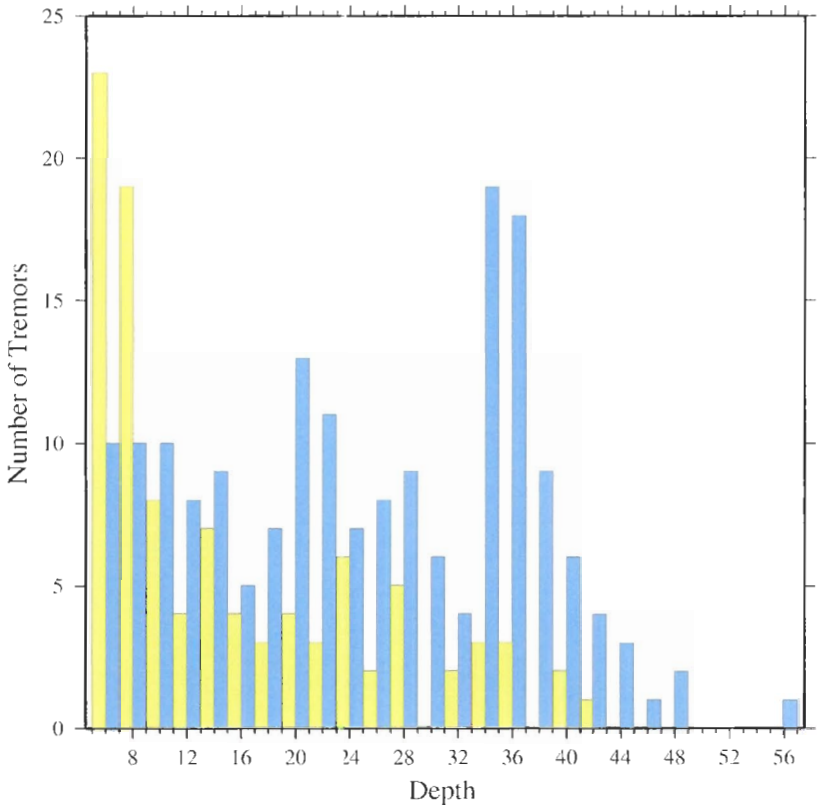

Figure 3.6: Comparison of well-located episodic and non-episodic tremor depths. Yellow bars indicate the number of September 2002 tremors within each 2-km depth bin. Blue bars indicate the number of February 2002 tremors within each depth bin. Episodic tremors are detected at greater depths than non-episodic tremors, and within both the subducting Juan de Fuca and overriding North America plates. Non-episodic tremors distribute more evenly along a shallower depth range of 5 - 10 km and in the North American plate.

3.4 Comparison of Tremor Amplitude and Frequency

Well-located episodic and non-episodic tremor amplitudes were compared to determine the magnitude of each tremor sequence. To correct for geometric spreading, the maximum trace amplitude from each seismograph station corresponding to a tremor event was multiplied by the radial distance from the tremor source to the recording station. Corrected trace amplitudes from recording stations were then averaged to yield an amplitude estimate for the tremor event. Tremor amplitude estimates for each day were averaged to produce a histogram of daily tremor amplitude (Figure 3.7(a), (b)). Amplitude estimates of the February 2002 sequence are significantly larger than those of the September 2002 sequence, perhaps indicating a larger amount of stress release during a period of aseismic slip. The amplitudes of non-episodic tremors shows larger variability than episodic tremors, which may signify a more unstable stress release process.

The frequency spectra of local earthquakes was compared to that of both episodic and non-episodic tremors to identify the distinctions between the above processes, and to verify that the tremors located in this study are unrelated to local earthquake seismicity. The 15 best-located tremor events (tremor sources with the least amount of spatial difference between locations identified using absolute trace amplitudes and those identified using trace envelope waveforms) and the 15 largest amplitude tremor events from the February 2002 and September 2002 sequences were isolated. The spectra of these 15 events were stacked to produce a representative spectra for each group. The spectra of 15 local earthquakes with local magnitudes less than 1.0, between 1.0 and 2.0, and greater than 2.0 were also stacked and compared to the stacked spectra of the largest and best-located episodic and non-episodic tremors (Figure 3.8). The spectral energy of tremor events peaks in the range of 2-4 Hz, whereas the spectral energy of earthquakes peaks at frequencies greater than 8 Hz. There is a substantial difference between the spectra of tremor events and that of local earthquakes with magnitudes greater than 1.0, indicating that earthquakes and tremors are distinct physical processes. The spectra of small ($M_L < 1.0$) local earthquakes and tremor events are similar at low frequencies in the range of 1-5 Hz. However, the higher frequency content (greater than 8 Hz) is much larger in these earthquakes than in tremor events.

3.5 Comparison of Tremor Waveform Coherence

Despite the differences in location and amplitude between episodic and non-episodic tremors, comparable degrees of waveform coherence have been obtained from tremor waveforms in February

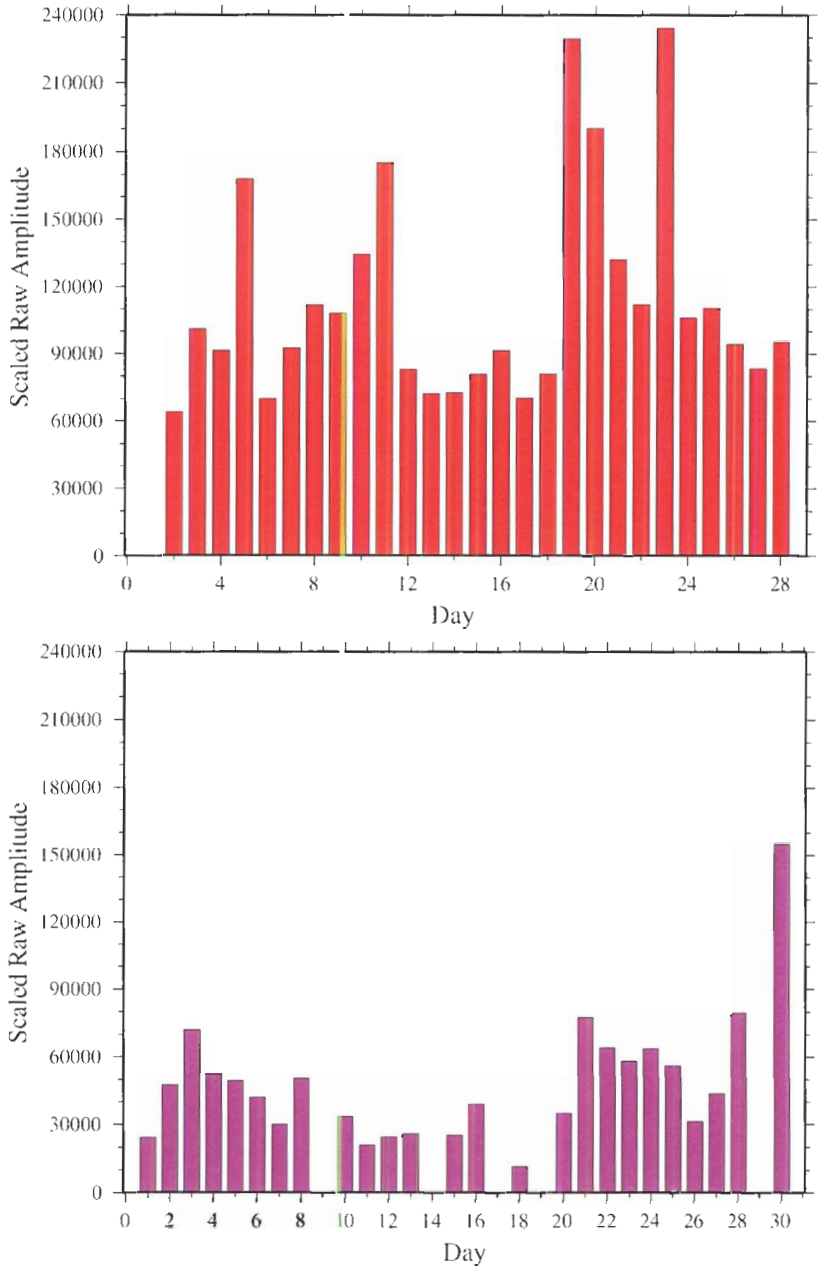

Figure 3.7: Histogram of daily-averaged, scaled tremor amplitudes (top) during February 2002 and (bottom) during September 2002. Raw waveform amplitudes corresponding to located tremor events were scaled by multiplying waveform amplitudes by the radial distance from the recording station to the tremor source. Larger episodic tremor amplitudes might indicate a larger amount of stress released during a slow slip episode.

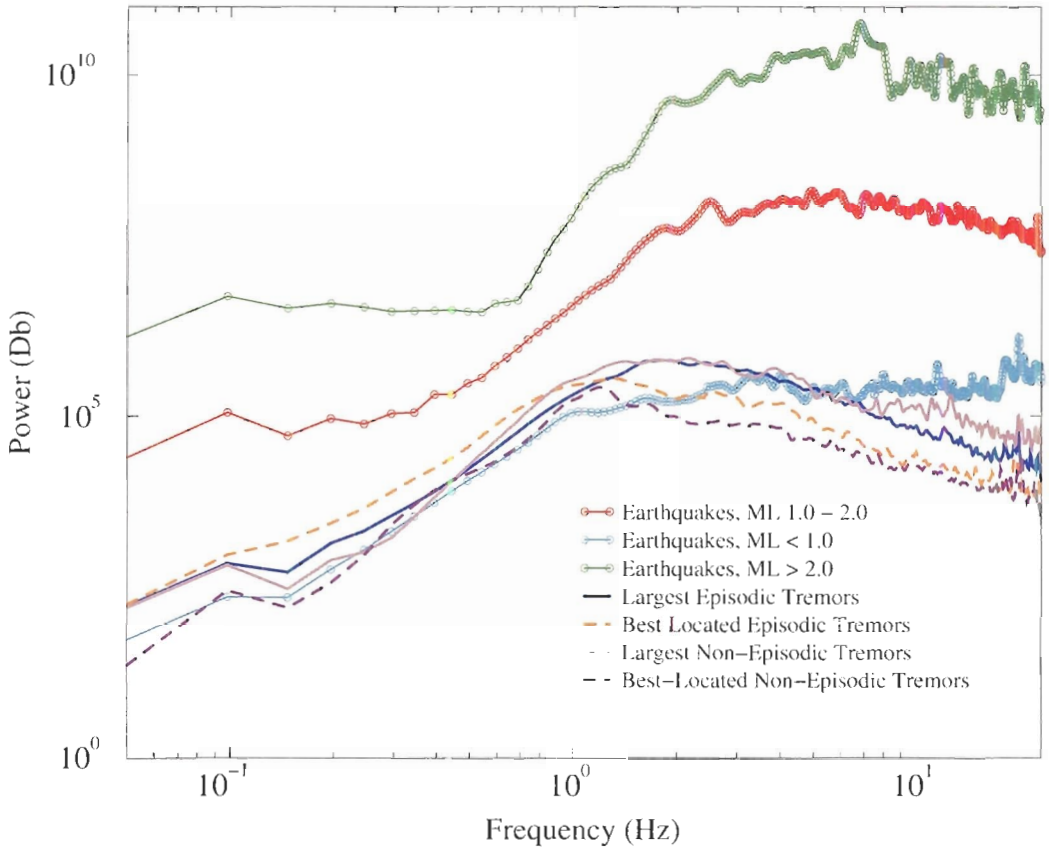

Figure 3.8: Comparison of the frequency spectra between local earthquakes, episodic tremors and non-episodic tremors. At frequencies between 1-5 Hz, the spectral energy of tremor events is similar to that of small (M_L <1.0) earthquakes. However, the energy of M_L <1.0 earthquakes peaks at approximately 10 Hz while that of tremors peaks between 2-4 Hz. The spectra of earthquakes with M_L 1.0 is very different from that of episodic and non-episodic tremors, indicating that tremor activity and earthquakes seismicity are distinct physical processes.

2002 and September 2002. The source locations and origin times of both episodic and non-episodic tremors were determined by brightness values greater than 0.7 using absolute trace amplitudes and greater than 1.0 using trace envelopes. There was no apparent dependency of waveform coherence on the depth of the tremor source. The brightness functions of two episodic and two non-episodic tremor events have been plotted along with their waveforms to indicate the comparable degrees of waveform coherence between both tremor classes (Figures 3.9, 3.10, 3.11, 3.12).

Similar amounts of spatial error were found for episodic and non-episodic tremor sequences. For each well-located tremor event, the location error was calculated by the decay of the brightness function away from its maximum value (Appendices A and B). As outlined in Chapter 2, the horizontal spatial error was estimated by the average spatial range in the $+x/-x/+y/-y$ directions that correspond to brightness values within 15% of the maximum value. Vertical error was calculated by the same method, yet averaging the spatial ranges along the $+z/-z$ direction. An average horizontal error of 7 km and an average vertical error of 9 km was found for both episodic and non-episodic tremors. These errors are largely attributed to a reduced station coverage, since they exceed an average horizontal error of 3 km and an average vertical error of 5 km found in previous tremor location studies in the Northern Cascadia subduction zone [26] that make use of a total of 40 broadband and short-period seismograph stations.

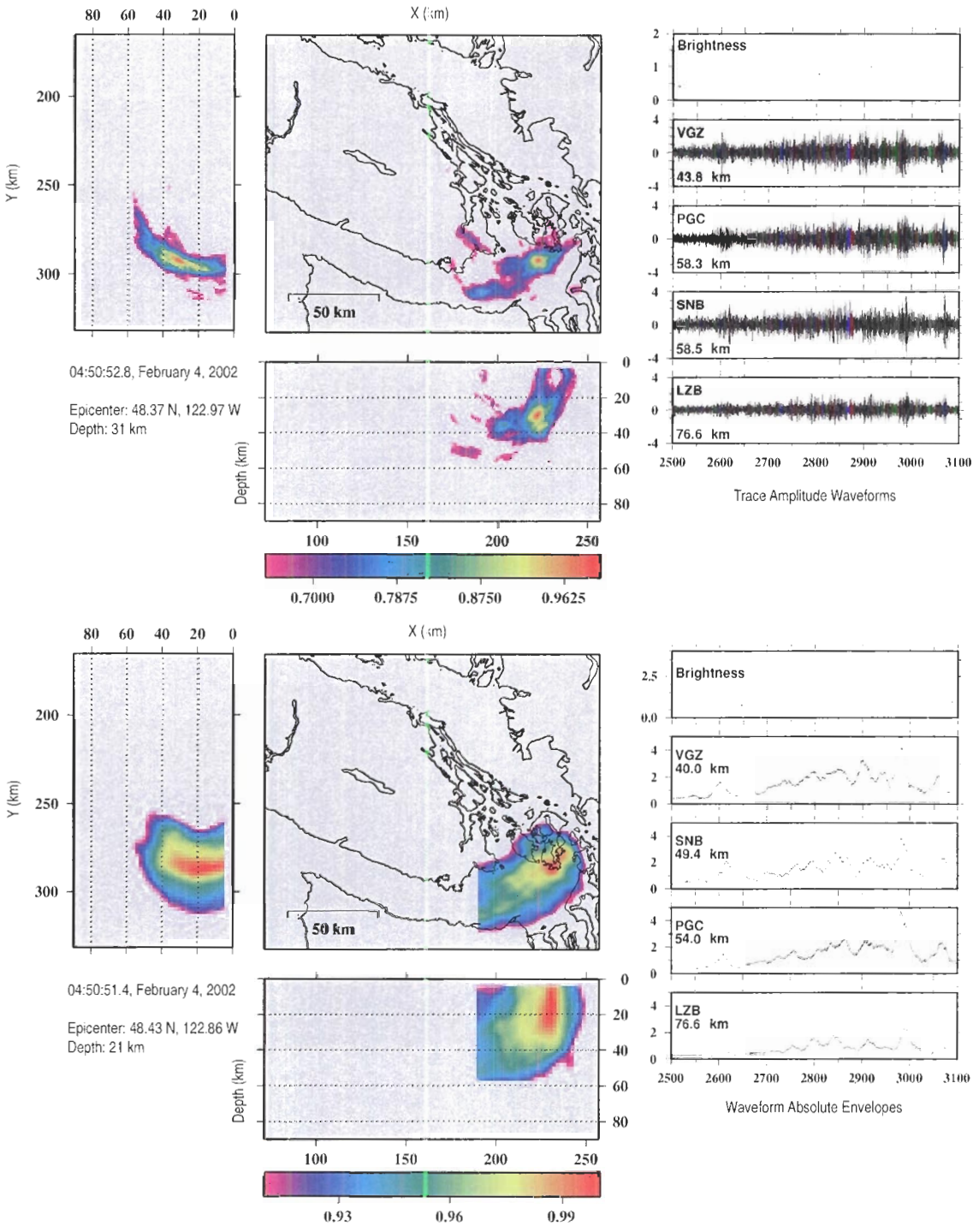

Figure 3.9: Map and profiles displaying a tremor event identified February 4 2002. Left: normalized brightness function obtained from (top) absolute trace amplitude waveforms and (bottom) trace envelopes. Right: trace amplitudes (top) and envelopes (bottom) indicate waveform coherence across the array.

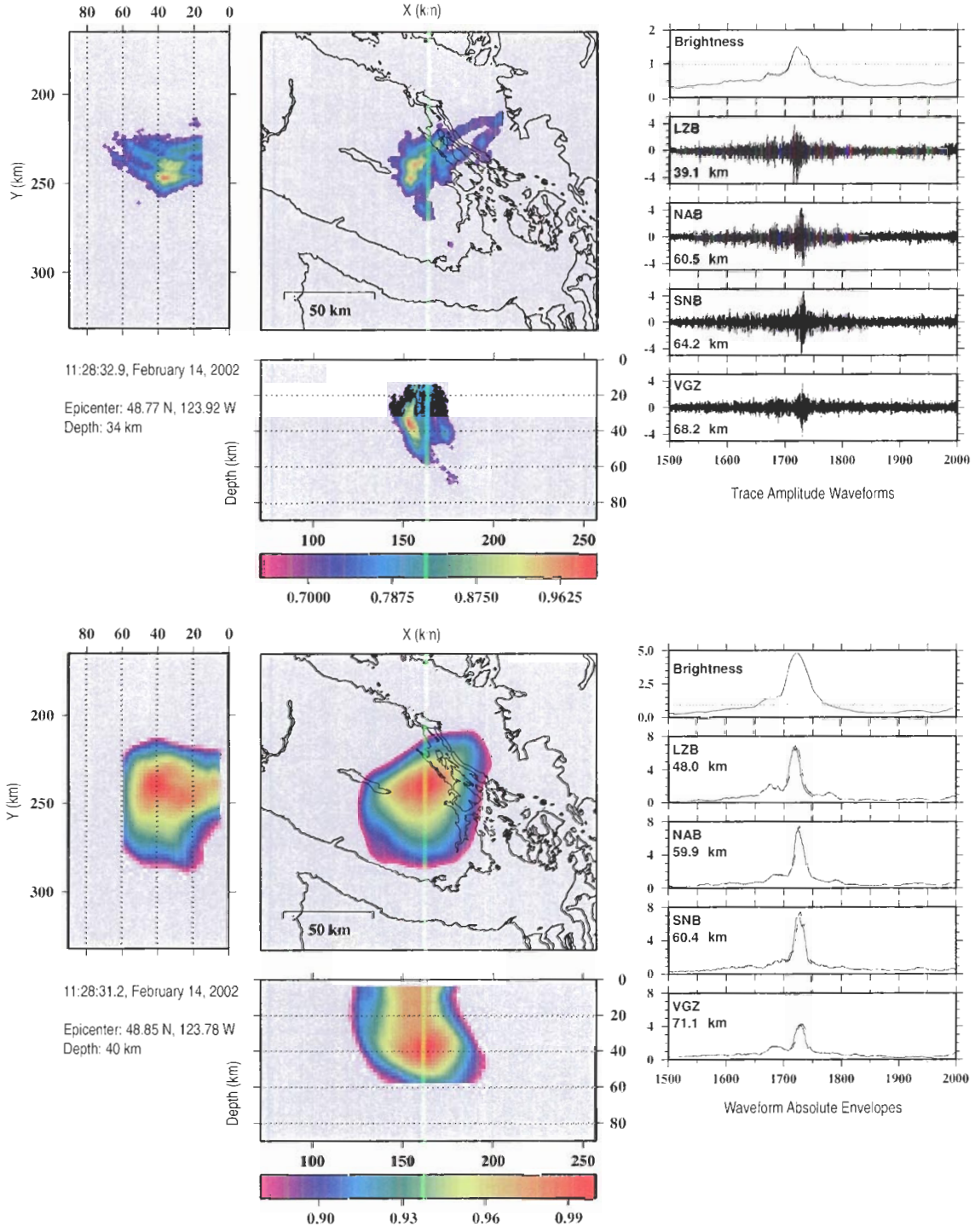

Figure 3.10: Map and profiles displaying a tremor event identified February 14, 2002. Left: normalized brightness function obtained from (top) absolute trace amplitude waveforms and (bottom) trace envelopes. Right: trace amplitudes (top) and envelopes (bottom) indicate waveform coherence across the array.

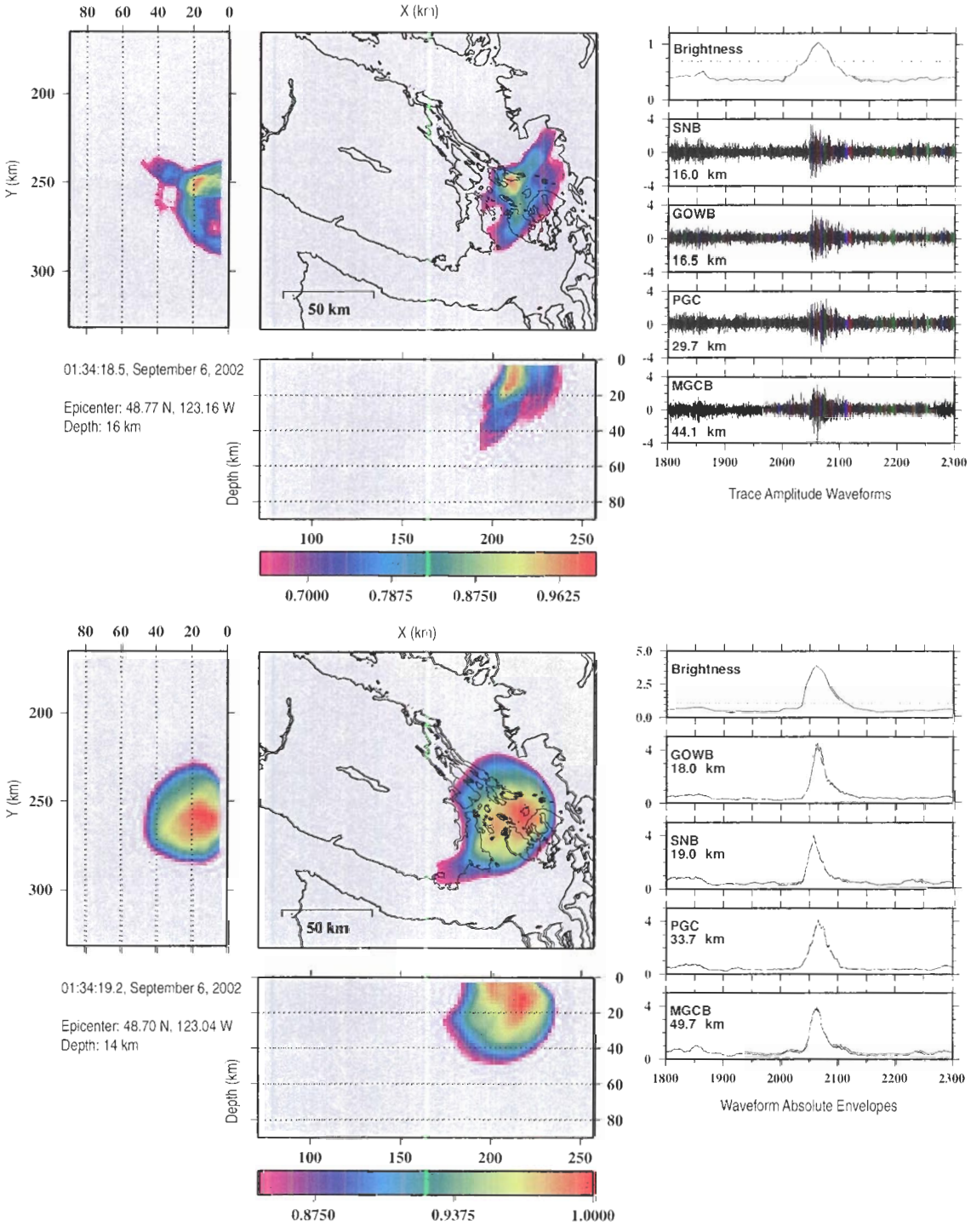

Figure 3.11: Map and profiles showing a shallow tremor event identified September 6, 2002. Left: normalized brightness function obtained from (top) absolute trace amplitude waveforms and (bottom) trace envelopes. Right: trace amplitudes (top) and envelopes (bottom) indicate waveform coherence across the array.

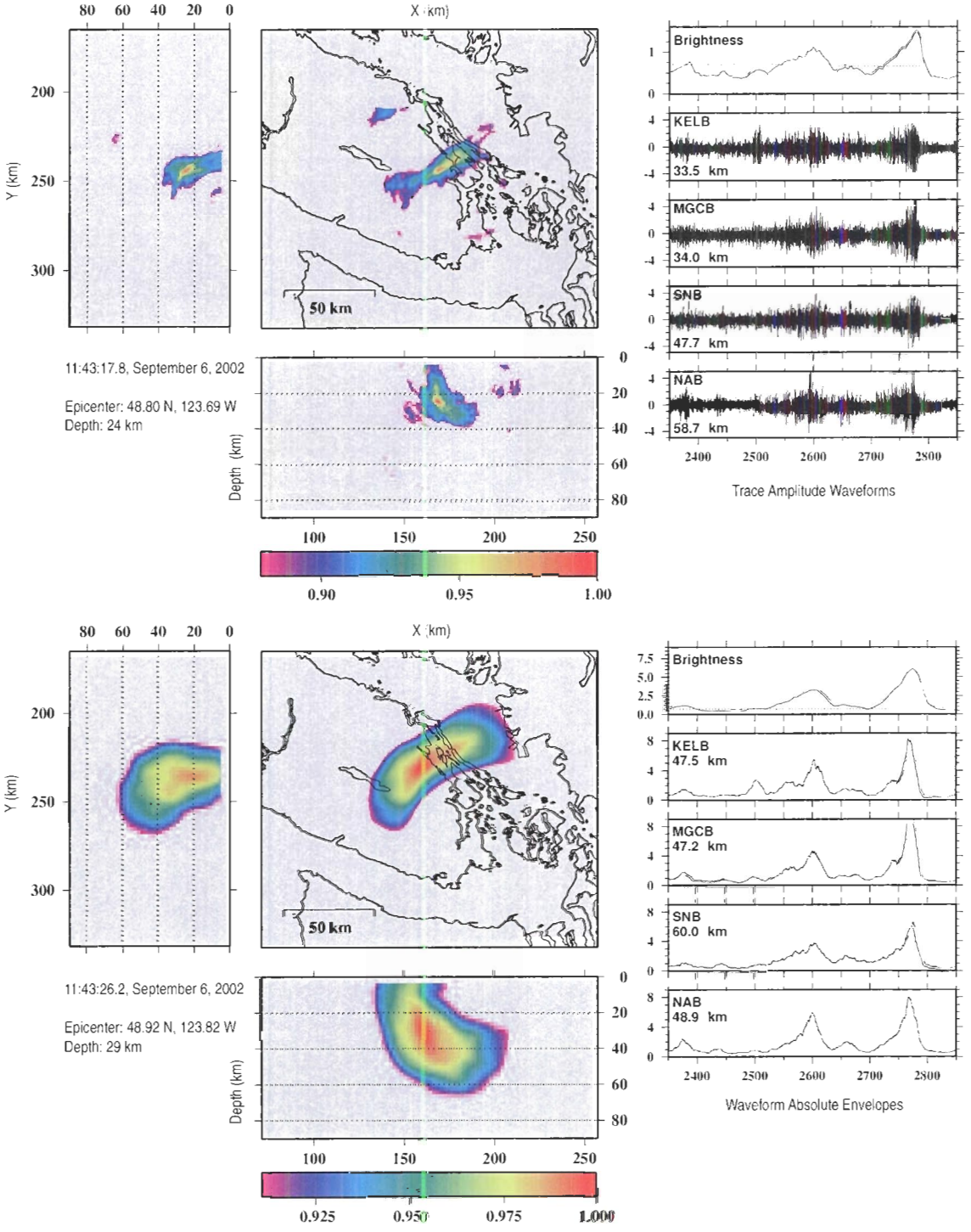

Figure 3.12: Map and profiles showing a tremor event identified September 6, 2002. The normalized brightness function (top left) obtained from trace absolute amplitude waveforms (top right) shows consistency with the normalized brightness function obtained from absolute envelope waveforms (bottom left and right).

Chapter 4

THE STRUCTURAL AND RHEOLOGICAL IMPLICATIONS OF TREMOR DISTRIBUTIONS

It has been suggested that the location of tremor sequences may be used to refine the estimated duration and periodicity of slow slip thrusting [46]. However, tremors may play a much more significant role in the accumulation and release of elastic strain, and therefore seismic hazard along the northern Cascadia subduction zone. In light of Julian's (1994) argument that tremors are generated by flow-induced oscillation in fluid-filled conduits [23], tremor activity may directly affect the local frictional stability regime by varying the local pore fluid pressure. Following a tremor sequence, the source region of tremors may undergo a decompression of pore fluids, resulting in a decrease in fluid pressure and an increase in effective normal shear strength. In this sense, tremor activity may regulate the local frictional stability regime [49] and constrain both the location and magnitude of aseismic slip and earthquake seismicity. Earthquake activity and aseismic sliding may equally regulate tremor activity because interfaces of stable sliding and fault systems may provide pathways for pore fluid flow. A thorough interpretation of tremor distributions and source mechanisms must therefore examine the stress interactions between tremors, earthquake seismicity, and aseismic sliding, each in relation to the structure of the megathrust interface. In this chapter, I will provide a brief rheological description of earthquake and aseismic slip source mechanisms, followed by a comparison of tremor distributions to the above processes and to the structure of the megathrust interface inferred from seismic reflection data. The spatial and temporal correlation of tremors from February

2002 and September 2002 to aseismic slip and earthquakes will provide valuable insight on how stress is accumulated, distributed, and released on the northern Cascadia margin. The interaction between the above processes will also clarify the rheological environment(s) necessary for tremor generation.

4.1 SEISMIC *vs.* ASEISMIC SLIDING AND FRICTION LAWS

Both earthquakes and aseismic slip may be described by stick-slip frictional instabilities [5]. Earthquakes are thought to occur predominantly by sudden slippage along pre-existing faults or interfaces, rather than by the conventional theory of brittle fracture [49]. The transition from seismogenic slip to aseismic slip occurs at the transition from elastic-brittle deformation to ductile flow [49, 48]. A number of authors have suggested that this transition is thermally constrained [48, 18, 19]. The observed maximum depth of crustal earthquakes and thermal modelling [18] indicate that beyond a critical temperature of about 350^{o}C, earthquake seismicity decreases rapidly. Ductile flow, however, need not occur strictly at depths corresponding to temperatures above the critical 350^{o}C limit, but also by the mechanism of cataclastic flow: a type of granular deformation which can occur in poorly consolidated sediments [49]. In this sense, slow slip need not occur exclusively at depth and along the megathrust interface, but may also release stress along shallow interfaces in the crust which exhibit poor sediment compaction and low shear strength.

In the standard model of stick-slip friction, it is assumed that sliding begins when the ratio of shear to normal stress on the fault surface reaches a value μ_s (the static friction coefficient) [49]. The slip may occur seismically or aseismically, depending on the rheology. The effective normal stress of the fault zone is given by the relation

$$\bar{\sigma} = \sigma - p \tag{4.1}$$

where σ is the applied normal stress (the lithostatic load) and p is the pore fluid pressure. Along subduction zones, increasing temperature and pressure conditions initially release large amounts of water from subducted sediment and oceanic crust through mineral dehydration reactions. This maintains high pore fluid pressures on the fault interface and limits the frictional build-up of shear stress and strain. If the pore fluid pressure p approaches the applied normal stress σ, the effective normal stress and shear strength drop. Once the shear stresses become greater than the shear strength of the fault, stable aseismic sliding may occur. At some point, however, the rate of fluid loss decreases,

increasing the effective stress and allowing build-up of elastic strain and seismogenic behaviour [34].

Both aseismic slip and earthquake activity may affect the distribution and magnitude of tremors. The location of slow slip defines interfaces of low shear strength and high pore fluid pressure. The relaxation of accumulated elastic stress in the form of slow slip may propagate fluids along slip interfaces and induce tremor activity. Sudden slippage in the form of an earthquake may lengthen pre-existing faults, or remove asperities along the fault plane. This might result in lengthening, interconnection, or broadening of conduits along which fluid may be introduced. Additionally, tremor activity may regulate the frictional regimes that control aseismic and seismic slip. The onset of a tremor sequence may indicate a more rapid release of local shear stress. The reduction of pore fluid pressure following tremor activity may increase the shear strength along an interface or fault, and potentially terminate a slow slip episode or induce earthquake seismicity. The spatio-temporal correlation of slow slip, earthquakes, and tremor activity will serve to support or disprove these theories.

4.2 ASSOCIATIONS BETWEEN ASEISMIC SLIP AND TREMOR SEQUENCES

Episodic transient surface displacement of GPS stations has been modelled by up to 3 cm of slip on a region of the interplate interface roughly bounded by the 30-40 km depth contours and 100 km landward of the locked seismogenic zone [15]. It has been proposed that fluid released from metamorphic dehydration reactions in the subducting slab results in an increase in pore fluid pressure and subsequent decrease in shear strength along strike [41, 46], leading to the episodic release of stress accumulated around the transition zone in the form of aseismic slip. The spatio-temporal association of episodic tremor sequences with slow slip events (the aforementioned regions of low shear strength) promotes the idea that fluid migration generates episodic tremor activity [46]. Nevertheless, the identification of tremor sequences outside the 13-16 month cycle may indicate that tremors originate from other source mechanisms besides fluid flow, and may nucleate in a variety of rheological environments (not strictly environments of low shear strength). There may exist two unique classes of non-volcanic tremor with distinct source mechanisms. Though the fact that episodic and non-episodic tremors share the same spectral content and waveform character would contradict this point. If episodic and non-episodic tremors are indeed regulated by slow slip, aseismic slip could be occurring more frequently on a smaller scale and undetected by transient surface deformation.

4.2.1 Coincidence of slow slip with episodic tremor sequences

The locations of episodic tremors from February 2002 coincide with the proposed spatial range of aseismic slip (Figure 4.1). Tremors have been located in both the subducting Juan de Fuca plate and overriding North America plate, and over a depth range of 5-60 km. The largest densities of tremors occur at discrete depth ranges of 33-36 km and at 19-22 km, both of which lie at depths where slow slip is possible. In addition, episodic tremors migrate to the northwest and along strike in a similar fashion to slow slip. The spatial and temporal correlation and migratory behaviour of episodic

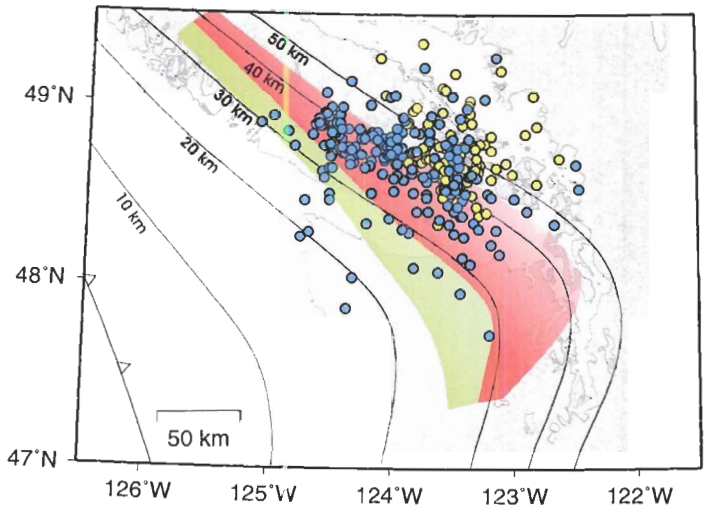

Figure 4.1: Epicenters of located episodic tremors (blue) and non-episodic tremors (yellow) superimposed on the proposed transition zone (green) and zone of full aseismic slip (orange) as determined from surface transient deformation studies [46]. Episodic tremors distribute along the zone of full slip, whereas non-episodic tremor cluster at the eastern margin and at shallower depths.

tremors and aseismic slip indicates that both processes are directly related and possibly co-regulated. If episodic tremors are the seismic expression of fluid flow through conduits, a non-uniform tremor depth distribution would suggest that fluid is constrained to flow along the two interfaces which correspond to the largest tremor densities. Tremor source locations therefore delineate interfaces of low shear strength, along which aseismic slip may be constrained and/or enhanced. As well, shearing along interfaces of slow slip may remove asperities, thereby allowing more fluid to propagate along the shear interface and inducing stronger tremor activity. These theories are supported by observations of increased tremor activity coinciding with slip episodes [46].

4.2.2 COINCIDENCE OF SLOW SLIP WITH NON-EPISODIC TREMOR SEQUENCES

September 2002 tremors were located at shallow depths, and immediately east of the proposed zone of slow slip. All tremors were located exclusively within the continental crust, and predominantly between depths of 5-10 km. Based on their spatial distribution, non-episodic tremors might not be the direct manifestation of fluid flow at depth, but instead liberate small amounts of stress in the brittle regime in response to shallow re-adjustment of the continental crust following a slip event. This, however, does not seems likely since the waveform character and frequency content of non-episodic tremors is identical to that of episodic tremors. A more plausible argument would be that shallow re-adjustment of the continental crust following the previous slow slip event generates, lengthens, or interconnects fault systems that serve as fluid pathways. Resonance of fluids through conduits extending into the crust would appear to generate shallow non-episodic tremor activity.

One distinction between episodic and non-episodic tremors is that non-episodic tremors are found to have on average lower waveform amplitudes. Time-depth-amplitude histograms of the February 2002 and September 2002 tremor sequences are displayed in Figure 4.2. The amplitudes of tremor events were calculated by first scaling the maximum amplitude of each tremor arrival from each recording station by the inverse of the radial distance between the recording station and the tremor source location. The scaled amplitudes from all recording stations and corresponding to one tremor event were then averaged to give a single corrected average amplitude for each tremor. The amplitudes of tremor events of the February 2002 sequence do not appear to have significant variability with respect to time and depth, though they are significantly greater, in general, than those of the September 2002 sequence. February 2002 tremor locations coincide with interfaces accommodating slow slip, and hence locate along extensive shear interfaces which may accommodate large amounts of fluid. Reduced amounts of fluid flow in the crust, relative to larger amounts of fluid migration along interfaces that accommodate slow slip, might explain lower amplitude tremors during September 2002. As well, shear interface or conduit geometry may play an important role. The surface area of fluid conduits through crustal fractures is likely much reduced and more variable than that of shear interfaces at depth, and might explain the larger variability in tremor amplitudes during September 2002.

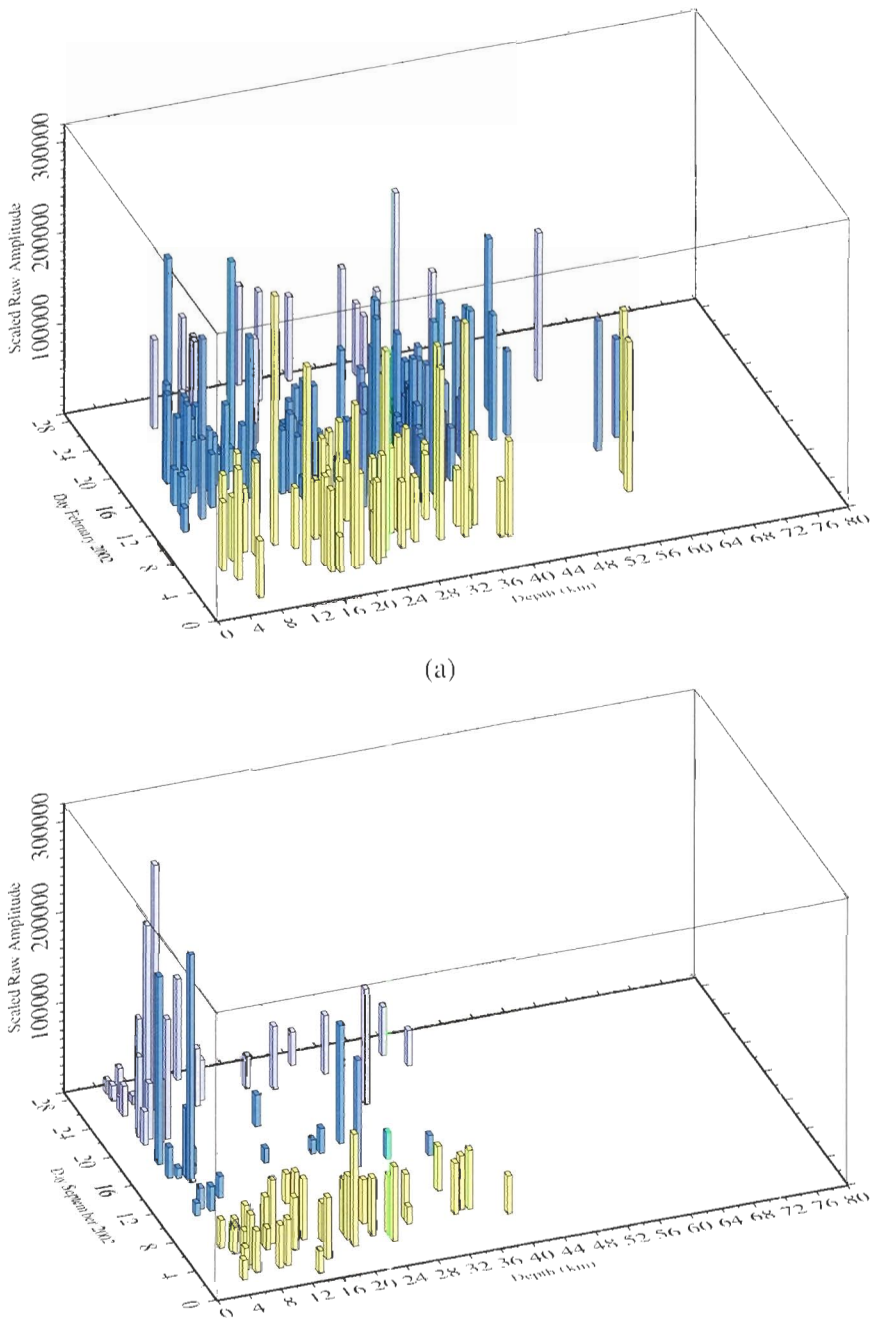

Figure 4.2: Time-depth-amplitude 3-D histograms of tremor events from the (a) February 2002 sequence and (b) September 2002 sequence. The amplitudes of tremor events were calculated by first scaling the maximum tremor arrival at each station by the inverse of the radial distance between the tremor source location and the station location, and averaging the scaled amplitudes.

4.3 COINCIDENCE OF EARTHQUAKE SEISMICITY WITH TREMOR SEQUENCES

Thermal and deformational modelling of the subduction interface [24, 18, 19] indicate that seismicity due to brittle fracture and frictional sliding is unlikely to occur in the subducting slab at depths greater than 35 km. Deep earthquakes within the slab are interpreted to originate by a process of embrittlement, during which internal pore fluid pressure due to dehydration of the slab reduces the effective normal stresses along faults [29]. Large increases in pore pressure are thought to cause fracture and frictional sliding along faults, or promote brittle reactivation of pre-existing faults [45, 28]. Shallow slab events most commonly occur along the Pacific coast, around southern Vancouver Island and the adjacent mainland [55], which correlates with the boundary of the zone of slow slip. This spatial correlation suggests that slow slip and in-slab seismicity may be related to a common process of slab dehydration [14], or stress interaction. Because episodic tremors and aseismic slip associate both temporally and spatially, a common stress interaction between slow slip and in-slab seismicity could indicate that the source mechanism(s) of episodic tremors and in-slab earthquakes are also related. Earthquake seismicity may remove asperities along faults and enable or enhance the propagation of fluids being dehydrated from the subducting slab, and in this sense, may induce tremor activity. Alternatively, the removal of asperities along fault systems may result in the fault clamping shut. Because strain changes caused by earthquakes can alter pore-fluid pressures in rocks at a distance from the hypocenter [22, 32], a relationship (whether direct or inverse) between tremors and earthquakes is likely. Tremor and earthquake distributions and magnitudes must therefore be compared in order to determine the exact association.

4.3.1 EPISODIC TREMOR AND EARTHQUAKE DISTRIBUTIONS

Elevated levels of tremor activity have been identified during February 2002, amounting to 482 identified tremors, 187 of which are considered well-located. Despite significant tremor activity, earthquake seismicity during this month is relatively quiescent. 13 weak ($M_L < 2.8$) crustal and in-slab earthquakes occurred during February 2002, and within the search region of this study. Reduced earthquake seismicity may be a consequence of the slow slip episode that occurs during this month. During the slow slip episode, fluids released from the subducting slab reduce the shear strength along the subduction interface, resulting in the aseismic release of shear stress. It is possible that an insufficient amount of the accumulated stress remains to generate earthquake seismicity.

Earthquake hypocenters do not coincide with the locations of episodic tremors (Figure 4.3), but

occur specifically where tremors do not. This has important implications for the rheological environ-

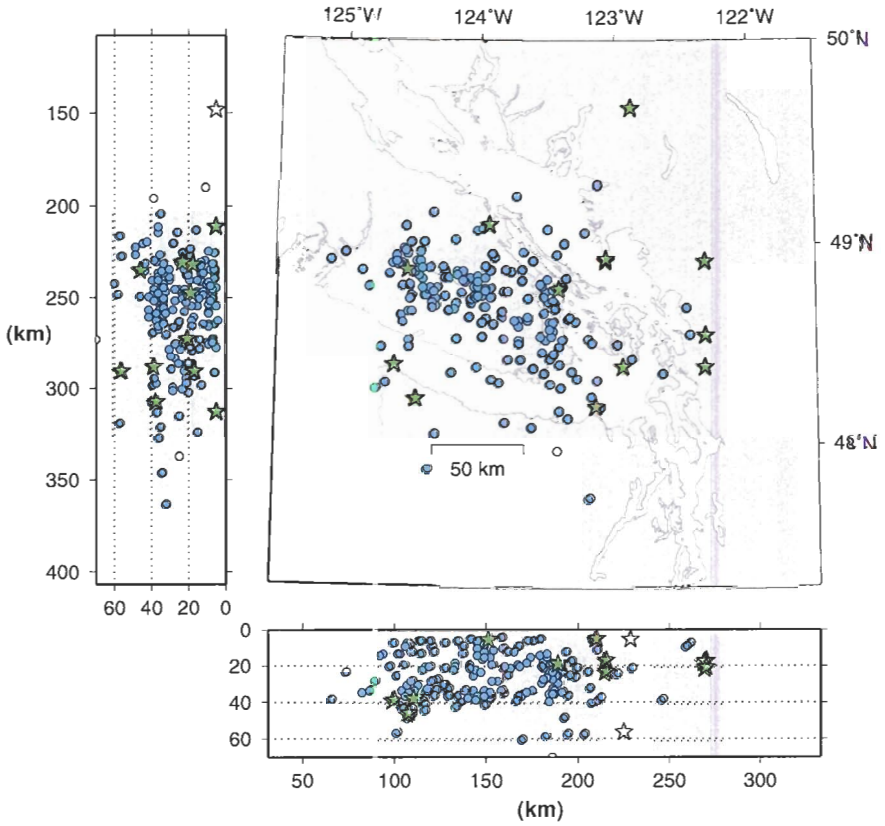

Figure 4.3: Comparison of episodic tremors and local in-slab and crustal earthquakes during February 2002. Blue circles indicate episodic tremors, green stars indicate earthquakes.

ment of episodic tremors. Large amounts of tremor activity that coincide spatially and temporally with slow slip rather than earthquake seismicity indicates that episodic tremors (at depths predominantly between 20-40 km) nucleate along shear interfaces (and low shear strength environments) that accommodate large amounts of fluid rather than along fault systems.

4.3.2 Non-episodic tremor and earthquake distributions

Lower levels of non-episodic tremor activity have been found during September 2002 than that of episodic tremor activity during February 2002. 194 tremors have been identified, 99 of which are considered well located. However, September 2002 experienced relatively large levels of weak

($M_L < 2.8$) crustal and in-slab earthquake seismicity, predominantly near the southeast tip of Vancouver Island. The majority of earthquakes during September appear to be crustal, indicating that large amounts of accumulated stress are being released in the crust 6 months following the previous slip event. There appears to be some spatial overlap between the location of tremors and earthquakes (Figure 4.4) which indicates that large amounts of accumulated stress are being released in the general region from which non-episodic tremors originate.

It is possible that slow slip may have been occurring during September 2002, though on a smaller and undetectable scale. However, aseismic slip and earthquakes require different frictional regimes (slow slip requires low shear strength, whereas earthquakes require high shear strength). High levels of earthquake activity in the crust indicates a high shear strength environment, unsuitable for slow slip. Furthermore, low levels of earthquake activity during the previous slow slip event supports the idea that these two processes are spatially disassociated. It is more likely that shallow re-adjustment of the crust following the previous slip event induces fracture and frictional sliding along faults, which may serve to remove roughness and asperities along fault systems, allow the propagation of fluid into the crust, and initiate the September 2002 tremor sequence.

4.4 MEGATHRUST STRUCTURE AND EPISODIC TREMOR DISTRIBUTIONS

The depth distribution of episodic tremors located during February 2002 may be characterized in relation to the two surges in tremor activity identified during February 1^{st}-10^{th}, and February 11^{th}-20^{th}, respectively. Tremors located during the first surge in activity distribute evenly over a broad depth range of 40 km, placing them in both the subducting Juan de Fuca and overriding North American plates. During the second and stronger surge in activity, the majority of tremors appear to distribute at two depths, approximately 20 and 34 km. If in fact the location of episodic tremors directly identifies the depth at which aseismic slip occurs, a segregated tremor depth distribution would indicate that slow slip occurs along more than one interface. Episodic tremor sequences have been projected laterally onto a seismic reflection profile (Figure 4.5) with superimposed *P*-wave velocities [42] to form a composite cross-section of the megathrust interface (Figure 4.6). A histogram of tremor depth distribution was generated by sorting located tremor depths into 2 km bins. The large number of tremors located at depths of 33-36 km coincides with the depth of the *F*-reflector. A second peak at 19-22 km coincides with the top of the *E*-reflector zone. It is important to note that the spatial correlation of episodic tremors to the proposed duplex thrust structure is apparent only during the second surge in tremor activity. It is possible that the first surge in tremor

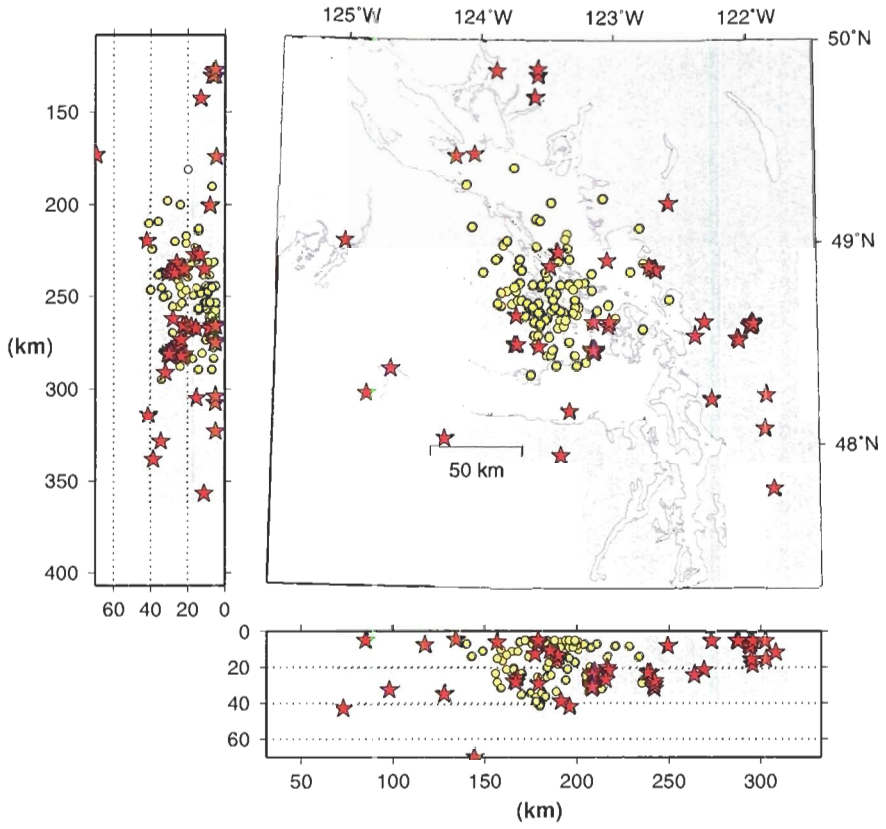

Figure 4.4: Comparison of non-episodic tremors and local in-slab and crustal earthquakes during September 2002. Yellow circles indicate non-episodic tremors, red stars indicate earthquakes. The majority of earthquakes occur at depths shallower than 30 km, and within the North American plate.

activity indicates a build-up in stress along the megathrust which is subsequently released in the form of deeper slow slip.

Another important distinction between first-surge and second-surge tremor sequences is the difference in migration rate. Tremors undergo a slow migration at the beginning of the month, while more rapid tremor migrations are observed during the second pulse in activity. This second pulse also corresponds to a re-distribution of many tremors along the two subsurface interfaces. Because fluid released from metamorphic dehydration reactions has been proposed to induce aseismic slip events [41, 46], the migration direction of the tremor sequence might indicate the direction of fluid flow in response to the redistribution of shear stress along the slow slip interface(s). Changes in pore pressure due to the release of shear stress during slow slip may drive the migration of fluids in

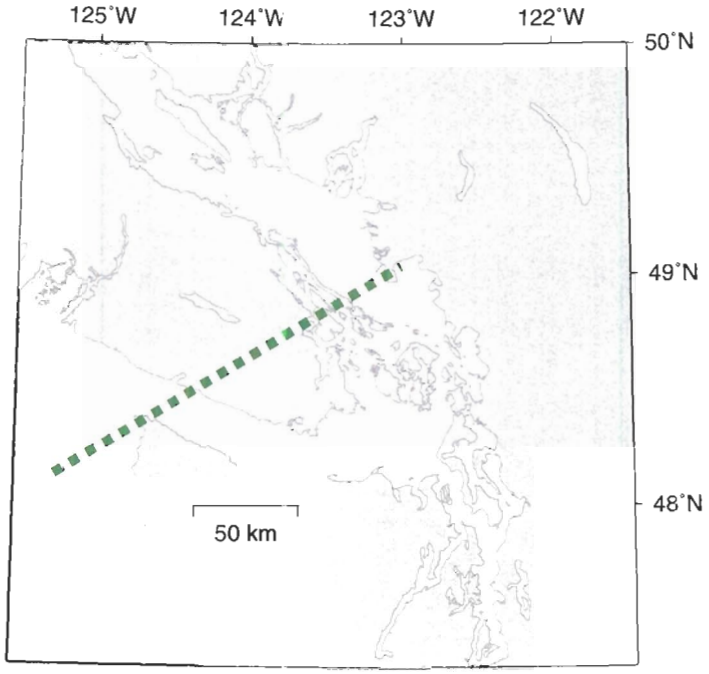

Figure 4.5: Azimuth of 063° onto which tremor sequences were projected for comparison to reflection data and *P*-wave velocities (Figure 4.6).

the direction of slow slip. The correspondence of large migration rates to a divided depth distribution could imply that the roof and floor thrust interfaces of a possible megathrust duplex structure accommodate fluid pathways which initiate aseismic slip and the associated tremor activity.

4.5 Megathrust Structure and Non-Episodic Tremor Distributions

Non-episodic tremors identified during September 2002 distribute predominantly at depths of 5-10 km, and eastward of the zone of aseismic slip. The distribution of non-episodic tremors appears unrelated to the depths of *E*- and *F*-reflectors (Figure 4.6), which suggests that the mechanisms which generate non-episodic tremors are unrelated to possible fluid migration and shear stress redistribution along these interfaces. The lack of tremor migration observed during September 2002 suggests that non-episodic tremors relate to a more localized stress change at shallow depths in the crust. If small and undetected amounts of deep aseismic slip are occurring on the megathrust, shallow tremors may originate from fluids released due to aseismic stress changes along the slip

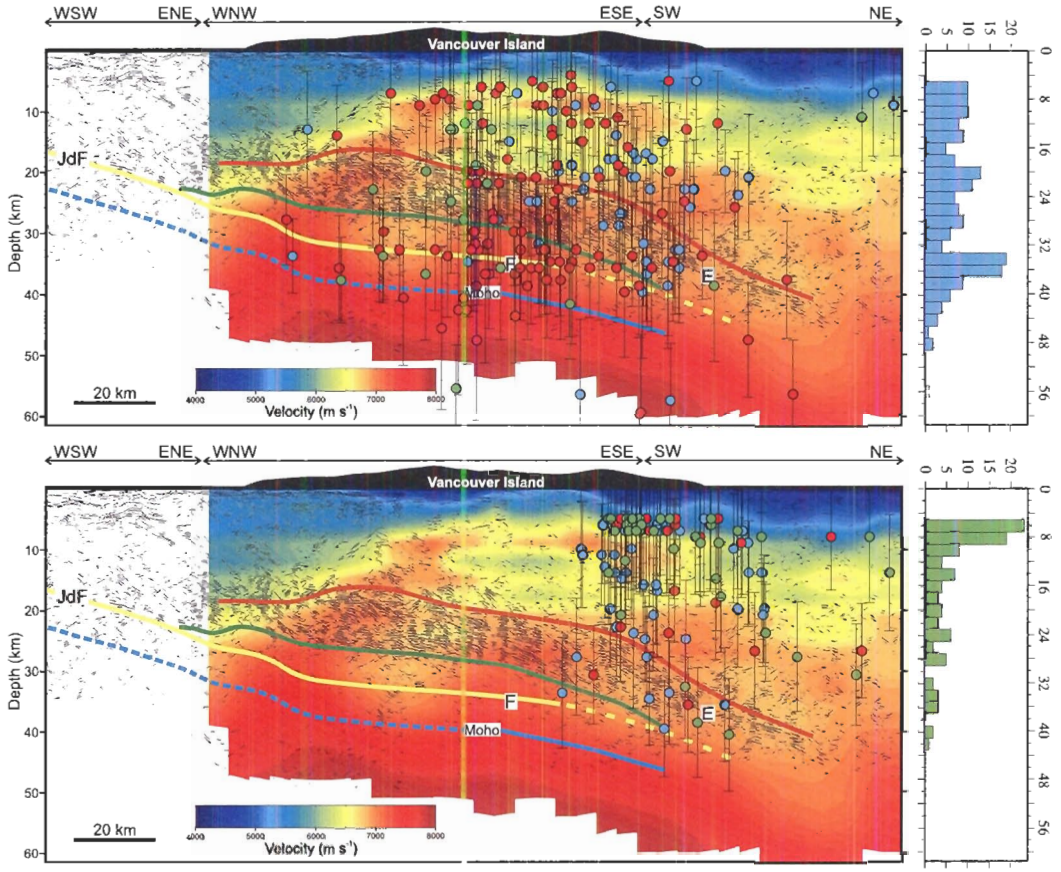

Figure 4.6: Composite seismic cross-section across the Cascadia forearc, showing migrated reflection data superimposed on *P*-wave velocities derived by 3-D tomographic inversion of first arrivals. Seismic profiles were projected onto an azimuth of 063^{o}, which is a representative dip direction for the subducting plate near the seismic profiles [7]. (a) Episodic tremor sequences were projected onto the same azimuth, and are color-coded in terms of 10-day period. Tremors located during February 1^{st} - 10^{th} are shown in blue, during February 11^{th} - 20^{th} in red, and during February 21^{st} - 28^{th} in green. A histogram of tremor depths (right) was generated by sorting tremor locations into bins of 2 km. Many tremors occur at the same depths as the *F*-reflector. A smaller peak in the distribution corresponds to the top of the *E*-reflectors. Largest tremor migrations occur during the second surge in tremor activity, during February 11^{th} - 20^{th}. (b) Non-episodic tremor sequences projected onto the same profile. Tremors located during September 1^{st} - 10^{th} are shown in blue, during September 11^{th} - 20^{th} in red, and during September 21^{st} - 28^{th} in green. Non-episodic tremors have no direct spatial association with the megathrust interface, and abruptly terminate at the top of the *F*-reflector. This indicates almost all non-episodic tremors are located in the continental crust.

interface(s) which propagate into the crust through fault systems. However, the magnitude of this deep aseismic slip must be considerably lower than in February 2002, because there is no evidence of comparable ground deformation in the GPS monitoring data.

Chapter 5

CONCLUSIONS AND SUGGESTIONS FOR FUTURE WORK

In this thesis I have imaged the source locations and origin times of the two tremor sequences that occurred during February and September of 2002, with the incentives of obtaining more accurate estimations of the region and duration of slow slip thrusting and the distribution of stresses along the northern Cascadia margin. The comparison of two tremor classes, one of episodic nature which co-incides spatio-temporally with slow slip, and the other which is non-episodic and crustal, has led to theories on the rheology and structure of the subduction thrust and the nature of stress accumulation and release along the northern Cascadia margin. It has become apparent that stress release along the megathrust manifests through a sequence of interrelated processes, namely slow slip, earthquakes, and tremor activity. The critical factor which appears to control the release of accumulated stress and the interaction of the above processes is pore fluid pressure. The propagation of large quantities of fluids dehydrated from the subducting slab has the effect of varying the pore fluid pressure, and therefore the frictional regime, in an apparently episodic manner that is precursory to episodic sequences of tremor activity and slow slip thrusting. These fluids seem to propagate along a large portion of the megathrust (corresponding to the region of slow slip) and at shallow depths into the crust (corresponding to the depths of the September 2002 tremor sequence), allowing seismic and aseismic processes that nucleate in different regions along the subduction thrust to become co-dependent and co-regulated. Flow modelling of fluids dehydrated from the subducting slab will be a very important aspect of future research into the state of stress of the northern Cascadia margin. In this chapter I will outline the conclusions drawn from my thesis research, and present important

avenues for future research based on my results.

5.1 CONCLUSIONS

Episodic and non-episodic tremors corresponding the sequences of February and September of 2002, respectively, are identified by *S*-wave arrivals with a frequency content in the range of 1-5 Hz, and an emergent waveform character that has been attributed to a common source mechanism of resonance in fluid-filled conduits [23, 22, 41]. Both tremor sequences have been imaged using the source-scanning algorithm, which identifies the source locations and origin times of tremors based on the coherence of tremor *S*-wave arrivals across the seismograph network. Episodic and non-episodic tremors differ in terms of their spatial distributions, their migratory behaviour, and their magnitudes. The majority of tremors of the February 2002 sequence distribute at depths greater than 15 km and migrate from the southeast tip of Vancouver Island to the northwest. Non-episodic tremors of the September 2002 sequence generally locate between depths of 5-10 km at the southeast tip of Vancouver Island, and show no migratory behaviour. The amplitudes of September 2002 tremors are significantly lower than those of February 2002, which indicates reduced fluid flow and stress release associated with the non-episodic tremor sequence.

Episodic tremors are spatially and temporally linked to slow slip through the propagation of fluids along the megathrust interface(s). Their source region and migration indicate the region and propagation direction of fluids dehydrated from the subducting slab. Two 8-day periods of elevated tremor activity were identified during February 2002, separated by a short two-day period of reduced detection. During the first period, tremor locations were fairly evenly distributed over a depth range of 15-40 km. The second period of enhanced tremor activity is accompanied by a more rapid migration to the northwest and a redistribution of tremors along two interfaces at depths of approximately 19-22 km and 33-36 km. The depths which correspond to the largest tremor populations identify two interfaces which accommodate large amounts of fluid such that the shear strength is sufficiently reduced to allow slow slip. In lieu of this argument, the structure of the megathrust interface may in fact be a duplex thrust structure, with shear and slow slip occurring on both the upper and lower thrust interface. Episodic tremor locations have an average spatial error of 7 km in the horizontal direction and 9 km in the vertical direction, and may therefore be used to further constrain the depths at which slow slip occurs (in addition to surface-based deformation monitoring). The spatial error of tremor locations may be reduced by using horizontal-component seismometer data in addition to the vertical-component data used in this thesis, and a larger number of seismograph stations. Episodic

tremors appear to nucleate where local earthquakes do not, which further supports the theory that tremors are generated by fluid flow which decreases the shear strength along faults.

Non-episodic tremors do not correlate spatially nor temporally to slow slip, though temporally coincide with elevated crustal earthquake seismicity. Non-episodic tremors distribute in a localized area in the crust, predominantly at depths of 5-10 km. The large spatial segregation of episodic and non-episodic tremors, despite their common source mechanism, indicates that fluid propagation along the northern Cascadia margin is abundant and wide-spread. Elevated pore-fluid pressures may result from both dewatering reactions at depth and poor sediment compaction at shallow depths in the crust, which may reduce effective stresses over a broad depth range corresponding to the distributions of episodic and non-episodic tremor sequences. High pore-fluid pressures along a significant portion of the northern Cascadia subduction zone would further indicate a weak coupling of the subduction fault. Non-episodic tremors occur during a period of elevated crustal earthquake seismicity, which has led to the theory that this tremor class is generated by the lengthening and interconnection of fault systems due to crustal seismicity which provide fluid pathways to shallow depths in the crust. As in the case of episodic tremors, non-episodic tremor locations do not coincide with earthquake hypocenters, which may indicate reduced shear strength along fault systems from which tremors originate due to fluid infiltration.

The imaging tremor sequences may be used to map the movement of fluid in the subduction zone. Because tremors are generated by fluid flow, the location of tremor sequences may isolate regions of high pore fluid pressure and low effective stress, which define areas of low seismicity and higher probability of shear. The February 2002 tremor sequence indicates the propagation of large amounts of fluid on the deeper (19- to 36-km) part of the northern Cascadia subduction zone interface, which has the effect of generating rheological or frictional instabilities that induce stable sliding. Transient deformation associated with slip increases the stress along the up-dip locked plate interface [46]. Consequently, the possibility of triggering a megathrust earthquake would be expected to increase as the frequency and magnitude of slow slip increases [46, 31]. The September 2002 tremor sequence indicates fluid-saturated fault systems at shallow (5- to 10-km) depths in the continental crust. High crustal pore pressures reduces the probability of large crustal earthquakes. The imaging of non-volcanic tremor sequences is therefore a sensitive indicator of stress variation and a valuable tool to assess seismic hazard both along the megathrust and at crustal depths. My most general suggestion for future tremor research is to acquire and image tremor waveform data over an entire slow slip period (13-16 months) to develop statistical relationships between tremor occurrence, slow slip and earthquakes. More observational data and robust statistical correlations

will be required to address some important questions that arise from the interpretations of this thesis, as will be outlined in the following section.

5.2 SUGGESTIONS FOR FUTURE WORK

DO EARTHQUAKES TRIGGER TREMOR ACTIVITY?

There is evidence that small- to moderate-sized earthquakes may trigger tremor activity by causing strain changes that can alter local pore fluid pressures [32, 22]. It may be that shallow non-episodic tremor are dependant on earthquake seismicity to:

1. re-activate and interconnect fault systems which may become infiltrated with fluids dehydrated from the subducting slab, and
2. induce local pore fluid pressure gradients which drive fluids through fault systems.

This may be verified by correlating shallow non-episodic tremor sequences with crustal earthquake seismicity. Additionally, it would be interesting to see if shallow non-episodic tremor has any effect on the focal mechanisms of crustal earthquakes. Systematic differences in the focal mechanisms of earthquakes accompanied by tremor may be used to quantify the amount of stress released by the non-episodic tremor sequence.

ARE EPISODIC TREMORS PRECURSORS TO SLOW SLIP?

Episodic tremors of the February 2002 sequence were found to have two 8-day pulses of elevated activity. During the first pulse, tremors were located fairly evenly over a broad (5- to 40-km) depth range and showed no significant source migration. The majority of the tremors of the second pulse were located along two shear interfaces an undergo a rapid source migration, and are therefore interpreted to accompany slow slip. It is possible that fluid propagation associated with the first pulse of elevated tremor activity is necessary to sufficiently hydrate the slip interface(s), reduce the effective stress, and induce the slip episode. This may be verified by determining the occurrence rate of tremor activity during several slip episodes. If an initial pulse in tremor activity characteristically precedes episodes of aseismic slip, the magnitude of these tremors may indicate the amount of stress accumulation required to induce slow slip.

What are there no in-slab earthquakes during September 2002?

Following an episodic tremor and slip event, one would expect the subducting slab to be sufficiently embrittled due to the propagation of large amounts of dehydrated fluids. Because deep earthquakes within the slab are interpreted to originate by a process of embrittlement [29], it is surprising that earthquake seismicity in September 2002 following the slip event is uniquely crustal. This might indicate that aseismic slip releases most of the accumulated stress in the subducting slab, and an insufficient amount of stress remains at depths beyond 35 km to generate earthquake seismicity. Temporal correlations between slow slip and in-slab seismicity may clarify any dependencies one process has on the other.

Can the Coherence of Tremor Waveforms Verify the Source Mechanism(s)?

It might be possible to verify or constrain the source mechanism(s) of non-volcanic tremors by correlating tremor events with the same source location but occur at different origin times. A large waveform coherence between common source-point tremor events (though with different origin times) would indicate that the tremor source mechanism is repeatable. This would indicate that the tremor source mechanisms are repeatable, and give further credibility to the assumption that non-volcanic tremor are generated by flow-induced resonance in fluid conduits. In addition, a large degree of waveform coherence between common source-point tremor events might indicate that these tremors were generated in the same fluid pathway, which may isolate the number of fluid pathways that generate an entire tremor sequence.

Appendix A

EPISODIC TREMOR SOURCES

February 2002 locations							
date	hour	seconds	lat	lon	depth	dh	dz
yyyymmdd	hr	after hour	(^{o})	(^{o})	(km)	(km)	(km)
20020202	06	660.690	48.55	-122.43	7	5.909	10.52
20020203	12	1598.16	48.42	-123.47	18	6.909	9.995
20020203	14	2873.69	48.28	-123.39	20	5.728	9.635
20020203	14	624.210	48.49	-123.40	18	4.432	7.164
20020203	17	3053.55	48.36	-123.31	17	5.163	7.208
20020203	21	2429.06	48.52	-123.19	23	5.007	8.234
20020204	04	3051.45	48.42	-122.86	21	8.347	10.48
20020204	07	2746.67	48.24	-123.16	40	6.238	11.04
20020204	09	2251.98	48.32	-123.12	39	7.679	10.42
20020204	10	154.750	48.52	-123.37	23	6.548	9.679
20020204	12	1823.12	48.50	-122.97	24	6.986	7.298
20020204	14	1424.01	48.30	-123.47	23	4.514	8.112
20020204	20	1968.25	48.66	-123.51	17	4.105	8.320
20020204	20	2047.86	48.38	-123.59	6	3.084	9.231
20020205	05	1426.74	48.52	-123.50	27	5.185	8.274
20020205	05	1668.12	48.11	-123.80	35	9.536	9.144
20020205	08	1467.04	48.35	-123.51	21	5.031	9.460
20020205	08	442.770	48.16	-123.40	25	6.889	10.03
20020205	08	711.460	48.08	-123.60	15	5.102	12.12
20020205	10	476.740	47.73	-123.17	32	9.468	9.900
20020205	17	3291.46	47.96	-123.41	25	7.096	9.040
20020205	18	1977.50	48.40	-123.40	29	7.680	9.092

Table A.1: February 2002 tremors

February 2002 locations							
date yyyymmdd	hour hr	seconds after hour	lat (^{o})	lon (^{o})	depth (km)	dh (km)	dz (km)
20020206	04	741.890	48.62	-123.33	36	10.70	9.167
20020206	07	259.310	48.51	-123.16	5	9.131	12.09
20020206	11	2252.87	48.18	-123.09	37	7.784	8.773
20020206	17	134.480	48.61	-123.47	35	7.102	9.911
20020207	04	617.430	48.61	-123.28	26	5.337	7.433
20020207	04	899.910	48.13	-123.33	57	8.852	12.42
20020207	09	347.180	48.45	-123.44	27	4.457	8.451
20020207	10	2943.34	48.46	-123.52	29	6.017	7.313
20020207	11	2602.51	48.30	-123.85	28	6.086	7.410
20020207	11	2873.19	48.54	-123.97	7	6.789	10.04
20020207	14	1555.48	48.71	-123.48	15	9.698	9.967
20020207	15	945.130	48.53	-123.81	10	6.768	8.452
20020207	19	2031.01	48.42	-123.78	25	9.946	8.754
20020207	19	209.940	48.62	-123.63	6	5.962	9.723
20020208	03	2226.70	48.86	-123.76	21	5.694	11.73
20020208	06	2195.07	48.57	-123.44	32	7.323	10.41
20020208	07	1050.19	48.52	-123.70	9	6.474	7.924
20020208	08	404.540	48.64	-123.63	18	9.069	6.881
20020208	11	2590.46	48.50	-123.70	19	4.068	8.271
20020208	11	3195.03	48.30	-124.68	13	8.000	9.728
20020208	13	1812.63	48.61	-123.44	18	9.075	10.54
20020208	22	3312.67	48.42	-123.68	20	10.09	11.86
20020208	23	944.530	47.88	-124.36	34	5.837	6.143
20020209	09	2548.07	48.95	-123.42	20	7.331	6.896
20020209	09	2637.18	48.62	-123.70	9	6.031	8.451
20020209	13	2437.19	48.76	-123.50	58	8.105	9.468
20020209	14	2372.64	48.68	-122.45	9	5.934	8.442
20020209	18	3072.59	48.54	-123.46	70	6.180	10.11
20020209	20	2987.69	48.77	-123.44	23	11.20	11.65
20020209	20	3193.42	48.71	-123.43	33	6.719	10.74
20020209	20	3330.30	48.68	-123.43	35	5.714	12.25
20020209	23	3525.37	48.92	-123.60	33	7.550	10.65
20020209	23	48.4000	48.72	-123.44	35	12.45	6.015
20020210	01	3217.00	48.32	-123.27	21	4.551	8.206
20020210	02	196.060	48.54	-123.54	14	6.569	7.404
20020211	03	865.850	49.07	-123.49	26	6.049	8.094
20020211	04	2030.17	48.96	-123.66	35	10.88	9.900
20020211	12	1312.81	48.87	-123.68	36	8.015	10.59
20020211	15	285.510	48.28	-124.75	28	9.109	7.481
20020212	01	3508.37	48.78	-123.38	34	7.845	7.265
20020212	02	1803.36	48.64	-123.82	4	9.337	8.510
20020212	02	253.300	48.83	-123.49	13	4.377	8.496

Table A.2: February 2002 tremors

February 2002 locations							
date yyyymmdd	hour hr	seconds after hour	lat (^{o})	lon (^{o})	depth (km)	dh (km)	dz (km)
20020212	02	69.8400	48.63	-123.32	25	6.023	9.992
20020212	08	2783.47	48.79	-124.00	38	8.535	9.891
20020212	12	2338.31	48.73	-123.63	34	6.408	8.465
20020212	12	3517.42	48.74	-123.51	27	12.34	10.84
20020212	13	141.070	48.32	-123.90	37	9.050	9.079
20020212	13	1782.25	48.35	-124.20	74	6.311	11.39
20020212	14	3121.01	48.74	-123.91	35	4.393	13.64
20020212	21	3310.48	49.05	-123.21	57	4.006	8.969
20020213	01	1768.20	48.64	-124.07	37	10.26	7.544
20020213	03	2379.26	48.83	-123.35	12	9.519	8.652
20020213	07	2509.51	48.77	-124.00	7	5.968	7.073
20020213	12	951.820	48.79	-123.53	20	9.805	11.45
20020214	01	1364.76	48.82	-123.68	60	9.450	12.91
20020214	03	2129.25	48.76	-123.81	21	8.016	9.972
20020214	04	1545.80	48.59	-123.70	36	7.974	8.283
20020214	04	479.060	48.80	-123.54	5	9.404	9.836
20020214	07	1684.16	48.69	-123.96	35	8.005	8.622
20020214	10	454.970	48.79	-124.03	25	9.400	8.762
20020214	11	1160.41	48.61	-123.95	9	9.440	10.33
20020214	11	1711.24	48.84	-123.77	40	6.532	10.89
20020214	11	2218.18	48.35	-122.63	38	11.83	9.732
20020214	11	3079.76	48.66	-123.82	33	7.739	9.480
20020214	12	1037.48	48.60	-123.89	28	5.436	10.82
20020214	14	2765.11	48.83	-124.06	19	8.228	12.56
20020214	14	951.350	48.71	-124.16	18	10.15	10.52
20020214	16	1335.28	48.38	-124.01	22	5.367	9.019
20020214	18	2706.40	48.53	-124.16	20	9.758	9.698
20020214	19	2606.09	48.48	-124.71	14	7.464	8.321
20020214	20	1495.57	48.68	-124.18	22	9.158	7.080
20020215	00	3162.18	48.76	-124.12	39	5.259	8.897
20020215	01	3247.33	48.83	-124.41	39	8.617	9.290
20020215	02	290.110	48.87	-124.15	6	6.922	10.83
20020215	02	773.850	48.63	-123.95	33	9.741	8.953
20020215	03	1149.07	49.15	-124.34	35	4.333	8.951
20020215	03	1155.83	48.74	-123.97	23	7.428	9.168
20020215	03	465.760	48.75	-124.40	41	6.889	10.49
20020215	03	999.590	48.85	-124.24	33	6.367	11.66
20020215	04	2713.05	48.87	-124.11	13	8.858	8.449
20020215	07	2631.89	48.87	-124.25	21	5.889	8.691
20020215	07	3093.17	48.73	-124.31	33	9.533	9.199
20020215	07	3347.59	48.83	-124.25	30	10.94	8.946
20020215	12	3423.08	48.70	-124.31	33	6.643	10.25

Table A.3: February 2002 tremors

February 2002 locations							
date yyyymmdd	hour hr	seconds after hour	lat (^{o})	lon (^{o})	depth (km)	dh (km)	dz (km)
20020215	13	1501.98	48.71	-124.06	5	6.437	11.61
20020215	13	1591.23	48.79	-124.56	33	8.944	10.08
20020215	13	1715.73	48.75	-124.38	20	8.063	11.58
20020215	13	439.150	48.61	-123.97	36	9.316	9.310
20020215	13	640.830	48.67	-124.22	32	7.358	9.139
20020215	16	1958.01	48.79	-124.30	27	6.889	9.412
20020215	21	1463.30	48.65	-124.57	41	5.484	11.20
20020215	22	1739.03	48.61	-124.56	33	4.383	8.505
20020216	02	3350.15	48.79	-124.00	7	9.820	12.91
20020216	04	3255.98	48.78	-123.91	15	9.984	8.857
20020216	06	1916.11	48.71	-124.34	9	8.800	12.51
20020216	06	885.020	48.87	-124.5	43	7.966	8.973
20020216	07	1439.14	48.78	-124.37	32	9.248	8.826
20020216	07	2175.99	48.79	-124.36	20	7.027	10.26
20020216	08	2880.38	48.77	-124.33	12	7.413	9.073
20020216	09	1235.62	48.74	-124.25	7	6.778	10.95
20020216	10	1496.11	48.75	-124.49	46	8.989	13.52
20020216	10	1720.17	48.78	-123.95	12	6.042	8.608
20020216	12	2900.54	48.84	-124.00	6	6.506	9.310
20020216	13	1129.83	48.87	-123.91	34	8.667	10.68
20020216	13	2597.40	48.73	-124.06	21	6.765	11.74
20020216	13	787.570	48.82	-124.00	10	6.459	12.25
20020216	14	1809.44	48.78	-124.41	22	6.936	8.448
20020216	15	2300.01	48.89	-123.95	8	10.18	12.36
20020216	16	789.740	48.52	-124.51	7	11.65	10.40
20020216	17	2100.57	48.74	-124.03	33	7.639	9.351
20020216	17	2202.66	49.07	-124.01	36	8.093	8.252
20020216	17	2715.21	49.00	-123.36	48	9.279	9.455
20020216	22	1515.42	48.73	-124.51	8	8.041	9.864
20020217	01	2988.53	48.93	-123.88	11	4.663	8.507
20020217	01	3160.46	48.85	-124.44	30	4.118	13.16
20020217	01	3367.18	48.85	-124.15	36	5.366	8.143
20020217	04	2823.89	48.92	-124.46	37	10.03	14.76
20020217	04	3190.75	48.86	-124.47	33	6.749	9.270
20020217	05	149.990	48.79	-124.51	34	7.397	10.16
20020217	06	2924.92	48.49	-124.51	30	8.121	11.25
20020217	06	3272.18	49.08	-123.97	16	10.05	11.97
20020217	07	1618.01	48.87	-123.80	20	7.436	7.631
20020217	07	2344.70	48.05	-124.31	36	6.812	8.648
20020217	10	2196.46	48.95	-123.90	19	9.687	8.160
20020217	11	1199.81	48.81	-124.10	33	12.14	10.77
20020217	11	729.510	48.82	-124.11	9	8.848	11.05
20020217	14	1704.70	48.89	-124.26	30	6.712	8.773

Table A.4: February 2002 tremors

February 2002 locations							
date yyyymmdd	hour hr	seconds after hour	lat (^{o})	lon (^{o})	depth (km)	dh (km)	dz (km)
20020217	14	3015.50	48.58	-123.47	39	10.51	8.587
20020217	16	104.960	48.76	-123.78	12	11.49	9.516
20020217	17	2680.80	48.73	-124.02	38	9.865	9.635
20020217	18	3335.96	48.67	-124.52	9	8.087	9.140
20020218	00	2273.53	48.62	-123.73	12	10.29	12.49
20020218	01	779.610	48.77	-123.95	36	8.155	11.44
20020218	03	3150.43	48.91	-124.57	43	6.173	14.10
20020218	03	3418.15	48.83	-124.22	36	6.518	7.524
20020218	04	2163.45	48.80	-124.51	8	8.116	9.350
20020218	09	1229.05	48.88	-124.44	6	7.268	8.836
20020218	09	811.190	48.96	-124.43	6	8.729	9.355
20020218	10	223.700	49.01	-124.50	28	9.598	9.624
20020218	11	217.550	48.74	-124.00	14	5.676	8.875
20020218	13	1645.17	49.01	-124.40	44	8.764	7.843
20020218	14	2160.32	48.88	-124.36	6	7.828	9.078
20020219	09	2147.17	48.79	-124.81	33	7.754	8.611
20020219	19	2915.95	48.83	-123.95	15	9.893	8.072
20020219	20	1456.18	48.91	-124.63	7	6.656	9.935
20020220	07	243.180	48.95	-124.53	48	8.260	13.16
20020221	10	1560.77	48.98	-124.55	19	8.998	9.455
20020221	22	3330.14	49.02	-124.17	42	10.02	9.129
20020222	09	2400.84	48.86	-124.50	12	9.082	8.295
20020222	19	2203.40	48.94	-124.61	56	5.081	7.185
20020222	23	1420.34	49.29	-123.12	11	6.594	9.031
20020223	01	2828.93	48.92	-125.10	38	5.915	7.091
20020224	01	1520.24	48.90	-124.58	13	9.346	13.98
20020225	11	463.620	48.97	-124.54	9	5.664	10.21
20020226	03	241.970	48.92	-124.43	13	11.57	9.998
20020226	05	551.520	48.90	-124.59	13	7.763	12.07
20020226	08	2709.46	48.92	-124.61	25	6.849	11.88
20020226	15	1258.90	48.96	-124.99	23	6.639	9.679
20020227	06	2062.64	48.87	-124.86	34	7.449	7.812
20020227	10	2818.05	48.85	-124.66	20	6.710	9.253
20020227	12	423.600	49.09	-124.54	36	5.158	11.93
20020227	13	827.070	48.67	-124.49	37	5.944	10.98
20020228	02	220.290	49.23	-123.72	39	4.727	12.58
20020228	09	1054.24	48.69	-124.34	28	6.317	11.89
20020228	23	1422.67	48.88	-124.41	22	8.739	11.64

Table A.5: February 2002 tremors

Appendix B

NON-EPISODIC TREMOR SOURCES

September 2002 locations							
Date yyyymmdd	hour hr	seconds after hour	lat (^{o})	lon (^{o})	depth (km)	dh (km)	dz (km)
20020901	06	549.230	48.68	-123.62	14	7.56	8.56
20020902	03	566.320	48.67	-123.57	5	7.15	9.87
20020902	18	1393.21	48.99	-123.82	16	5.51	7.90
20020902	18	1525.78	48.80	-123.21	7	6.87	10.6
20020902	18	1584.85	48.69	-123.82	10	5.92	9.78
20020902	21	2639.03	48.70	-123.74	11	5.90	8.46
20020903	07	757.340	48.68	-123.25	6	5.60	11.1
20020903	15	2198.16	48.83	-123.49	25	4.78	9.75
20020903	17	2366.12	49.37	-123.74	20	3.46	9.74
20020903	20	1243.69	48.66	-123.36	7	3.11	10.4
20020904	08	1110.53	48.67	-123.46	7	6.75	10.3
20020904	10	1120.59	48.78	-123.54	40	7.74	8.07
20020904	14	2839.18	48.70	-123.55	25	10.4	7.11
20020904	16	3217.44	48.76	-123.78	13	9.36	8.43
20020904	19	1404.65	48.76	-123.72	23	7.07	9.14
20020904	21	3156.44	48.45	-123.48	20	3.11	9.72
20020905	01	1031.83	48.62	-123.39	7	5.43	10.8
20020905	05	3515.07	48.45	-123.28	17	7.14	10.9
20020905	06	1480.64	48.54	-123.47	10	11.0	11.6
20020905	10	386.260	48.88	-123.70	28	8.81	8.26
20020905	13	2006.53	48.92	-123.69	6	9.72	9.81
20020905	13	3315.78	48.35	-123.60	34	6.83	9.27

Table B.1: September 2002 tremors

September 2002 locations							
Date yyyymmdd	hour hr	seconds after hour	lat (^{o})	lon (^{o})	depth (km)	dh (km)	dz (km)
20020905	15	1284.18	48.80	-123.25	10	9.99	9.03
20020905	16	2191.05	48.50	-123.56	6	4.62	9.86
20020905	17	2908.61	48.85	-123.16	20	6.11	8.94
20020905	21	1798.35	48.85	-123.96	11	6.26	8.77
20020905	21	1932.77	48.92	-123.86	15	5.81	7.92
20020905	21	2143.65	49.12	-123.57	36	8.27	9.46
20020905	22	1444.06	48.97	-123.34	14	5.49	8.58
20020905	23	116.150	48.40	-123.41	14	10.0	8.42
20020905	23	2346.93	48.86	-123.68	35	9 76	7.80
20020905	23	2956.71	48.70	-123.85	28	10.9	9.75
20020906	01	1458.74	49.01	-123.79	21	8.77	9.36
20020906	01	2058.58	48.69	-123.04	14	11.9	10.0
20020906	05	2524.63	49.04	-123.34	21	9.46	8.62
20020906	11	2365.16	48.92	-123.87	23	7.23	8.21
20020906	11	2597.85	48.80	-123.69	24	8.58	12.5
20020906	11	2780.63	48.68	-123.28	5	9.42	12.7
20020906	21	2682.14	48.60	-123.55	7	6.80	9.50
20020907	08	1586.46	48.72	-123.70	11	9.75	8.68
20020907	21	3168.29	48.77	-123.16	9	9.36	13.9
20020908	18	3479.92	48.79	-123.53	34	12.4	8.65
20020910	15	1685.14	48.59	-123.40	16	6.03	9.96
20020911	04	3535.45	48.63	-123.48	5	8.62	11.8
20020911	10	3116.63	48.59	-123.36	7	8.21	10.3
20020911	21	1922.54	48.67	-123.39	6	10.5	9.97
20020912	19	108.460	48.92	-123.32	9	7.79	9.20
20020913	10	2022.65	48.85	-123.50	36	5.50	8.01
20020913	14	2013.03	49.02	-123.35	27	8.68	9.72
20020913	22	2825.84	48.75	-123.83	31	8.86	8.19
20020915	08	2972.06	48.40	-123.27	7	10.9	12.6
20020916	02	640.010	49.28	-124.1	7	11.8	10.1
20020916	03	1029.37	48.42	-123.20	24	9.03	8.2
20020916	04	3215.32	48.76	-123.47	17	7.41	8.58
20020916	05	270.614	48.45	-123.46	6	6.93	10.3
20020916	06	756.650	48.72	-123.68	23	7.74	9.04
20020916	10	2320.27	48.65	-123.27	8	6.84	9.14
20020916	10	2405.54	48.86	-122.87	8	5.79	8.87
20020916	10	2506.25	48.62	-123.35	5	6.82	9.56
20020916	21	3267.46	48.90	-122.78	27	8.61	7.86
20020918	08	51.3500	48.80	-123.32	5	6.16	10.0
20020918	11	229.530	48.61	-123.58	5	7.47	11.3
20020920	21	1516.44	48.60	-123.16	19	7.69	9.44
20020921	00	3332.00	48.67	-123.58	6	5.93	10.8

Table B.2: September 2002 tremors

September 2002 locations							
Date yyyymmdd	hour hr	seconds after hour	lat (^{o})	lon (^{o})	depth (km)	dh (km)	dz (km)
20020921	01	2655.10	48.66	-123.54	7	7.78	10.5
20020921	02	776.030	48.66	-123.54	5	8.85	9.06
20020921	03	338.660	48.75	-123.42	33	7.11	8.66
20020921	04	1332.70	48.68	-123.43	5	9.64	10.2
20020921	07	664.440	48.67	-123.12	7	10.5	9.70
20020921	08	460.680	48.66	-123.29	8	6.02	9.60
20020921	08	864.920	48.72	-123.44	10	9.09	8.37
20020921	16	1588.05	48.70	-123.63	5	5.62	9.43
20020921	17	1634.87	48.62	-123.50	6	8.17	9.95
20020922	03	1040.60	48.59	-123.54	6	7.03	9.68
20020922	05	907.120	48.68	-123.59	5	10.9	10.4
20020923	13	2562.60	48.60	-123.54	7	10.2	11.4
20020924	17	1534.68	49.07	-122.80	14	7.20	9.63
20020924	22	2581.29	49.11	-123.54	41	8.37	9.42
20020925	01	1530.00	49.20	-123.46	24	8.71	8.03
20020925	02	2172.77	48.63	-122.98	8	6.46	7.51
20020925	04	328.040	48.55	-123.58	5	5.42	9.62
20020925	05	1880.73	48.79	-123.39	9	6.97	10.6
20020925	05	2177.95	48.91	-123.40	18	5.04	9.20
20020925	07	1896.26	48.55	-123.55	7	3.27	9.48
20020925	08	3327.34	48.79	-123.32	15	6.97	8.60
20020925	10	2057.96	48.77	-123.29	9	6.66	9.25
20020925	18	1324.71	48.64	-123.65	5	6.37	10.6
20020925	18	821.620	48.78	-123.73	21	9.26	7.92
20020925	19	3234.74	49.22	-123.08	31	11.0	8.48
20020926	10	1667.12	48.79	-123.59	7	10.4	9.83
20020926	19	388.140	48.98	-123.57	39	6.44	9.17
20020927	06	742.180	48.51	-123.32	5	5.81	9.40
20020927	13	894.240	48.72	-123.28	6	7.87	10.7
20020927	14	1151.03	48.58	-122.78	28	8.27	9.14
20020927	22	1345.94	48.48	-123.44	12	9.79	8.21
20020928	06	1375.36	48.72	-123.28	5	8.52	10.2
20020928	08	1824.34	49.08	-124.05	14	6.88	8.60
20020930	06	3198.15	48.72	-122.59	8	7.01	11.0
20020930	11	1341.52	48.66	-123.55	7	7.86	9.64

Table B.3: September 2002 tremors

Appendix C

IMPLEMENTING SOURCESCAN

C.1 PROGRAM AND SCRIPTS

In this appendix I will describe the methods, scripts and programs I have implemented to obtain, preprocess, and image tremor waveform data. Several scripts and programs written by other researchers have been used, and will referred to but not included. They may be obtained directly from their authors, and are as follows:

`mkPmodel_new.f` (H. Kao): Converts a 3D *P*-wave velocity model to a C binary input file `velP3d_new` required by the 3D raytracing program `punch.c`.

`punch.c` (J. Hole and C. Zelt): Calculates first arrival travel times within a gridded 3-D velocity model [16]. `pnch.par` and `velP3d_new` are the required input files.

`pnch.par` (J. Hole and C. Zelt): Parameter file for `punch.c`, specifying the name and size of the velocity model and the grid size of the volume discretization.

`mkPref.csh` (H. Kao): Script to calculate the reference *P*-wave velocity travel-times from each seismograph station to each grid point in the scanning volume. Station names, (*x*, *y*, *z*) positions and latitude-longitude coordinates are read from an input file `station.dat`, of the form

```
LZB  159.2930   265.3800   -0.8440   48.6117   -123.8236
MGB  95.8430    221.1600   -1.3000   49.0000   -124.6975
NAB  146.9000   197.3600   -0.2560   49.2222   -124.0039
```

and `punch.c` is executed. Travel-time reference files are named according to their reference station and corresponding phase velocity.

`mkSref.f` (H. Kao): Reads in a *P*-wave velocity travel-time reference file and multiplies the travel-time by 1.73 to produce the corresponding *S*-wave velocity travel-time reference file. Travel-time reference files are named according to their reference station and corresponding phase velocity.

`sacssplot_040616.f` (H. Kao): Generates a SAC (Seismic Analysis Code) macro (`readsta.m`) to plot, decimate (sample interval=0.1 s), and high-pass filter the vertical-component seismograms. Seismograph station instrument response files must be first acquired from the National Waveform Archive [38], which are used to transform waveforms to a unified instrument.

`preSS_040621.f` (H. Kao): Reads in a series of SAC-format filtered waveform files, normalizes the waveforms, and outputs two ASCII-format waveform files used by sourcescan to calculate 'brightness' values. The first contains normalized waveform absolute amplitudes (*.obs1), the second contains normalized waveform envelopes (*.env1).

`sourcescanV040531.f` (H. Kao): Tremor source-scanning algorithm, which scans through a set of seismograms for coherent signals and locates the corresponding source point [25].

`sourcescan.inc` (H. Kao): Include file for `sourcescanV040531.f`, which provides the dimensions of the scanning volume and the number of grid elements in the volume discretization.

I have written the following programs and scripts to supplement the above programs and produce an automated method to obtain tremor waveforms and image tremor events efficiently on the WestGrid cluster facility at the University of British Columbia [53].

`reqfile.csh`: Requests the waveform data from the National Waveform Archive [38].

`sacdir.csh`: Organizes the waveform data into directories according to their date and time.

`hpsac.csh`: Submits the SAC waveform data to `sacssplot_040616.f`.

`runpress.csh`: Generates the input files for `preSS_040621.f`.

`mkinput.csh`: Generates the input files for `sourcescanV040531.f`.

`mkrun.csh`: Submits the `sourcescanV040531.f` jobs to run on the WestGrid cluster.

`fmparm.csh`: Identifies *x*-, *y*-, and *z*-positions and occurrence times corresponding to large brightness values in the output files of the first run of `sourcescanV040531.f`.

`fm.c`: Used by `fmparm.csh` to identify spatial positions and occurrence times corresponding to brightness values above a specified brightness threshold.

`disc.csh`: Defines the spatial range and time period for scanning in the second run of sourcescan.

`disc1.c`: Used by `disc.csh`.

`disc2.c`: Used by `disc.csh`.

`frparm.csh`: Generates the input files for second run of `sourcescanV040531.f`.

`fr.c`: Used by `frparm.csh`.

`findmax.csh`: Generates the input files for final run of `sourcescanV040531.f`.

`maxbri.c`: Used by `findmax.csh`.

C.2 SETUP

The user must first

1. download and install the Seismic Analysis Code (SAC)

   `http://www.llnl.gov/sac/`

2. download and install `rdseed`

   `http://www.iris.edu/pub/programs/`

3. download and install Generic Mapping Tool (GMT)

   `http://gmt.soest.hawaii.edu/`

Several directories will need to be generated. As an example, I suggest the following:

1. `/tremor/src`
2. `/tremor/bin`
3. `/tremor/velmodel`
4. `/tremor/allref/P`
5. `/tremor/allref/S`
6. `/tremor/sac`
7. `/tremor/obs1`
8. `/tremor/env1`
9. `/tremor/input`
10. `/tremor/output5sec`
11. `/tremor/output0.1sec`
12. `/tremor/outputssfnl`
13. `/tremor/polezero`

Program executables and scripts should be placed in `/tremor/bin`. The paths to `sac`, `rdseed`, `gmt`, and `/tremor/bin` should be defined in `.cshrc` so that programs may be executed in all directories.

VELOCITY MODELS

A 3-D *P*-wave velocity model for northern Cascadia, `velocity-merged.dat_z87km`, was first acquired from K. Ramachandran [42]. `mkPmodel_new.f` was executed to produce a direct-access C-binary *P*-wave velocity model named `velP3d_new` of (x, y, z) dimensions $361 \times 451 \times 91$ km with a grid-size of 1 km.

WAVEFORM DATA

Waveform data from available CNSN and broad-band seismograph stations in southwestern British Columbia were requested and downloaded from the National Waveform Archive [38] in one-hour time-interval segments by executing `reqfile.csh`. The instrument response files for available stations were downloaded from the Canadian National Seismograph Network [37], and placed in `/tremor/polezero`. Seismograms are downloaded in seed-format, and are converted to SAC-format using the `rdseed` program. The script `sacdir.csh` executes `rdseed` and places SAC-format waveforms in directories corresponding to their dates and times, for example, `/day/hour`. The seismograph station position file `station.dat` was generated using information available from the Canadian National Seismograph Network website [37]. The Generic Mapping Tool (GMT) was used to convert latitudes and longitudes to (x, y, z) positions.

```
#!/bin/csh -f
# reqfile.csh
# Gillian Royle
# Generates the email request files for waveform data
# from specified stations for the specified day. Data are
# downloaded in one-hour time intervals. This example generates
# the request from stations LZB, MGB, NAB, for Feb.1/2002.
set year = 2002
set month = 02
set day = 01
set hr = 0
set sec = 0000
set mail = gtroyle@sfu.ca
set sta = 'LZB MGB NAB'
while ( $hr <= 23)
  while ($hr <= 9)
    echo "BEGIN" > req_$year$month$day'0'$hr
    echo "EMAIL "$mail >> req_$year$month$day'0'$hr
    echo "DATE1 "$year$month$day'0'$hr$sec >> \
req_$year$month$day'0'$hr
    echo "DUR 3600" >> req_$year$month$day'0'$hr
    echo "FORMAT SEED" >> req_$year$month$day'0'$hr
    echo "STA_LIST "$sta >> req_$year$month$day'0'$hr
    echo "CHA_LIST *Z" >> req_$year$month$day'0'$hr
```

```
    echo "WAVEFORM" >> req_$year$month$day'0'$hr
    echo "STOP" >> req_$year$month$day'0'$hr
    @ hr = $hr + 1
  end
  echo "BEGIN" > req_$year$month$day$hr
  echo "EMAIL "$mail >> req_$year$month$day$hr
  echo "DATE1 "$year$month$day$hr$sec >> req_$year$month$day$hr
  echo "DUR 3600" >> req_$year$month$day$hr
  echo "FORMAT SEED" >> req_$year$month$day$hr
  echo "STA_LIST "$sta >> req_$year$month$day$hr
  echo "CHA_LIST *Z" >> req_$year$month$day$hr
  echo "WAVEFORM" >> req_$year$month$day$hr
  echo "STOP" >> req_$year$month$day$hr
@ hr = $hr + 1
end
set finp = `/bin/ls req_*`
foreach file ($finp)
  echo "mailx -s "data" autodrm@seismo.nrcan.gc.ca <" $file \
>>request
  echo "sleep 600" >> request
end
chmod +x request

#!/bin/csh
# sacdir.csh
# Gillian Royle
# Reads seed-format data and outputs sac-format data.
# Uses rdseed.
# Renames the waveform file by recording station and date.
# Places in a directory labelled by the day and hour of the data.
set flist = `ls CNSN_*.*`
foreach file ($flist)
  `/global/home/gtroyle/rdseed/rdseed -d -f $file -o 1`
  set saclist = `ls *.SAC`
  foreach sfile ($saclist)
    set ddir = `echo $sfile | cut -c6-8`
    set hdir = `echo $sfile | cut -c10-11`
    set sdir = `echo $sfile | cut -c13-14`
    set sacstnm = `echo $sfile | cut -c27-29`
    set saccmpt = `echo $sfile | cut -c32-34`
    set sacfnm = `echo $sacstnm.$saccmpt | tr "[A-Z]" "[a-z]"`
    mv $sfile $sacfnm
    mkdir $ddir
```

```
    cd $ddir
    mkdir $hdir'_'$sdir
    cd ..
    mv $sacfnm $ddir'/'$hdir'_'$sdir
    cp $file $ddir'/'$hdir'_'$sdir
  end
  rm rdseed.err*
  mkdir CNSN
  mv CNSN_* CNSN
end
```

REFERENCE TRAVEL-TIME FILES

`mkPref.csh` was executed to calculate the reference travel-time files from each seismograph station to each grid point in the scanning volume. `mkPref.csh` inputs `velP3d_new`, `station.dat`, and `pnch.par` to `punch.c`. The travel-time reference files corresponding to the *P*-wave velocity model were placed in `/allref/P`. Travel-times corresponding to *S*-wave velocities were subsequently calculated by executing `mkSref.f` and placed in `/allref/S`.

WAVEFORM PREPROCESSING

In directories containing SAC waveform files, `hpsac.csh` was executed to generate the file `fn_list` that is input to `sacssplot_040616.f`. `fn_list` specifies the sampling interval and vertical-component waveforms for `sacssplot_040616.f`, which then generates the SAC macro `readsta.m` that decimates and high-pass filters the waveform files. The following lines of `sacssplot_040616.f` will need to be specified:

- lines 28 and 35: give the correct path to `station.dat`.
- lines 185, 187, 201, and 206: give the correct path to `/tremor/polezero`.

```
#!/bin/csh
# hpsac.csh
echo S >! fn_list # S for southern Vancouver Island target area
echo 0.1 >> fn_list  # specify 0.1 sampling interval of output
ls *z >> fn_list  # take vertical component waveforms
sacssplot < fn_list  # create SAC macro \texttt{readsta.m}
sac readsta.m  # run \texttt{readsta.m} to output filtered waveforms
# (filtered waveforms end with extension \texttt{dec_hp}).
```

The waveform data is then normalized. Input files for `preSS_040621.f` are first generated, and have the extension `*.preSS`. The first line indicates the beginning hour, minute and second, the total duration of the waveform (in seconds), the N-th root factor for data processing (refer to Section C.6), and the normalization type (-1 indicates no normalization, 0 indicates linear normalization

with two standard deviations, 1 indicates mean linear normalization with the maximum amplitude being this positive value). For example, to apply a linear normalization with two standard deviations to waveforms recorded at 12:00:0.0 on February 1, 2002 and lasting 3600 s, use the following commands:

```
echo 12 0 0.0 3600 1 0 >! 2002032_1200.preSS
ls *hp >> 2002032_1200.preSS
echo 2002032_1200.preSS | preSS
```

The input files for `preSS_040621.f` are named according to the date and hour of the waveform data, of the form `yearjulianday_hour.preSS`.

```
#!/bin/csh
# runpress.csh
# script to make .preSS input file and run preSS
# Gillian Royle
# Example generates the *.preSS files and runs preSS for data
# acquired over the entire day of February 1, 2002 (julian day 032)
# applying a linear normalization with two standard deviations.
# note: assume the starting directory is /tremor/sac/032/00_00
set yr = 2002
set day = 032
set hour = `pwd | cut -c17-18`
while ( $hour <= 23)
    while ($hour <= 9)
      set hr = `echo $hour | cut -c2-2`
      set fnm = $yr$day_0$hr'00'
      echo $hr 0 0.0 3600 1 0 >! $fnm.preSS
      ls *hp >> $fnm.preSS
      echo *.preSS | /tremor/bin/preSS
      mv *obs* /tremor/obs1
      mv *env* /tremor/env1
      @ hour = $hour + 1
      cd ../$hour_00
    end
    set hr = `echo $hour | cut -c1-2`
    set fnm = $yr$day_$hr'00'
    echo $hr 0 0.0 3600 1 0 >! $fnm.preSS
    ls *hp >> $fnm.preSS
    echo *.preSS | /tremor/bin/preSS
    mv *obs* /tremor/obs1
    mv *env* /tremor/env1
    @ hr = $hr + 1
    cd ../$hour_00
```

`end`

The are four ASCII output files are:

1. `2002032_1200.obs1`: contains the normalized trace amplitudes
2. `2002032_1200.obs1_abs`: contains the absolute trace amplitudes
3. `2002032_1200.env1`: contains the envelopes of the normalized trace amplitudes, calculated by taking a 25-point running average of normalized amplitudes
4. `2002032_1200.env1_abs`: contains the envelopes of the absolute trace amplitudes, calculated by taking a 25-point running average of absolute amplitudes

All `*.obs1` files are placed in `/tremor/obs1` and all `*.env1` files in `/tremor/env1`.

C.3 THE FIRST RUN OF SOURCESCAN

As outlined in Chapter 2, `sourcescanV040531.f` is applied to the waveform data in three stages. In the first run, waveform data are scanned at a time interval of 5 s, and a spatial grid interval of 10 km.

INPUT FILES FOR THE FIRST RUN

The input files for `sourcescanV040531.f` should be generated in the directory `/tremor/input`, and are labelled according to the date and time of the waveform data to be scanned (for example, `2002032_1200.input`. For this example, `2002032_1200.input` should be,

```
0.0 3600.0 2.5 5.0 1 1 0 0.7 1 1 1.0 70.0 100.0 1
1 361 1 451 1 91 10
/tremor/allref/S
2002032_1200.obs1  (or 2002032_1200.env1)
/tremor/output5sec/2002032_1200.out
/tremor/station.dat
/tremor/allref/S/1D_S
```

The format is (refer to Section C.6 for lines 1 and 2):

- Line1: t1min t1max dt1 dtwindow ilim iweight igrid bthre mbf Nroot stthre ttmax rlim ioutrlim
- Line2: ixmin ixmax iymin iymax izmin izmax kmint
- Line3: path_to_ref_files
- Line4: filename_of_input_waveforms (normalized waveforms or envelopes)
- Line5: filename_of_output

- Line6: filename_of_station_coordinates_in_X/Y/Z
- Line7: filename_of_traveltime_table_of_1D_velocity_model

Note: Lines 6 and 7 are needed only when the 3-D travel time reference files for one or more stations can not be found in the path_to_ref_files (line 3) directory. The input files for `sourcescanV040531.f` may be generated using one script `mkinput1.csh` within the directory of either the *.obs1 files or the *.env1 files `/tremor/obs1` or `tremor/env1`.

```
#!/bin/csh
# mkinput.csh
# script to make .input files for sourcescan
# Gillian Royle
# Generates the *.input files first run of sourcescan
# for *.obs1 files of the form 2002032_1200.obs1
set finp = '/bin/ls *.obs1'
foreach file ($finp)
  set yrdaytime = 'echo $file | cut -c1-12'
  echo 0.0 3600.0 2.5 5.0 1 1 0 0.7 1 1 1.0 70.0 100.0 1 > \
$yrdaytime.input
  echo 1 361 1 451 1 91 10 >> $yrdaytime.input
  echo /tremor/allref/S >> $yrdaytime.input
  echo $file >> $yrdaytime.input
  echo /tremor/output5sec/$yrdaytime.out >> $yrdaytime.input
  echo /tremor/station.dat >> $yrdaytime.input
  echo /tremor/allref/S/1D_S >> $yrdaytime.input
end
```

`sourcescanV040531.f` is run on the WestGrid cluster facility at the University of British Columbia. The program `sourcescanV040531.f` is not yet parallelized, so one node of the cluster is used for each job submitted. Input files must be generated to submit jobs (execute `sourcescanV040531.f`) on the cluster. These are generated using the script `mkrun1.csh`, which is executed in the directory containing the *.input files.

```
#!/bin/csh
# mkrun1.csh
# script to generate run scripts for sourcescan jobs
# Gillian Royle
# Generates the submit scripts for the first run of sourcescan
# for *.obs1 files of the form 2002032_1200.obs1
#!/bin/csh
# mkrun.csh
set finp = '/bin/ls *.input'
foreach file ($finp)
  set date = 'echo $file | cut -c1-7'
```

```
  set day = `echo $date | cut -c5-7`
  set hr = `echo $file | cut -c9-12`
  echo '#PBS -S /bin/csh' >> 'r'$day'_'$hr.csh
  echo '#PBS -o $date'_'$hr.out' >> 'r'$day'_'$hr.csh
  echo '#PBS -e $date'_'$hr.err' >> 'r'$day'_'$hr.csh
  echo '#PBS -q ice' >> 'r'$day'_'$hr.csh
  echo '#PBS -l walltime=2:00:00' >> 'r'$day'_'$hr.csh
  echo 'cd /tremor/input' >> 'r'$day'_'$hr.csh
  echo 'time /tremor/bin/sourcescan < /tremor/input/'$finp >> \
'r'$day'_'$hr.csh
end
```

To submit all jobs to the queue:

```
set runlist = `/bin/ls r*.csh`
foreach file ($runlist)
  qsub $file
end
```

C.4 THE SECOND RUN OF SOURCESCAN

SORTING THROUGH OUTPUT FILES

Once the first run of `sourcescanV040531.f` has completed, the output files have the form:

```
5.00000  191  171    4  0.5657  0.4017  0.0334    -24.55   7   4   7 T LZB
10.00000 251  171   14  0.5157  0.3556  0.0325    -27.47   7   4   7 T LZB
15.00000 211  241    4  0.4866  0.3729  0.0222     -4.16   7   3   7 T LZB
20.00000 211  241    4  0.4518  0.3591  0.0180      0.84   7   3   7 T LZB
25.00000  61  321   14  0.4387  0.3635  0.0200     -6.62   7   4   7 T LZB
30.00000 111  351   44  0.4424  0.3609  0.0237      2.48   7   4   7 T VGZ
35.00000 171  341   24  0.4515  0.3821  0.0215     12.99   7   2   7 T VGZ
```

The output files are scanned for brightness values in excess of a specified brightness threshold. `fmparm.csh` is executed, which isolates output files with large brightness values and moves them to a directory labelled by the brightness threshold (for example, the directory bthre0.7 contains output files with brightness values equal or greater than 0.7).

```
#!/bin/csh -f
# This script isolates times and locations corresponding
# to large brightness values
# fmparm.csh
# Gillian Royle
set finp = `/bin/ls *.out`
foreach file ($finp)
```

```
  set fn = `echo $file | cut -c1-12`
  set line = `awk 'END {print NR}' $file`
  awk '{print $1, $2, $3, $4, $5}' < $file > findmax.in
  echo $line | fm
  set tloc = `awk '{print $1}' 'findmax.out'`
  set tfin = `echo $tloc[1] | cut -c1-6`
  mv findmax.out $fn'_'$tfin.out
  mv $fn'_'$tfin.out bthre0.7
  rm findmax.in
end
```

`fmparm.csh` uses the program `fm.c`.

```
# Program: fm.c
#include <stdio.h>
#include <math.h>
#define INPUT "findmax.in"
#define OUTPUT "findmax.out"

int main(void)
{
int *xloc,*yloc,*zloc,i=0,j=0,line;
int line;
double *tloc,*bri;
FILE *input;
FILE *output;
input = fopen(INPUT,"r");
output = fopen(OUTPUT,"w");
scanf("%i", &mem);
xloc=(int *)malloc(mem*(sizeof(int)));
yloc=(int *)malloc(mem*(sizeof(int)));
zloc=(int *)malloc(mem*(sizeof(int)));
tloc=(double *)malloc(mem*(sizeof(double)));
bri=(double *)malloc(mem*(sizeof(double)));
for (i=0; i<=(mem-1); i++) {
  fscanf(input,"%lf %i %i %i %lf\n", &tloc[i],&xloc[i],&yloc[i],\
&zloc[i],&bri[i]);
  }
for (j=0; j <= (mem-1); j++) {
  while (bri[j] > 0.7) {
    fprintf(output,"%lf %i %i %i %lf\n", tloc[j],xloc[j],yloc[j],\
zloc[j],bri[j]);
    j++;
    }
```

```
  }
fclose(input);
fclose(output);
free(xloc);
free(yloc);
free(zloc);
free(tloc);
free(bri);
return 0;
}
```

Output files in the directory bthre0.7 are scanned to determine the time interval of temporally-consecutive large brightness values. Tremor events typically last 30 s to a minute. In each output file, the x-, y-, and z-positions and occurrence times corresponding to consecutive brightness values equal or greater than 0.7 over a time period of at least 30 s were isolated by executing `disc.csh`.

```
#!/bin/csh -f
# determines the time interval over which large brightness values
# are measured.
# disc.csh
set filein = `/bin/ls *.out`
foreach file ($filein)
  set line = `awk 'END {print NR}' $file`
  set fn = `echo $file | cut -c1-12`
  awk '{print $1, $2, $3, $4, $5}' < $file > findrange.in
  set beg = 1
  echo $beg $line | disc1
  set linemax2 = `awk 'END {print NR}' < max2.out`
  echo $linemax2 | disc2
  unset linemax2
  set tloc = `awk '{print $(NF-4)}' 'max3.out'`
  set tshort = `echo $tloc[1] | cut -c1-6`
  set finp = $fn'_'$tshort.disc
  mv max3.out $finp
  rm max2.out
  set linemax3 = `awk 'END {print NR}' < $finp`
  @ acc = $linemax3 + 1
  while ( $acc <= $line)
    echo $acc $line | disc1
    unset linemax3
    set linemax2 = `awk 'END {print NR}' < max2.out`
    echo $linemax2 | disc2
    unset linemax2
    set tloc = `awk '{print $(NF-4)}' 'max3.out'`
```

```
    set tshort = `echo $tloc[1] | cut -c1-6`
    set finp = $fn'_'$tshort.disc
    mv max3.out $finp
    rm max2.out
    set linemax3 = `awk 'END {print NR}' < $finp`
    @ acc = $acc + $linemax3
    unset tloc
    unset tshort
    unset finp
  end
rm findrange.in
end
```

disc.csh uses the two programs disc1.c and disc2.c.

```
# disc1.c
#include <stdio.h>
#include <math.h>
#define INPUT "findrange.in"
#define OUTPUT "max2.out"

int main(void)
{
int *xloc,*yloc,*zloc,i=0,j=0,k=0,beg,mem;
double *tloc, *bmax;
FILE *input;
FILE *output;
input = fopen(INPUT,"r");
output = fopen(OUTPUT,"w");
scanf("%i %i", &beg, &mem);
xloc=(int *)malloc(mem*(sizeof(int)));
yloc=(int *)malloc(mem*(sizeof(int)));
zloc=(int *)malloc(mem*(sizeof(int)));
tloc=(double *)malloc(mem*(sizeof(double)));
bri=(double *)malloc(mem*(sizeof(double)));
if (mem == 1) {
  fscanf(input,"%lf %i %i %i %lf\n",&tloc[0],&xloc[0],&yloc[0],\
&zloc[0],&bmax[0]);
  fprintf(output,"%lf %i %i %i %lf\n",tloc[0],xloc[0],yloc[0],\
zloc[0],bmax[0]);
  }
else if (beg == mem) {
  for (i=0; i<=(mem-1); i++) {
    fscanf(input,"%lf %i %i %i %lf\n",&tloc[i],&xloc[i],&yloc[i],\
```

```
&zloc[i],&bmax[i]);
    }
  fprintf(output,"%lf %i %i %i %lf\n",tloc[mem-1],xloc[mem-1],\
yloc[mem-1],zloc[mem-1],bmax[mem-1]);
  }
else {
  for (j=0; j<=(mem-1); j++) {
    fscanf(input,"%lf %i %i %i %lf\n", &tloc[j],&xloc[j],&yloc[j],\
&zloc[j],&bmax[j]);
    }
  for (k=beg; k<=(mem-1); k++) {
  if (tloc[k] - tloc[k-1]>30 ) {
    fprintf(output,"%lf %i %i %i %lf\n",tloc[k-1],xloc[k-1],yloc[k-1],\
zloc[k-1],bmax[k-1]);
    break;
    }
  else {
    if (tloc[k] - tloc[k-1]<=30 ) {
      fprintf(output,"%lf %i %i %i %lf\n", tloc[k-1],xloc[k-1],\
yloc[k-1],zloc[k-1],bmax[k-1]);
      fprintf(output,"%lf %i %i %i %lf\n", tloc[k],xloc[k],yloc[k],\
zloc[k],bmax[k]);
      }
    }
  }
}
fclose(input);
fclose(output);
free(xloc);
free(yloc);
free(zloc);
free(tloc);
free(bri);
return 0;
}

# disc2.c
#include <stdio.h>
#include <math.h>
#define INPUT "max2.out"
#define OUTPUT "max3.out"

int main(void)
```

```
{
int *xloc, *yloc, *zloc, j=0, k=0, mem;
double *tloc, *bmax;
FILE *input;
FILE *output;
input = fopen(INPUT,"r");
output = fopen(OUTPUT,"w");
scanf("%i", &mem);
xloc=(int *)malloc(mem*(sizeof(int)));
yloc=(int *)malloc(mem*(sizeof(int)));
zloc=(int *)malloc(mem*(sizeof(int)));
tloc=(double *)malloc(mem*(sizeof(double)));
bri=(double *)malloc(mem*(sizeof(double)));
if (mem==1) {
  fscanf(input,"%lf %i %i %i %lf\n", &tloc[0],&xloc[0],&yloc[0],\
&zloc[0],&bmax[0]);
  fprintf(output,"%lf %i %i %i %lf\n", tloc[0],xloc[0],yloc[0],\
zloc[0],bmax[0]);
  }
else if (mem == 2) {
  for (j=0; j<=(mem-1); j++) {
    fscanf(input,"%lf %i %i %i %lf\n", &tloc[j],&xloc[j],&yloc[j],\
&zloc[j],&bmax[j]);
    fprintf(output,"%lf %i %i %i %lf\n", tloc[j],xloc[j],yloc[j],\
zloc[j],bmax[j]);
    }
  }
else {
  for (j=0; j<=(mem-1); j++) {
    fscanf(input,"%lf %i %i %i %lf\n", &tloc[j],&xloc[j],&yloc[j],\
&zloc[j],&bmax[j]);
    }
  for (k=0; k<=(mem-2); k=k+2) {
    fprintf(output,"%lf %i %i %i %lf\n", tloc[k],xloc[k],yloc[k],\
zloc[k],bmax[k]);
    }
  fprintf(output,"%lf %i %i %i %lf\n", tloc[mem-1],xloc[mem-1],\
yloc[mem-1],zloc[mem-1],bmax[mem-1]);
  }
fclose(input);
fclose(output);
free(xloc);
```

```
free(yloc);
free(zloc);
free(tloc);
free(bri);
return 0;
}
```

Once all the large brightness files have been discretized into time-intervals and regions (x-, y-, and z-positions) of interest, a new set of input files are generated for the second run of `sourcescanV040531.f`. These input files specify the scanning time interval and subvolume specified by occurrence times and positions corresponding to large brightness values. For the second run, a time step of 0.1 s and grid spacing of 1 km is used by `sourcescanV040531.f`.

```
#!/bin/csh -f
# This generates the revised input files for
# the second run of sourcescan
# frparm.csh
# Gillian Royle
set finp = `/bin/ls *.disc`
foreach file ($finp)
  set fn = `echo $file | cut -c1-12`
  set line = `awk 'END {print NR}' $file`
  awk '{print $1, $2, $3, $4, $5}' < $file > findrange.input
  echo $line | fr
  set tmin = `awk '{print $(NF-1)}' 'findtime.output'`
  set tmax = `awk '{print $NF}' 'findtime.output'`
  set ttmin = `echo $tmin | cut -c1-6`
  set ttmax = `echo $tmax | cut -c1-6`
  set xmin = `awk '{print $(NF-5)}' 'findrange.output'`
  set xmax = `awk '{print $(NF-4)}' 'findrange.output'`
  set ymin = `awk '{print $(NF-3)}' 'findrange.output'`
  set ymax = `awk '{print $(NF-2)}' 'findrange.output'`
  set zmin = `awk '{print $(NF-1)}' 'findrange.output'`
  set zmax = `awk '{print $NF}' 'findrange.output'`
  echo $ttmin $ttmax 0.1 2.5 1 1 0 0.7 1 1 1.0 250 150.0 1 >! \
$fn'_'$ttmin.input
  echo $xmin $xmax $ymin $ymax $zmin $zmax 1 >> \
$fn'_'$ttmin.input
  echo '/tremor/allref/S' >> $fn'_'$ttmin.input
  echo '/tremor/obs1/'$fn.obs1 >> $fn'_'$ttmin.input
  echo '/tremor/output0.1sec/'$fn'_'$ttmin.out >> \
$fn'_'$ttmin.input
  echo '/tremor/station.dat' >> $fn'_'$ttmin.input
```

```
  echo '/tremor/allref/S/1D_S' >> $fn'_'$ttmin.input
  rm findrange.input
  rm findrange.output
  rm findtime.output
end
```

The x, y, and z spatial ranges for the second run of `sourcescanV040531.f` are defined using the program `fr.c`.

```
# fr.c
#include <stdio.h>
#include <math.h>
#define INPUT "findrange.input"
#define OUTPUTRANGE "findrange.output"
#define OUTPUTTIME "findtime.output"

int main(void)
{
int *xloc,*yloc,*zloc,xmax,xmin,ymax,ymin,zmax,zmin,i=0;
int npts,mem;
double *tloc,*bmax,tmin,tmax,tfmin,tfmax;
scanf("%i", &mem);
npts = mem-1;
xloc = (int *)malloc(mem*(sizeof(int)));
yloc = (int *)malloc(mem*(sizeof(int)));
zloc = (int *)malloc(mem*(sizeof(int)));
tloc = (double *)malloc(mem*(sizeof(double)));
bmax = (double *)malloc(mem*(sizeof(double)));
FILE *input;
FILE *outputr;
FILE *outputt;
int min_x(int x[], int n);
int min_y(int y[], int n);
int min_z(int z[], int n);
int max_x(int x[], int n);
int max_y(int y[], int n);
int max_z(int z[], int n);
input = fopen(INPUT,"r");
outputr = fopen(OUTPUTRANGE,"w");
outputt = fopen(OUTPUTTIME,"w");
for (i=0; i<=npts; i++) {
  fscanf(input,"%lf %i %i %i %lf\n", &tloc[i],&xloc[i],&yloc[i],\
&zloc[i],&bmax[i]);
  }
```

```
tmin = tloc[0];
if (tmin < 20.0000) {
  tmin = 20.0000;
  }
tfmin = tmin - 20;
tmax = tloc[npts];
if (tmax > 3580.00) {
  tmax = 3580.00;
  }
tfmax = tmax + 20;
fprintf(outputt,"%lf %lf", tfmin, tfmax);
fprintf(outputr,"%i %i %i %i %i %i", min_x(xloc, npts), \
max_x(xloc, npts),min_y(yloc, npts), max_y(yloc, npts), \
min_z(zloc, npts), max_z(zloc, npts));
fclose(input);
fclose(outputr);
fclose(outputt);
return 0;
}
/*-------------------------------------------------------------*/
/* Function to return min value of x */
int min_x(int xloc[], int n)
{
int j;
int xmin;
xmin = xloc[0];
for (j=1; j<=n; j++) {
  if (xloc[j] < xmin) {
    xmin = xloc[j];
    }
  }
if (xmin < 101) {
  xmin = 101;
  }
return xmin - 100;
}
/*-------------------------------------------------------------*/
/* Function to return min value of y */
int min_y(int yloc[], int n)
{
int k;
int ymin;
```

```
ymin = yloc[0];
for (k=1; k<=n; k++) {
  if (yloc[k] < ymin) {
    ymin = yloc[k];
    }
  }
if (ymin < 101) {
  ymin = 101;
  }
return ymin - 100;
}
/*-------------------------------------------------------------*/
/* Function to return min value of z */
int min_z(int zloc[], int n)
{
int l;
int zmin;
zmin = zloc[0];
for (l=1; l<=n; l++) {
  if (zloc[l] < zmin) {
    zmin = zloc[l];
    }
  }
if (zmin < 81) {
  zmin = 81;
  }
return zmin - 80;
}
/*-------------------------------------------------------------*/
/* Function to return max value of x */
int max_x(int xloc[], int n)
{
int m;
int xmax;
xmax = xloc[0];
for (m=1; m<=n; m++) {
  if (xloc[m] > xmax) {
    xmax = xloc[m];
    }
  }
if (xmax > 261) {
  xmax = 261;
```

```
  }
return xmax + 100;
}
/*-------------------------------------------------------------*/
/* Function to return max value of y */
int max_y(int yloc[], int n)
{
int q;
int ymax;
ymax = yloc[0];
for (q=1; q<=n; q++) {
  if (yloc[q] > ymax) {
    ymax = yloc[q];
    }
  }
if (ymax > 351) {
  ymax = 351;
  }
return ymax + 100;
}
/*-------------------------------------------------------------*/
/* Function to return max value of z */
int max_z(int zloc[], int n)
{
int p;
int zmax;
zmax = zloc[0];
for (p=1; p<=n; p++) {
  if (zloc[p] > zmax) {
    zmax = zloc[p];
    }
  }
if (zmax > 17) {
  zmax = 17;
  }
return zmax + 80;
}
/*-------------------------------------------------------------*/
```

All previous input files in `/tremor/input` should be erased and replaced by the input files for the second run of `sourcescanV040531.f`. All jobs for the second run may be submitted to the cluster by again executing `mkrun1.csh`, followed by the commands:

```
set runlist = '/bin/ls r*.csh'
```

```
foreach file ($runlist)
  qsub $file
end
```

C.5 THE THIRD RUN OF SOURCESCAN

Once the output files for the second run of `sourcescanV040531.f` are generated, a unique tremor origin time and refined spatial range must be defined for the third and final run. This involves searching through the output files and finding the origin time that corresponds to the largest tremor brightness. The spatial range is generated by taking the grid-point location corresponding to the largest brightness, and padding this position by 50 km on in the x-, y-, and z-directions to generate a small search volume.

```
#!/bin/csh -f
# Finds the origin time and defines the
# search volume for the forward calculation
# of sourcescan
# findmax.csh
# Gillian Royle
set finp = `/bin/ls *.out`
foreach file ($finp)
  set fn = `echo $file | cut -c1-12`
  set line = `awk 'END {print NR}' $file`
  awk '{print $1, $2, $3, $4, $5}' < $file > brimax.input
  echo $line | maxbri
  set ttbri = `awk '{print $NF}' 'brimaxt.output'`
  set tbri = `echo $ttbri | cut -c1-8`
  set xmin = `awk '{print $(NF-5)}' 'brimaxsp.output'`
  set xmax = `awk '{print $(NF-4)}' 'brimaxsp.output'`
  set ymin = `awk '{print $(NF-3)}' 'brimaxsp.output'`
  set ymax = `awk '{print $(NF-2)}' 'brimaxsp.output'`
  set zmin = `awk '{print $(NF-1)}' 'brimaxsp.output'`
  set zmax = `awk '{print $NF}' 'brimaxsp.output'`
  echo $tbri $tbri 1 2.5 1 1 1 0.5 0 1 1.0 250.0 50.0 1 >! \
$fn'_'$tbri.input
  echo $xmin $xmax $ymin $ymax $zmin $zmax 1 >> $fn'_'$tbri.input
  echo '/tremor/allref/S' >> $fn'_'$tbri.input
  echo '/tremor/obs1/'$fn.obs1 >> $fn'_'$tbri.input
  echo '/tremor/outputssfnl/'$fn'_'$tbri.out >> $fn'_'$tbri.input
  echo '/tremor/station.dat' >> $fn'_'$tbri.input
  echo '/tremor/allref/S/1D_S' >> $fn'_'$tbri.input
  rm brimax.input
  rm brimaxt.output
```

```
  rm brimaxsp.output
end
```

findmax.csh uses the program maxbri.c.

```
# maxbri.c
#include <stdio.h>
#include <math.h>
#define INPUT "brimax.input"
#define OUTPUTSPACE "brimaxsp.output"
#define OUTPUTTIME "brimaxt.output"

int main(void)
{
int *xloc,*yloc,*zloc,i=0;
int mem, npts;
int xbri, ybri, zbri;
double *tloc,*bri,bmax,tbri;
scanf("%i", &mem);
npts = mem - 1;
xloc = (int *)malloc(mem*(sizeof(int)));
yloc = (int *)malloc(mem*(sizeof(int)));
zloc = (int *)malloc(mem*(sizeof(int)));
tloc = (double *)malloc(mem*(sizeof(double)));
bri = (double *)malloc(mem*(sizeof(double)));
FILE *input;
FILE *outputsp;
FILE *outputt;
input = fopen(INPUT,"r");
outputsp = fopen(OUTPUTSPACE,"w");
outputt = fopen(OUTPUTTIME,"w");
double max_bri(double b[],int n);
double tloc_bri(double b[],double t[],int n);
int xloc_min(double b[],int x[],int n);
int xloc_max(double b[],int x[],int n);
int yloc_min(double b[],int y[],int n);
int yloc_max(double b[],int y[],int n);
int zloc_min(double b[],int z[],int n);
int zloc_max(double b[],int z[],int n);
for (i=0; i<=npts; i++) {
  fscanf(input,"%lf %i %i %i %lf\n", &tloc[i],&xloc[i],&yloc[i],\
&zloc[i],&bri[i]);
  }
fprintf(outputt,"%lf", tloc_bri(bri,tloc,npts));
```

```
fprintf(outputsp,"%i %i %i %i %i %i", xloc_min(bri,xloc,npts),\
xloc_max(bri,xloc,npts),yloc_min(bri,yloc,npts),\
yloc_max(bri,yloc,npts),zloc_min(bri,zloc,npts),zloc_max(bri,zloc,npts));
fclose(input);
fclose(outputsp);
fclose(outputt);
free(xloc);
free(yloc);
free(zloc);
free(tloc);
free(bmax);
return 0;
}
/*-------------------------------------------------------------*/
/* Function to return max bri value */
double max_bri(double bri[], int n)
{
int j;
double bmax;
bmax = bri[0];
for (j=1; j<=n; j++) {
  if (bri[j] > bmax) {
    bmax = bri[j];
    }
  }
return bmax;
}
/*-------------------------------------------------------------*/
/* Function to return max bri value */
double tloc_bri(double bri[], double tloc[], int n)
{
int k;
double bmax;
double tbri;
bmax = bri[0];
for (k=1; k<=n; k++) {
  if (bri[k] > bmax) {
    bmax = bri[k];
    tbri = tloc[k];
    }
  }
if (tbri < 0.0000) {
```

```
  tbri = 0.0000;
  }
return tbri;
}
/*-------------------------------------------------------------*/
/* Function to return x-value of bmax */
int xloc_min(double bri[], int xloc[], int n)
{
int m;
double bmax;
int xbri;
bmax = bri[0];
for (m=1; m<=n; m++) {
  if (bri[m] > bmax) {
    bmax = bri[m];
    xbri = xloc[m];
    }
  }
if (xbri < 81) {
  xbri = 81;
  }
return xbri - 80;
}
/*-------------------------------------------------------------*/
/* Function to return x-value of bmax */
int xloc_max(double bri[], int xloc[], int n)
{
int p;
double bmax;
int xbri;
bmax = bri[0];
for (p=1; p<=n; p++) {
  if (bri[p] > bmax) {
    bmax = bri[p];
    xbri = xloc[p];
    }
  }
if (xbri > 281) {
  xbri = 281;
  }
return xbri + 80;
}
```

```
/*-------------------------------------------------------------*/
/* Function to return x-value of bmax */
int yloc_min(double bri[], int yloc[], int n)
{
int q;
double bmax;
int ybri;
bmax = bri[0];
for (q=1; q<=n; q++) {
  if (bri[q] > bmax) {
    bmax = bri[q];
    ybri = yloc[q];
    }
  }
if (ybri < 81) {
  ybri = 81;
  }
return ybri - 80;
}
/*-------------------------------------------------------------*/
/* Function to return x-value of bmax */
int yloc_max(double bri[], int yloc[], int n)
{
int r;
double bmax;
int ybri;
bmax = bri[0];
for (r=1; r<=n; r++) {
  if (bri[r] > bmax) {
    bmax = bri[r];
    ybri = yloc[r];
    }
  }
if (ybri > 371) {
  ybri = 371;
  }
return ybri + 80;
}
/*-------------------------------------------------------------*/
/* Function to return x-value of bmax */
int zloc_min(double bri[], int zloc[], int n)
{
```

```
int s;
double bmax;
int zbri;
bmax = bri[0];
for (s=1; s<=n; s++) {
  if (bri[s] > bmax) {
    bmax = bri[s];
    zbri = zloc[s];
    }
  }
if (zbri < 81) {
  zbri = 81;
  }
return zbri - 80;
}
/*-------------------------------------------------------------*/
/* Function to return x-value of bmax */
int zloc_max(double bri[], int zloc[], int n)
{
int t;
double bmax;
int zbri;
bmax = bri[0];
for (t=1; t<=n; t++) {
  if (bri[t] > bmax) {
    bmax = bri[t];
    zbri = zloc[t];
    }
  }
if (zbri > 17) {
  zbri = 17;
  }
return zbri + 80;
}
/*-------------------------------------------------------------*/
```

The output files from the third run of `sourcescanV040531.f` define the brightness distribution for each located tremor event.

C.6 GLOSSARY OF VARIABLES

t1min time mark for the beginning of process

t1max time mark for the end of process

dt1 time shift for each step

dtwindow time duration of moving window centered at each t1

ilim 0 if searching through the entire model, 1 if a subvolume is specified in the next line

iweight 0 means Gaussian weighting will be used, 1 means equal weighting will be used

igrid 0 means the max, average, and standard deviation of each time step will be outputed, 1 means each time step will output a file containing the brightness/location/occurrence times of each point if its brightness is >= bthre

bthre only points with brightness >= bthre*bmax will be outputted

mbf 0 means the t1min and t1max are referred as the time limits at the source (origin times, i.e. forward calculation for the first and second run of `sourcescanV040531.f`), 1 means the t1min and t1max are the time limits at the reference station (arrival times, i.e. backward calculation for the third run of `sourcescanV040531.f`)

Nroot This will raise the calculated brightness to its N-th power (to sharpen the image)

stthre only points calculated from (stthre)% of total stations are kept

ttmax only traveltime <= ttmax will be used in brightness calculation

rlim any positive number (e.g., 150.0) means that the calculation of brightness will be limited to the region (+/- rlim) from the station with the largest absolute amplitude. In this case, the program will load in the absolute amplitude information from the file named "$file-name_of_input_waveform"_abs (which was generated by `preSS_040621.f` previously). The two files' format is exactly the same. <= 0.0 means that no constraints from the absolute amplitude is used in the calculation. *Note*: We should set rlim whenever possible. Even a more generous rlim (=100.0) can save calculation time by as much as 50%

ioutrlim 0 means that all points outside the (+/- rlim) region will be ignored (when rlim is set to a positive value). 1 means that, when a point is outside of the (+/- rlim) region from the station with the largest absolute amplitude (Station MaxAm), its brightness will still be calculated if it is located closer the Station MaxAm than to any other stations. *Note*: This parameter is not used if rlim is set to be <= 0. When rlim is > 0, the calculation times for ioutrlim=0 and ioutrlim=1 sometimes is limited (<1%). Thus, it is suggested to use ioutrlim=1 all the time

ixmin minimum x-coordinate

ixmax maximum x-coordinate

iymin minimum y-coordinate

iymax maximum y-coordinate

izmin minimum z-coordinate

izmax maximum z-coordinate *Note*: This line should be a blank line if ilim = 0.

kmint calculation will be performed every kmint points

Bibliography

[1] J. Adams and S. Halchuk, *Knowledge of in-slab earthquakes needed to improve seismic hazard estimates for southwestern British Columbia*, Geological Survey of Canada Open File 3938: Proceedings of the Geological Society of America Penrose Conference: Great Cascadia Earthquake Tricentennial, 2000, p. 5.

[2] J. Adams, S. Halchuk, and D. H. Weichert, *Lower probability hazard, better performance? Understanding the shape of the hazard curves from Canada's Fourth Generation seismic hazard results*, Paper 1555, 12^{th} World Conference on Earthquake Engineering, Auckland, 30^{th} January-4^{th} February, 2000, p. 8.

[3] B. F. Atwater, A. A. Nelson, and J. J. Clague et al., *Consensus about past great earthquakes at the Cascadia subduction zone*, Earthquake Spectra **11** (1995), 1–18.

[4] N. J. Balmforth, R. V. Craster, and A. C. Crust, *Instability in flow through elastic conduits and volcanic tremor*, J. Fluid Mech. **527** (2005), 353–377.

[5] W. F. Brace and J. D. Byerlee, *Stick slip as a mechanism for earthquakes*, Science **153** (1966), 990–992.

[6] T. Brocher, R. Wells, S. Johnson, C. Weaver, S. Kirby, T. Pratt, R. Blakely, and P. McCrory.

[7] A. J. Calvert, *Seismic reflection imaging of two megathrust shear zones in the northern Cascadia subduction zone*, Nature **428** (2004), 163–167.

[8] A. J. Calvert and R. M. Clowes, *Deep, high-amplitude reflections from a major shear zone above the subducting Juan de Fuca plate*, Geology **18** (1990), 1091–1094.

[9] J. Cassidy and R. M. Ellis, *S-wave velocity structure of the northern Cascadia subduction zone*, J. Geophys. Res. **98** (1993), 4407–4421.

[10] J. J. Clague, *Evidence for large earthquakes at the Cascadia subduction zone*, Rev. Geophys. **35** (1997), 430–460.

[11] R. M. Clowes and R. D. Hyndman, *Geophysical studies of the northern Cascadia subduction zone off western Canada and their implications for great earthquake seismotectonics: A review*, pp. 1–23, Terra Scientific Publishing Company, 2002.

[12] R. M. Clowes, C. J. Yorath, and R. D. Hyndman, *Reflection mapping across the convergent margin of western Canada*, Geophys. J. R. Astron. Soc. **89** (1987), 79–84.

[13] C. DeMets, R. G. Gordon, D. F. Argus, and S. Stein, *Current plate motions*, Geophys. J. Int. **101** (1990), 425–478.

[14] H. Dragert, S. Mazzotti, and K. Wang, *Aseismic slip on the northern Cascadia subduction zone: Impacts on seismic hazard estimates*, 2002.

[15] H. Dragert, K. Wang, and T. S. James, *A silent slip event on the deeper Cascadia subduction zone*, Science **292** (2001), 1525–1528.

[16] J. A. Hole and B. C. Zelt, *3-d finite-difference reflection traveltimes*, Geophys. J. Int. **121** (1995), 427–434.

[17] R. D. Hyndman, *Dipping seismic reflectors, electrically conductive zones, and trapped water in the crust over a subduction plate*, J. Geophys. Res. **93** (1988), 13391–13405.

[18] R. D. Hyndman and K. Wang, *Thermal constraints on the zone of major thrust earthquake failure: the Cascadia subduction zone*, J. Geophys. Res. **98** (1993), 2039–2060.

[19] ———, *The rupture of Cascadia great earthquakes from current deformation and thermal regime*, J. Geophys. Res. **100** (1995), 22133–22154.

[20] S. Y. Johnson, *Evidence for a margin truncating transcurrent fault (pre-late Eocene) in western Washington*, Geology **12** (1984), 538–541.

[21] D. L. Jones, N. J. Silberling, and J. Hillhouse, *Wrangellia - a displaced terrane in northwestern North America*, Can. J. Earth Sci. **14** (1977), 2565–2577.

[22] B. Julian, *Seismological detection of slab metamorphism*, Science **296** (2002), 1625–1627.

[23] B. R. Julian, *Volcanic tremor: nonlinear excitation by fluid flow*, J. Geophys. Res. **99** (1994), 11 859–11 877.

[24] B. R. Julien, *Seismological detection of slab metamorphism*, Science **296** (2002), 1625–1626.

[25] H. Kao and S.-J. Shan, *The Source-Scanning Algorithm: mapping the distribution of seismic sources in time and space*, Geophys. J. Int. **157** (2004), 589–594.

[26] H. Kao, S.-J. Shan, H. Dragert, G. Rogers, J. F. Cassidy, and K. Ramachandran, *A wide depth distribution of seismic tremors along the northern Cascadia margin*, Nature **436** (2005), 841–844.

[27] A. Katsuma and N. Kamaya, *Low-frequency continuous tremor around the Moho discontinuity away from volcanoes in southwest Japan*, J. Geophys. Res. **30** (2003), 20–21.

[28] S. H. Kirby, *Taking the temperature of slabs*, Nature **403** (2000), 31–34.

[29] S. H. Kirby and K. Wang, *Introduction to a global systems approach to Cascadia slab processes and associated earthquake hazard*, The Cascadia Subduction Zone and Related Subduction Systems (S. H. Kirby, K. Wang, and S. G. Dunlop, eds.), U.S. Geological Survey Open-File Report 02-328, Geological Survey of Canada Open File 4350, 2002, pp. 37–42.

[30] R. D. Kurtz, J. M. Delaurier, and J. C. Gupta, *The electrical conductivity distribution beneath Vancouver Island: A region of active plate subduction*, J. Geophys. Res. **95** (1990), 10,929–10,946.

[31] A. T. Linde and P. G. Silver, *Elevation changes and the great 1960 Chilean earthquake: Support for aseismic slip*, Geophys. Res. Lett. **16** (1989), 1305–1308.

[32] N. Matsumoto, *Regression analysis for anomalous changes of ground water level due to earthquakes*, Geophys. Res. Lett. **19** (1997), no. 12, 1193–1196.

[33] S. Mazzotti and J. Adams, *Variability of near-term probability for the next great earthquake on the Cascadia subduction zone*, Bull. Seis. Soc. Am. **94** (2004), no. 5, 1954–1959.

[34] J. C. Moore and D. Saffer, *Updip limit of the seismogenic zone beneath the accretionary prism of Southwest Japan; an effect of diagenetic to low-grade metamorphic processes and increasing effective stress*, Geology **29** (2001), 183–186.

[35] J. E. Muller, *Evolution of the pacific margin, Vancouver Island, and adjacent regions*, Can. J. Earth Sci. **14** (1977), 2062–2085.

[36] ———, *Chemistry and origin of Eocene Metchosin Volcanics, Vancouver Island, British Columbia*, Can. J. Earth Sci. **17** (1980), 199–209.

[37] National Resources Canada, *Canadian National Seismograph Network Station Book*, World Wide Web, http://www.seismo.nrcan.gc.ca/cnsn/stn_book, 2005.

[38] ———, *Event-Related Waveform Data Request Form*, World Wide Web, http://www.seismo.nrcan.gc.ca/nwfa/index, 2005.

[39] ———, *Overview of the National Earthquake Database*, World Wide Web, http://seismo.nrcan.gc.ca/nedb/bull, 2005.

[40] M. R. Nedimović, R. D. Hyndman, K. Ramachandran, and G. D. Spence, *Reflection signature of seismic and aseismic slip on the northern Cascadia subduction zone*, Nature **424** (2003), 416–420.

[41] K. Obara, *Nonvolcanic deep tremor associated with subduction in southwest Japan*, Science **296** (2002), 1679–1681.

[42] K. Ramachandran, *Velocity structure of S.W. British Columbia and N.W. Washington from 3-d non-linear seismic tomography*, Ph.D. thesis, University of Victoria, Department of Earth Sciences, 2001.

[43] K. Ramachandran, S. E. Dosso, and G. D. Spence, *Forearc structure beneath southwestern British Columbia: A three-dimensional tomographic velocity model*, J. Geophys. Res. **110, B02303** (2005), no. B2.

[44] K. Ramachandran, R. D. Hyndman, and T. M. Brocher, *Structure of the Northern Cascadia Subduction Zone: A 3-D Tomographic P-wave Velocity Model*, AGU Fall Meeting Abstracts (2004), 167.

[45] C. B. Rayleigh, *Tectonic implications of serpentine weakening*, Geophys. J. Royal Astro. Soc. **14** (1967), 113–118.

[46] G. Rogers and H. Dragert, *Episodic tremor and slip on the Cascadia subduction zone: The chatter of silent slip*, Science **300** (2003), 1942–1943.

[47] K. Satake, K. Shimazaki, Y. Tsuji, and K. Ueda, *Time and size of a giant earthquake in Cascadia inferred from Japanese tsunami records of January 1700*, Nature **379** (1996), 246–249.

[48] J. C. Savage, M. Lisowski, and W. S. Prescott, *Strain accumulation in western Washington*, J. Geophys. Res. **96** (1991), 14 493–14 507.

[49] C. H. Scholtz, *Earthquakes and friction laws*, Nature **391** (1998), 37–42.

[50] G. D. Spence, R. M. Clowes, and R. M. Ellis, *Seismic structure across the active subduction zone of western Canada*, J. Geophys. Res. **89** (1985), 79–84.

[51] J. Vidale, *finite-difference calculation of reflection traveltimes in three dimensions*, Geophysics **55** (1990), 521–526.

[52] K. Wang, H. Jiangheng, H. Dragert, and S. J. Thomas, *Three-dimensional viscoelastic interseismic deformation model for the Cascadia subduction zone*, Earth Planets Space **53** (2001), 295–306.

[53] Western Canada Research Grid, *Westgrid: The Innovation Grid*, World Wide Web, http://www.westgrid.ca/home.html, 2005.

[54] C. J. Yorath, A. G. Green, R. M. Clowes, A. Sutherland-Brown, M. T. Brandon, E. R. Kanasewich, R. D. Hyndman, and C. P. Spencer, *Lithoprobe - southern Vancouver Island: seismic reflection sees through Wrangellia to the Juan de Fuca plate*, Geology **13** (1985), 759–762.

[55] D. Zhao, K. Wang, G. C. Rogers, and S. M. Peacock, *Tomographic image of low P velocity anomalies above slab in northern Cascadia subduction zone*, Earth Planets Space **53** (2001), 285–293.